# ARS JOURNAL

## RUSSIAN SUPPLEMENT

**Igor Jurkevich, Editor**





*Published Under National Science Foundation Grant-in-Aid*

# Some Properties of a System of Nearly Canonical Differential Equations[1]

L. A. BEKLEMISHEVA

Department of Differential Equations
Moscow University

THE SOLUTIONS of general canonical systems show a very complex behavior; various aspects of the subject have been considered in the literature (1–4).[2] The nature of the first integral sometimes serves to indicate some properties of the solution; for example, if every line $U(x,y) =$ constant is bounded, then every solution of the system

$$\frac{dx}{dt} = \frac{\partial U(x,y)}{\partial y} \qquad \frac{dy}{dt} = -\frac{\partial U(x,y)}{\partial x}$$

is also bounded. Atkinson (5) has examined the equation

$$\ddot{x} + x^{2n-1} + f(t)x = 0 \qquad [*]$$

which is readily given the canonical form for $f(t) \equiv 0$; then the first integral is $\dot{x}^2 + x^{2n}/n$. Atkinson has formulated the conditions on $f(t)$ sufficient to give the function $\dot{x}^2(t) + x^{2n}(t)/n$ a finite limit as $t \to \infty$, if $x(t)$ is any solution of Eq. [*].

The method adopted here is applicable to any system of $2n$ equations very similar to a canonical one. In particular, Theorem 2a states restrictions on the right sides of the equations

$$\ddot{x}_i = -\frac{\partial V(x,x_2,\ldots,x_n)}{\partial x_i} + y_i(x_1,\ldots,x_n,\dot{x}_1,\ldots,\dot{x}_n,t) + h_1(x_1,\ldots,x_n,\dot{x}_1,\ldots,\dot{x}_n,t)$$

sufficient to make all solutions of this system bounded as $t \to \infty$. Theorem 1 states the condition sufficient to make

$$\lim_{t\to\infty} H(x(t),y(t),t) = C$$

for each bounded solution[3] of

$$\frac{dx_i}{dt} = \frac{\partial H(x,y,t)}{\partial y_i} + g_{i1}(x,y,t) + h_{i1}(x,y,t)$$

$$\frac{dy_i}{dt} = -\frac{\partial H(x,y,t)}{\partial x_i} + g_{i2}(x,y,t) + h_{i2}(x,y,t)$$

$$i = 1, \ldots, n \qquad \ldots\ldots\ldots\ldots\ldots\ldots\ldots\ldots\ldots\ldots [1]$$

This is a generalization of Ascoli's (6) theorem.

In Section 2, some conditions are given sufficient to insure that $\ddot{x} + f(x,\dot{x},t) = 0$ has solutions that resemble the solutions of the corresponding canonical equation, namely ones that tend to constant limits as $t \to \infty$. In Section 3, the equation $\ddot{x} + x = f(x,\dot{x},t)$ is used to demonstrate the results given by the theorems in this simple case.

## §1

Consider the real range of the system of Eq. 1; all functions appearing on the right are defined in the space $XYT$, which is the product of the space $XY$ of the variables $x_1, \ldots, x_n$ and $y_1, \ldots, y_n$ by the half-axis $t \geqslant T$. It is assumed that $H(x,y,t)$ and the solutions $x_1(t), \ldots, x_n(t)$ and $y_1(t), \ldots, y_n(t)$ are continuous. It is possible that system 1 has a definite and continuous solution provided that $T \leqslant t < \tau < \infty$, but the solution cannot be extended continuously beyond the point $\tau$. This is an inextensible solution; the equation $\ddot{x} + x + t^{-100}x^2 = 0$ has an infinite number of such solutions, for example.

The method presented here is applicable to any solution without change in the form given to the theorems, so in the following solutions to Eq. 1 will be dealt with that are defined and continuous for $T \leqslant t < \tau \leqslant \infty$, and also with the asymptotic behavior for $t \to \tau$.

### Theorem 1

Let $R$ be some region in $XY$, and in $RT$ let the functions $H$, $\partial H/\partial x_i$, $\partial H/\partial y_i$ $(i = 1, \ldots, n)$ be bounded (as regards modulus) by a constant $C$; further, let

$$\sum_{i=1}^{n}\left(\frac{\partial H}{\partial x_i}h_{i1} + \frac{\partial H}{\partial y_i}h_{i2}\right)$$

be of constant sign. Finally, let there be a function $\varphi(t)$ such that

$$\int_T^\tau \varphi(t)dt < \infty$$

and that in the range $T \leqslant t < \tau$ we have

$$|H'_t(x,y,t)| + \sum_{i=1}^{n}(|g_{i1}(x,y,t)| + |g_{i2}(x,y,t)|) \leqslant \varphi(t) \qquad [2]$$

for all $x$ and $y$ in $R$. Then there exists a finite limit

$$\lim_{t\to\tau} H(x(i),y(t),t)$$

for each solution $x(t)$, $y(t)$ of Eq. 1 for $R$ in the range $T \leqslant t < \tau$.

---

Translated from *Vestnik Moskovskogo Universiteta* (*Bulletin of Moscow University, Series 1, Mathematics-Mechanics*), 1960, no. 4, pp. 26–36. Translated by Research Information Service, New York.

[1] Some of these theorems have been presented previously [e.g., ref. (10)], but without proof.

[2] Numbers in parentheses indicate References at end of paper.

[3] Here and elsewhere the arguments of the functions are given in condensed form; $H(x, y, t)$ denotes $H(x_1, \ldots, x_n, y_1, \ldots, y_n, t)$, and $x(t)$, $y(t)$ denote $x_1(t), \ldots, x_n(t)$ and $y_1(t), \ldots, y_n(t)$, and so on.

**Proof**

Let us suppose that

$$\sum_{i=1}^{n}\left(\frac{\partial H}{\partial x_i}h_{i1}+\frac{\partial H}{\partial y_i}h_{i2}\right)\leqslant 0$$

The conditions imposed imply that $|H(x(t),y(t),t)|\leqslant C$ for $T\leqslant t<\tau$, so the set of $H(x(t),y(t),t)$ has at least one limit point for $t\to\tau$. Let us suppose that there are not less than two such points; then the continuity in $H$, $x(t)$ and $y(t)$ implies that there are numbers $\alpha$ and $\beta$ ($\beta>\alpha$) and a monotonic sequence $t_k\to\tau$ such that for all $k$

$$H(x(t_{2k}),y(t_{2k}),t_{2k})=\alpha \qquad H(x(t_{2k+1}),y(t_{2k+1}),t_{2k+1})=\beta \qquad [3]$$

The total derivative $dH/dt$ along $x(t),y(t)$ in the intervals $(t_{2k},t_{2k+1})$ is found by taking

$$\frac{dH(x(t),y(t),t)}{dt}=\sum_{i=1}^{n}\left(\frac{\partial H}{\partial x_i}g_{i1}+\frac{\partial H}{\partial y_i}g_{i2}\right)+\sum_{i=1}^{n}\left(\frac{\partial H}{\partial x_i}h_{i1}+\frac{\partial H}{\partial y_i}h_{i2}\right)+\frac{\partial H}{\partial t}\leqslant\left|\sum_{i=1}^{n}\left(\frac{\partial H}{\partial x_i}g_{i1}+\frac{\partial H}{\partial y_i}g_{i2}\right)+H'_t\right|\leqslant$$

$$\leqslant\sum_{i=1}^{n}\left(\left|\frac{\partial H}{\partial x_i}\right|\cdot|g_{i1}|+\left|\frac{\partial H}{\partial y_i}\right|\cdot|g_{i2}|\right)+|H'_t|\leqslant 2nC\varphi(t)+\varphi(t)=(2nC+1)\varphi(t) \qquad [4]$$

which is to be integrated between the limits $t_{2k}$ and $t_{2k+1}$ in conjunction with Eq. 3 to give

$$\beta-\alpha\leqslant\int_{t_{2k}}^{t_{2k+1}}(2nC+1)\varphi(t)dt$$

in which $\beta-\alpha$ is a positive constant. The integral is a function of $k$ and decreases without bound as $k$ increases; in fact, $\varphi(t)\in L_{T1,\tau}$ when $t_k\to\tau$, so Eq. 4 is contradictory if $k$ is large. This means that we were wrong to suppose that $H$ has several limiting points. *Q.E.D.*

Further, Eq. 2 implies that $\lim_{t\to\tau}H(x,y,t)$ exists for each point $(x,y)\in R$; let that limit be $U(x,y)$. If Theorem 1 is true, then all points $\Omega$ of the limiting set of the loci $x(t)$, $y(t)$ lie on a surface $U(x,y)=$ constant.

In what follows it shall be supposed that $U(x,y)$ is continuous; the difference $H(x,y,t)-U(x,y)$ will be denoted by $\psi(x,y,t)$. We shall now prove several theorems analogous to Theorem 1, except in that no bounds are imposed on $H$, $\partial H/\partial x_i$ and $\partial H/\partial y_i$. These theorems can be used to examine the unbounded solutions of Eq. 1 that tend to zero. The mode of proof is the same in all cases, which are formulated here as a lemma. The notation which shall be used is $U(x(t),y(t))\equiv U(t)$, $\psi(x(t),y(t),t)\equiv\psi(t)$, and so on.

**Lemma**

We are given a set $R\subseteq XY$, a solution $x(t)$, $y(t)$ and an infinite monotonically increasing sequence $t_k\to\tau$ ($T\leqslant t_k$) such that the points $(x(t),y(t))$ lie in $R$ for $t_{2k}\leqslant t\leqslant t_{2k+1}$. Conditions that are obeyed are

$$|\psi(x,y,t)|\leqslant c\,|U(x,y)| \qquad c<1 \qquad [5]$$

$$\frac{\epsilon}{U(x,y)}\sum_{i=1}^{n}\left(\frac{\partial H}{\partial x_i}h_{i1}+\frac{\partial H}{\partial y_i}h_{i2}\right)\geqslant 0 \qquad [6]$$

in which $\epsilon$ takes the value $+1$ or $-1$; let there be a function $\varphi(t)\in L^1_{T,\tau}$ such that for $(x,y)\in R$ and $T\leqslant t<\tau$ we have

$$|\psi'_t(x,y,t)|+\left|\sum_{i=1}^{n}\left(\frac{\partial H}{\partial x_i}g_{i1}+\frac{\partial H}{\partial y_i}g_{i2}\right)\right|\leqslant\varphi(t)\,|U(x,y)| \qquad [7]$$

Then we assert that we cannot have simultaneously for all $k$

$$U(t_{2k})=q^{\epsilon}U(t_{2k+1}) \qquad [8]$$

if $q\geqslant(1+c)/(1-c)$ is a positive number.

**Proof**

We produce along $x(t)$, $y(t)$ the derivative

$$\frac{d\ln H}{dt}=\frac{1}{H}\cdot\frac{dH}{dt}=\frac{1}{H}\left\{\sum_{i=1}^{n}\left(\frac{\partial H}{\partial x_i}g_{i1}+\frac{\partial H}{\partial y_i}g_{i2}\right)+\sum_{i=1}^{n}\left(\frac{\partial H}{\partial x_i}h_{i1}+\frac{\partial H}{\partial y_i}h_{i2}\right)+\psi'_t\right\} \qquad [9]$$

and integrate the two sides of Eq. 9 from $t_{2k}$ to $t_{2k+1}$; let $\epsilon$ equal $+1$, and suppose that Eq. 8 applies to that interval. Then we have for the left-hand side that

$$L=\ln\frac{H(t_{2k+1})}{H(t_{2k})}=\ln\frac{U(t_{2k+1})+\psi(t_{2k+1})}{U(t_{2k})+\psi(t_{2k})}=\ln\left(\frac{U(t_{2k+1})}{U(t_{2k})}\cdot\frac{1+\psi(t_{2k+1})/U(t_{2k+1})}{1+\psi(t_{2k})/U(t_{2k})}\right)\leqslant\ln\left(q^{-\epsilon}\cdot\frac{1+c}{1-c}\right)=$$

$$\ln\left(\frac{1}{q}\cdot\frac{1+c}{1-c}\right)=\text{const}<0 \qquad [10]$$

and for the right that

$$L=\int_{t_{2k}}^{t_{2k+1}}\left\{\frac{1}{H}\sum_{i=1}^{n}\left(\frac{\partial H}{\partial x_i}g_{i1}+\frac{\partial H}{\partial y_i}g_{i2}\right)+\frac{1}{H}\sum_{i=1}^{n}\left(\frac{\partial H}{\partial x_i}h_{i1}+\frac{\partial H}{\partial y_i}h_{i2}\right)+\frac{\psi'_t}{H}\right\}dt=$$

$$\int_{t_{2k}}^{t_{2k+1}}\frac{1}{1+\psi/U}\left\{\frac{1}{U}\sum_{i=1}^{n}\left(\frac{\partial H}{\partial x_i}g_{i1}+\frac{\partial H}{\partial y_i}g_{i2}\right)+\frac{1}{U}\sum_{i=1}^{n}\left(\frac{\partial H}{\partial x_i}h_{i1}+\frac{\partial H}{\partial y_i}h_{i2}\right)+\frac{\psi'_t}{U}\right\}dt$$

Now we estimate a lower limit to this expression. The condition implies that $1/(1+\psi'/U)\geqslant 1/(1-c)>0$; the second sum in the integral is not negative ($\epsilon=+1$), so

$$L\geqslant\int_{t_{2k}}^{t_{2k+1}}\frac{1}{1+\psi/U}\left\{\frac{1}{U}\sum_{i=1}^{n}\left(\frac{\partial H}{\partial x_i}g_{i1}+\frac{\partial H}{\partial y_i}g_{i2}\right)+\frac{\psi'_t}{U}\right\}dt\geqslant-$$

$$\int_{t_{2k}}^{t_{2k+1}}\frac{1}{1+\psi/U}\left\{\frac{1}{U}\sum_{i=1}^{n}\left(\frac{\partial H}{\partial x_i}g_{i1}+\frac{\partial H}{\partial y_i}g_{i2}\right)+\left|\frac{\psi'_t}{U}\right|\right\}dt\geqslant-\frac{1}{1-c}\int_{t_{2k}}^{t_{2k+1}}\varphi(t)dt$$

(The last inequality follows from Eqs. 5 and 7.) Now $\varphi(t)$ is integrable, so the right part becomes negative for $t_k\to\tau$, but the modulus can be made as small as may be desired when $k$ is large. This estimate of $L$ conflicts with that given by Eq. 10, so Eq. 8 is contradictory for $k$ large.

In what follows we shall examine the solution $x(t),y(t)$ to Eq. 1, which we suppose to be defined for $T\leqslant t<\tau$ and to lie in some manifold $K\subseteq XY$. The case $K=XY$ corre-

sponds to an arbitrary solution to Eq. 1; the case $K \subset XY$ enables us to examine at least some of the solutions to Eq. 1, if the restrictions on the complement are not complied with throughout the whole of $XY$.

The following theorems are presented in condensed form, and similar proofs are omitted, with a view to economy in space.

**Theorem 2**

We define a set $R_{C1}[R_{C2}]$ of points $(x,y)$ by means of the relations $(x,y) \in K$, $U(x,y) > C$ $[<C]$. Let there be a $C$ such that Eqs. 5, 6 and 7 apply to this set, and let $\epsilon$ equal $-1$. Then

$$U(x(t),y(t)) < \text{const } [> \text{const}] \text{ for } T \leqslant t < \tau$$

**Proof**

We assume the converse, i.e., that $U(t_\alpha) \to +\infty$ along some sequence $t_\alpha \to \tau$.[4] We take some number

$$q > \frac{(1+c)}{(1-c)}$$

(in which $c$ is defined by Eq. 5) and use the fact that $U(t)$ is continuous to select a new monotonically increasing sequence $t_k \to \tau$, such that

$$U(t_{2k+1}) = qU(t_{2k}) \qquad [11]$$

$$U(t_{2k}) \leqslant U(t) \leqslant U(t_{2k+1}) \text{ for } t_{2k} \leqslant t \leqslant t_{2k+1} \qquad [12]$$

Now Eq. 12 shows that $(x(t),y(t)) \in R_{C1}$ for $t_{2k} \leqslant t \leqslant t_{2k+1}$, so we have the conditions of the lemma. But $\epsilon = -1$, so Eq. 11 contradicts the assertion in the lemma. The theorem is thus proved. A simple consequence is as follows.

**Theorem 2a**

We have the system

$$\ddot{x}_i = -\frac{\partial V(x)}{\partial x_i} + \frac{\partial \psi(x,t)}{\partial x_i} + g_i(x,\dot{x},t) + h_i(x,\dot{x},t) \qquad [13]$$

$$i = 1,\ldots,n$$

Let $V(x)$ be continuous; let

$$\lim V(x) = \infty \text{ for } \sum x_i^2 \to \infty$$

$$U(x,y) = V(x) + \frac{1}{2}\sum_{i=1}^{n} y_i^2$$

$$\ldots\ldots\ldots\ldots\ldots\ldots\ldots\ldots\ldots\ldots\ldots\ldots [14]$$

and let us suppose that outside a certain sphere $S$ within the space of $x$ and $y$ we have for $t \geqslant T$ that

$$\sum_{i=1}^{n} y_i h_i(x,y,t) \leqslant 0$$

$$|\psi'_t(x,y,t)| + |\sum_i y_i g_i(x,y,t)| \leqslant \varphi(t)\cdot|U(x,y)|$$

$$\int_T^\infty \varphi(t)dt < \infty \qquad |\psi(x,t)| < c|U(x,y)| \qquad c < 1$$

$$\ldots\ldots\ldots\ldots\ldots\ldots\ldots\ldots\ldots\ldots\ldots\ldots [15]$$

Then all extensible solutions of Eq. 13, together with their derivatives, are bounded for $t \to \infty$.

*Note:* If the right sides of Eq. 13 are continuous and obey the conditions, the system has no unbounded solutions; the absence of unbounded inextensible solutions is demonstrated as for unbounded extensible ones (Eq. 15 is applied to a finite range in $t$).

[4] We prove the first assertion in the theorem.

**Proof of Theorem 2a**

The conditions are those of Theorem 2. We introduce variables $y_i = \dot{x}_i$; then Eq. 13 takes the form of Eq. 1, with $\partial\psi/\partial y_i \equiv h_{i1} \equiv g_{i1} \equiv 0$, and

$$U(x,y) + \psi(x,y,t) = H(x,y,t) = V(x) + \frac{1}{2}\sum_{i=1}^{n} y_i^2 + \psi(x,t)$$

Then the $R_{C1}$ of Theorem 2 is found by putting $K = XY$ and using the fact that the set of points $(x,y)$, as defined by

$$V(x) + \frac{1}{2}\sum_{i=1}^{n} y_i^2 > \text{const}$$

for values of that constant sufficiently large, lies outside that sphere. The assertion of Theorem 2 amounts to the assertion that along any solution

$$V(x(t)) + \frac{1}{2}\sum_{1}^{n} \dot{x}_i^2(t) < \text{const} \qquad [16]$$

so $V(x(t)) <$ constant, which in conjunction with condition 14 gives[5] for $t \to +\infty$

$$\sum_{i=1}^{n} x_i^2(t) < \text{const}$$

The continuity of $V(x)$, in conjunction with Eq. 14, implies that $V(x) >$ constant for all $x$. This, with Eq. 16, gives us

$$\sum_{i=1}^{n} \dot{x}_i^2(t) < \text{const for } t \to +\infty$$

**Theorem 3**

Let conditions 5, 6 and 7 be complied with for some $C$ in the set $R_{C1}[R_{C2}]$, and let $\epsilon$ be $+1$. Then if

$$\overline{\lim_{t\to\tau}}\, U(x(t),y(t)) = +\infty \quad [\lim\ldots = -\infty]$$

the more exact relation

$$\lim_{t\to\tau} U(x(t),y(t)) = +\infty \quad [-\infty]$$

is also obeyed.

Now several theorems will be given that can be used to examine the solutions to Eq. 1 near the equilibrium point of the abbreviated canonical equation. The proofs of Theorems 3 to 5 are omitted because they are merely simple deductions from the lemma.

**Theorem 4**

We define a set $R_{C3}[R_{C4}]$ by the relations

$$(x,y) \in K \qquad 0 \leqslant U(x,y) \leqslant C \qquad [0 \geqslant U(x,y) \geqslant C]$$

Let conditions 5, 6 and 7 be complied with for some $C$ in the set, and let $\epsilon$ be $+1$. Then if

$$\underline{\lim_{t\to\tau}}\, U(x(t),y(t)) \leqslant 0 \qquad [\overline{\lim_{t\to\tau}}\, U(x(t),y(t)) \geqslant 0]$$

[5] Condition 14 is used only at this point in the proof. The solutions to Eq. 13 can be shown to be bounded when less rigorous conditions are imposed on $V(x)$, for example

$$\overline{\lim_{R\to\infty}} \min_{\sum_1^n x_i^2 = R} V(x) = +\infty$$

which takes the form $\overline{\lim_{x\to\infty}}\, V(x) = +\infty$ for $n = 1$; it is the necessary and sufficient condition for all solutions of the abbreviated canonical equation $\ddot{x} = -V'(x)$ to be bounded.

we have for all $t$ sufficiently close to $\tau$ that

$$U(x(t),y(t)) \leqslant 0 \qquad [U(x(t),y(t) \geqslant 0]$$

**Theorem 5**

Let conditions 5, 6 and 7 be satisfied for some $C$ in the set, and let $\epsilon$ be $-1$; the fact that $x(t)$, $y(t)$ obeys

$$\overline{\lim_{t\to\tau}}\, U(x(t),y(t)) \leqslant 0 \qquad [\overline{\lim_{t\to\tau}}\, U(x(t),y(t)) \geqslant 0]$$

implies that a more exact relation

$$\overline{\lim_{t\to\tau}}\, U(x(t),y(t)) \leqslant 0 \qquad [\lim_{t\to\tau}\, U(x(t),y(t)) \geqslant 0]$$

is also obeyed.

**Theorem 4a**

We have system 13

$$\ddot{x}_i = -\frac{\partial V(x)}{\partial x_i} + \frac{\partial \psi(x,t)}{\partial x_i} + g_i(x,\dot{x},t) + h_i(x,\dot{x},t) \qquad [13]$$

$$i = 1, \ldots, n$$

and we suppose that in a region near the point 0 in the $XY$ plane the system obeys, for $t \geqslant T$, the conditions that $V(x)$ is continuous, that $V(0) = 0$, that $V(x) > 0$ for $x \neq 0$, and

$$\sum_{i=1}^{n} y_i h_i(x,y,t) \geqslant 0$$

$$|\psi'_t(x,t)| + \left|\sum_{i=1}^{n} y_i g_i(x,y,t)\right| \leqslant \varphi(t)\cdot|U(x,y)|$$

$$|\psi(x,t)| \leqslant c|U(x,y)|$$

$$c < 1 \qquad U(x,y) = V(x) + \frac{1}{2}\sum_{i=1}^{n} y_i^2$$

$$\int_T^\infty \varphi t(dt) < \infty$$

Then Eq. 13 has no solution that tends to zero along with its derivatives as $t \to \infty$.

**Proof**

Any region about the point $(0,0) \in XY$ contains at least one of the regions defined by the relations $0 \leqslant U(x,y) \leqslant C$. This means that set $R_{C\alpha}$ of Theorem 4 exists, so Theorem 4 applies to Eq. 13. Then if a solution to Eq. 13 exists that tends to zero as $t \to \infty$, for $t \geqslant T$ that solution satisfies

$$V(x) + \sum \frac{\dot{x}_i^2}{2} \leqslant 0$$

Now $V(x) \geqslant 0$, so it is necessary to have $V(x) = 0$ and $\dot{x}_i^2 \equiv 0$. But $V(x)$ is positive definite, so $x \equiv \dot{x} \equiv 0$.

## §2

Given here are theorems on the existence of solutions that tend to constant values for a nonlinear second-order equation; this is an extension of Villari's (7) theorem. The proof is omitted because it follows the lines of Villari's proof exactly.

We call the function $f(x,y,t)$ $\varphi$-continuous in the region $S$ of the variables $x$ and $y$ if for any $\epsilon > 0$ we can find a $\delta > 0$ such that if

$$(x_1,y_1) \in S \qquad (x_2,y_2) \in S$$

$$|x_1 - x_2| + |y_1 - y_2| < \delta$$

then

$$|f(x_1,y_1,t) - f(x_2,y_2,t)| < \epsilon\varphi(t)$$

for all $t$ within the region in which $f$ exists. We define a Lipschitz $\varphi$-condition in a similar way

$$|f(x_1,y_1,t) - f(x_2,y_2,t)| \leqslant \varphi(t)\{|x_1 - x_2| + |y_1 - y_2|\}$$

**Theorem 6**

We are given for $t \geqslant T$ that

$$\ddot{x} + f(x,\dot{x},t) = 0 \qquad [17]$$

together with a real number $c$. Let $f(c,0,t) \not\equiv 0$, and let there be for $t \geqslant T$ a function $\varphi(t)$ such that

1. $\varphi(t) \geqslant 0$, $\int_T^\infty t\varphi(t)dt < \infty$
2. $|f(c,0,t)| \leqslant \varphi(t)$ ..... [18]
3. In a certain region $S$ around the point $(c, 0)$ in the $XY$ plane the function $f(x,y,t)$ is $\varphi$-continuous.

Then Eq. 17 has a solution whose properties are

1. $x(t) \to c$, $\dot{x}(t) \to 0$ as $t \to \infty$ [19]
2. For any $\epsilon > 0$ there is a $t$ such that

$$|x(t) - c| < (1 + \epsilon)\int_t^\infty \varphi(s)ds$$

$$|\dot{x}(t)| < (1 + \epsilon)\int_t^\infty (s - t)\varphi(s)ds$$

That solution is unique if $f$ satisfies a Lipschitz $\varphi$-condition in $S$. Villari had

$$f(x,\dot{x},t) \equiv A(t)\cdot f(x)$$

$$0 < A(t) < \frac{L}{t^{\lambda+2}} \qquad \lambda > 0$$

Winter and Hartman (8) have shown that if for every region $S$ around $(c,0)$ on the $XY$ plane we have

$$\max_{(x,y)\in S} f(x,y,t) \leqslant -\varphi_S(t) \leqslant 0 \qquad \int^\infty t\varphi_S(t)dt = +\infty$$

then Eq. 17 has no solution whose asymptote is Eq. 19. Theorem 6 is, in this sense, correct.

**Theorem 7**

We are given for $t \geqslant T$ that

$$\dot{x} = f(x,y,t) \qquad y = g(x,y,t) \qquad [20]$$

and numbers $c_1$ and $c_2$ such that $|f(c_1,c_2,t) + g(c_1,c_2,t)| \not\equiv 0$. Let us suppose that we can select a function $\varphi(t)$ such that

1. $\int_T^\infty \varphi(t)dt < \infty$
2. $|f(c_1,c_2,t)| + |g(c_1,c_2,t)| \leqslant \varphi(t)$
3. $f(x,y,t)$ and $g(x,y,t)$ are $\varphi$-continuous in some region $S$ around the point $(c_1,c_2)$.

Then Eq. 20 has a solution whose asymptotic behavior is $x(t) \to c_1$, $y(t) \to c_2$ for $t \to \infty$. This solution is unique if $f$ and $g$ satisfy a Lipschitz $\varphi$-condition. This may be proved by means of Villari's method of successive approximations.

Villari (9) has given similar theorems for $n$th order equations; these may be reformulated in terms of integral estimates for the right sides.

## §3

In this section we shall discuss application to the equation

$$\ddot{x} + x = f(x,\dot{x},t) \qquad [21]$$

The foregoing theorems, applied to Eq. 21, give rise to the following conclusions. Suppose that $\varphi(t) \in L^1_{T,\infty}$.

1. If

$$|f(x,y,t)| \leqslant \varphi(t)\{|x| + |y|\} \qquad [22]$$

for some region $S$ in the $XY$ plane for $t \geqslant T$, then all extensible solutions of Eq. 21 are bounded as $t \to \infty$.

2. If $f(x,y,t)$ is also continuous, then all solutions of Eq. 21 are extensible.

3. If for every $R > 0$ we can select a $\varphi_R(t) \in L^1_{T,\infty}$ such that $x^2 + y^2 < R|f(x,y,t)| < \varphi_R(t)$, then any bounded solution of Eq. 21 has the property that $\lim_{t\to\infty} \{x^2(t) + y^2(t)\} =$ constant.

4. If $x_0$ and $y_0$ are such that

$$f(x_0 \cos t + y_0 \sin t, -x_0 \sin t + y_0 \cos t, t) \equiv 0$$

then Eq. 21 has as solution

$$x(t) = x_0 \cos t + y_0 \sin t$$

$$\dot{x}(t) = -x_0 \sin t + y_0 \cos t$$

5. If $x_0$ and $y_0$ are such that $x_0^2 + y_0^2 \neq 0$

$$f(x_0 \cos t + y_0 \sin t, -x_0 \sin t + y_0 \cos t, t) \not\equiv 0$$

and that in some region around the point $(x_0,y_0)$ this $f$ is $\varphi$-continuous and $\varphi$-bounded, then Eq. 21 has at least one solution whose asymptotic behavior is

$$x(t) = x_0 \cos t + y_0 \sin t + 0(1)$$

$$\dot{x}(t) = -x_0 \sin t + y_0 \cos t + 0(1) \qquad [23]$$

6. If the condition of $\varphi$-continuity in 5 is replaced by a Lipschitz $\varphi$-condition, we may say that one solution having the form of Eqs. 23 corresponds to the point $(x_0,y_0)$.

7. If Eq. 22 applies to some region around the point (0,0) in the $XY$ plane, then Eq. 21 has no solution that tends to zero.

Statements 1, 2 and 3 are direct applications of Theorems 2a, 1 and 4a; statement 4 is obvious. We may prove statements 5 and 6 by performing a substitution in Eq. 21, namely

$$x = \xi \cos t + \eta \sin t$$

$$\dot{x} = -\xi \sin t + \eta \cos t$$

This substitution is mutually continuous throughout the space $XYT$; then Eq. 21 becomes

$$\dot{\xi} = -\sin t \cdot f(\xi \cos t + \eta \sin t, -\xi \sin t + \eta \cos t, t)$$

$$\dot{\eta} = \cos t \cdot f(\xi \cos t + \eta \sin t, -\xi \sin t + \eta \cos t, t) \qquad [24]$$

Theorem 7 is applicable to Eqs. 24 if $(x_0,y_0)$ satisfies the requirements listed in statement 5. This gives us the solution

$$x(t) = [x_0 + 0(1)] \cos t + [y_0 + 0(1)] \sin t = x_0 \cos t + y_0 \sin t + 0(1)$$

Now we assume that there is a solution to Eq. 21 of the form

$$x(t) = x_0 \cos t + y_0 \sin t + 0_1(1) \equiv \xi(t) \cos t + \eta(t) \sin t$$

$$\dot{x}(t) = -x_0 \sin t + y_0 \cos t + 0_2(1) \equiv -\xi(t) \sin t + \eta \cos t$$

We solve these identities for $\xi(t)$ and $\eta(t)$ to get

$$\xi(t) = x_0 + 0_1(1) \cos t - 0_2(1) \sin t$$

$$\eta(t) = y_0 + 0_1(1) \sin t + 0_2(1) \cos t$$

Thus two different solutions having the form of Eqs. 23 correspond to two different solutions of Eq. 2 that tend to a single point $(x_0,y_0)$ [if $0_1(1) \cos t - 0_2(1) \sin t \equiv 0_1^*(1) \cos t - 0_2^*(1) \sin t$ and $0_1^*(1) \sin t + 0_2^*(1) \cos t \equiv 0_1(1) \sin t + 0_2(1) \cos t$, then $0_1(1) \equiv 0_1^*(1)$ and $0_2^*(1) \equiv 0_2(1)$]. This is impossible if statement 6 applies.

*—Received February 25, 1959*

## References


1 Moser, "Stabilitätsverhalten kanonischer Differentialgleichungen Systeme" (Stability of Canonical Differential Equation Systems), *Nachr. Akad. Wiss. Gottingen., Math.-Phys. Kl.*, 1955, vol. 6, pp. 87–120.

2 Moser, "New Aspects in the Theory of Stability of Hamiltonian Systems," *Communications in Pure and Appl. Math.*, 1958, vol. 11, no. 1, p. 81.

3 Slotnik, "Asymptotic Behavior of Solutions of Canonical Systems Near a Closed Unstable Orbit," *Ann. Math. Studies*, 1958, vol. 4, no. 41, pp. 85–110.

4 Malkin, I. D., *Some Problems in the Theory of Nonlinear Equations*, Gostekhizdat, 1956.

5 Atkinson, F. V., "On Linear Perturbation of Nonlinear Differential Equations," *Canadian J. Math.*, 1954, vol. 6, no. 4.

6 Ascoli, "Sopra una particolare equazione differenziale del secondo ordine" (A Particular Second-Order Differential Equation), *Rend. Inst. Lombardo Sci. Lettere*, 1936, vol. 69, pp. 167–184.

7 Villari, G., "Un teorema di essistenza e di unitita per una classe di soluzioni del'equazione z″ + A(t)f(z) = 0" (An Existence and Uniqueness Theorem for a Class of Solutions to the Equation z″ + A(t)f(z) = 0), *Riv. Mat. Univ. Parma*, 1953, vol. 4, no. 4–5.

8 Hartman, P. and Winter, A., "On the Non-increasing Solutions of y″ = f(x,y,y′)," *Amer. J. Math.*, 1951, vol. 73, no. 2.

9 Villari, G., "Sul comportamento asintotico degli integrali di una classe di equazioni differenziali non-lineari" (Asymptotic Behavior of the Integrals of a Class of Nonlinear Differential Equations), *Riv. Mat. Univ. Parma*, 1954, vol. 5, no. 1–3.

10 Beklemisheva, L. A., "Asymptotic Behavior of the Solutions to Some Nonlinear Systems of Differential Equations," *Doklady Akad. Nauk SSSR* (Trans. Acad. Sci. USSR), 1956, vol. 111, no. 2.

# Sequential Regression Analysis and Its Application to Some Problems of Automatic Control

I. I. PERELMAN

THE REGRESSION analysis of mathematical statistics makes it possible to estimate the unknown parameters in a functional dependence on the basis of a set of experimental results concerning the quantities in this dependence.

In the past, the amount of computing involved in making a regression analysis meant that it was suitable only for cases of stationary functional dependence.

Owing to the development of high speed automatic computers, regression analysis is now being applied more widely. In this article we describe the method of sequential, i.e., continuously refined, regression analysis and consider some of its possible applications to problems of automatic control and regulation.

Consider the dependence of the random variable $Y$ with arguments $x_1, x_2, \ldots, x_k$ of the form

$$Y = f(x_1, x_2, \ldots, x_k) + \delta y \qquad [1]$$

where the function $f(x_1, x_2, \ldots, x_k)$ is defined and $\delta y$ is a random quantity with expectation zero. In other words, $f(x_1, x_2, \ldots, x_k)$ is the conditional mathematical expectation of $Y$

$$M(Y/x_1, x_2, \ldots, x_k) = f(x_1, x_2, \ldots, x_k) \qquad [2]$$

We can use Eq. 2, which is usually called the regression equation of $Y$ on $x_1, x_2, \ldots, x_k$, to approximate to the expected value of $Y$ corresponding to given values of $x_1, x_2, \ldots, x_k$. It is obvious that the relative accuracy of this estimate of $Y$ will depend on the relation between the standard deviation of $Y$ and $f^2(x_1, x_2, \ldots, x_k)$.

Further, taking $\delta y$ to be independent of $x_1, x_2, \ldots, x_k$, we shall consider the regression equation in the form

$$M(Y/x_1, x_2, \ldots, x_k) = f(x_1, x_2, \ldots, x_k) = \sum_{i=1}^{l} a_i \psi_i(x_1, x_2, \ldots, x_k) \qquad [3]$$

where the $\psi_i(x_1, x_2, \ldots, x_k)$ are given single valued functions, and the $a_i$ are constant coefficients, the regression parameters.

The regression analysis of the random variable $Y$ satisfying conditions 1 and 3 consists in finding estimates of the unknown coefficients $a_i$.

If the regression parameters $a_i$ are unknown, then their estimates $\alpha_i$ can be found on the basis of some number $n (n \geq l)$ of actual values of $Y$ given in the form of $n$ points in $(k+1)$-dimensional space: $y_j, x_{1j}, x_{2j}, \ldots, x_{kj} (j = 1, \ldots, n)$. The estimate of the $a_i$ is usually found by the method of least squares, which consists in finding the $\alpha_i$ which make the function $Q$

$$Q = \sum_{j=1}^{n} \left[ y_j - \sum_{i=1}^{l} \alpha_i \psi_i(x_{1j}, x_{2j}, \ldots, x_{kj}) \right]^2 \qquad [4]$$

a minimum.

It is easy to show (1)[1] that when $\delta y$ has a normal distribution the method of least squares gives the maximum likelihood estimates $\alpha_i$.

Equating the partial derivatives of $Q$ to zero, we have

$$-2 \sum_{j=1}^{n} \psi_{ij} \left( y_j - \sum_{i=1}^{l} \alpha_i \psi_{ij} \right) = 0 \qquad (i = 1 \ldots l) \qquad [5]$$

where

$$\psi_{ij} = \psi_i(x_{1j}, x_{2j}, \ldots, x_{kj})$$

From Eq. 5 we obtain a system of $l$ equations to determine the $\alpha_i$

$$\alpha_i \sum_{j=1}^{n} \psi^2_{1j} + \alpha_2 \sum_{j=1}^{n} \psi_{1j}\psi_{2j} + \ldots + \alpha_l \sum_{j=1}^{n} \psi_{1j}\psi_{lj} = \sum_{j=1}^{n} \psi_{1j} y_j$$

$$\alpha_1 \sum_{j=1}^{n} \psi_{2j}\psi_{1j} + \alpha_2 \sum_{j=1}^{n} \psi^2_{2j} + \ldots + \alpha_l \sum_{j=1}^{n} \psi_{2j}\psi_{lj} = \sum_{j=1}^{n} \psi_{2j} y_j$$

$$\ldots\ldots\ldots\ldots\ldots\ldots\ldots\ldots\ldots\ldots\ldots\ldots\ldots\ldots\ldots\ldots\ldots\ldots\ldots\ldots$$

$$\alpha_1 \sum_{j=1}^{n} \psi_{lj}\psi_{1j} + \alpha_2 \sum_{j=1}^{n} \psi_{lj}\psi_{2j} + \ldots + \alpha_l \sum_{j=1}^{n} \psi^2_{lj} = \sum_{j=1}^{n} \psi_{lj} y_j \qquad [6]$$

The determinant of this system is Gram's determinant, which is equal to the sum of the squares of the $l$th order minors of the matrix $A$ (2)

$$A = \begin{vmatrix} \psi_{11}, \psi_{21}, \ldots, \psi_{l1} \\ \psi_{12}, \psi_{22}, \ldots, \psi_{l2} \\ \ldots\ldots\ldots\ldots \\ \psi_{1n}, \psi_{2n}, \ldots, \psi_{ln} \end{vmatrix} \qquad [7]$$

when $l < n$.

It follows from this that system 6 gives a unique solution for $\alpha_i (i = 1, \ldots, l)$ if $A$ contains at least $l$ linearly independent rows. This is equivalent to the condition that there is at

Translated from *Izvestiia Akademii Nauk SSSR, Otdelenie Tekhnicheskikh Nauk, Energetika i Avtomatika* (*Bulletin of the Academy of Sciences USSR, Div. Tech. Sci., Power and Automation*), 1960, no. 2. Translated by Research Information Service, New York.

[1] Numbers in parentheses indicate References at end of paper.

least one point among the $n$ points of the $l$-dimensional space generated by the axes $\psi_1, \psi_2, \ldots, \psi_l$ which does not lie on the same hyperplane of the $(l-1)$th order as all the others.

## Sequential Regression Analysis

Consider the process $Y(t)$ which changes over time, and depends on the arguments $x_1(t), x_2(t), \ldots, x_k(t)$ and the parameters $p_1, p_2, \ldots, p_r$ and is of the form

$$Y(t) = f[z_1(t), z_2(t), \ldots, z_{mk}(t), p_1, p_2, \ldots, p_r] + \delta y(t) \quad [8]$$

where

$$\begin{aligned} z_1(t) &= x_1(t), z_2(t) = x_2(t), \ldots, z_k(t) = x_k(t) \\ z_{k+1}(t) &= x_1(t - \Delta t), z_{k+2}(t) = x_2(t - \Delta t), \ldots, \\ &\quad z_{2k}(t) = z_k(t - \Delta t) \\ &\ldots\ldots\ldots\ldots\ldots\ldots\ldots\ldots\ldots\ldots\ldots\ldots \\ z_{(m-1)k+1}(t) &= x_1[t - (m-1)\Delta t], z_{(m-1)k+2}(t) = x_2[t - \\ &\quad (m-1)\Delta t], \ldots, z_{mk}(t) = x_k[t - (m-1)\Delta t] \end{aligned}$$

$\Delta t$ is a given time interval; $\delta y(t)$ is a random function of time with zero expectation

$$f[z_1(t), z_2(t), \ldots, z_{mk}(t), p_1, p_2, \ldots, p_r] = \sum_{i=1}^{l} a_i(p_1, p_2, \ldots, p_r)\psi_i[z_1(t), z_2(t), \ldots, z_{mk}(t)] \quad [9]$$

where $\psi_i$ are given single valued functions, and $a_i(p_1, p_2, \ldots, p_r)$ are the regression coefficients of $Y(t)$ on $z_1(t), z_2(t), \ldots, z_{mk}(t)$, to be determined.

We note that any function

$$\varphi = \varphi[z_{10} + z_1(t), z_{20} + z_2(t), \ldots, z_{mk0} + z_{mk}(t)]$$

which can be represented in the neighborhood of the point $Z_0(z_{10}, z_{20}, \ldots, z_{mk0})$ by a finite number of terms of its Taylor series expansion, satisfies condition 9 in the neighborhood of this point. We must also note that, to the necessary degree of accuracy, relation 9 expresses the dependence between the output variable $f(t)$ and the input variables (disturbances) $x_i(t)$ $(i = 1, \ldots, k)$ in a dynamic nonlinear system without feedback consisting of a set of linear dynamic stages $W$ together with static (memoryless) nonlinear stages $F$, where the relation between the output of a given ($n$th) dynamic stage, $u_n(t)$, and the input signal of this stage, $v_n(t)$, is defined by the equation

$$u_n(t) = \int_{-\infty}^{t} h_n(t - \tau)v_n(\tau)d\tau \quad [10]$$

where $h_n(t - \tau)$ is a continuous function satisfying the condition

$$|h_n(t - \tau)| < Ae^{-a(t-\tau)} \quad [11]$$

$$a > 0 \qquad A > 0 \qquad 0 \leqslant (t - \tau) < \infty$$

and the relation between the output of a given ($m$th) nonlinear stage, $u_m(t)$, and its input signals $v_{mj}(t)$ $(j = 1, \ldots l_m)$ is defined by the equation

$$u_m(t) = F_m[v_{m1}(t), v_{m2}(t), \ldots, v_{ml_m}(t)] \quad [12]$$

Here $F_m$ is a single valued function which has a convergent Taylor series expansion in the neighborhood of any point lying in the region of possible values of the arguments. These statements will be proved in the Appendix.

Let the process $Y(t)$ satisfy conditions 8 and 9 at integral moments of relative time $\bar{t}(\bar{t} = 1,2, \ldots, m, \ldots, n-1, n)$ where $\bar{t} = t/\Delta t$, and $\Delta t$ is a given, sufficiently small time interval, and suppose that observations are made during the process, giving data about the $n - m + 1$ sets of values of $y(i), z_1(j), z_2(j), \ldots, z_{mk}(j)$. This is with the convention that knowing the functions $\psi_i[z_1(\bar{t}), z_2(\bar{t}), \ldots, z_{mk}(\bar{t})]$ is equivalent to knowing the $n - m + 1$ sets of quantities

$$y(j), \psi_i(j) \qquad (j = m \ldots n, i = 1 \ldots l)$$

where

$$\psi_i(j) = \psi_i[z_1(j), z_2(j), \ldots, z_{mk}(j)]$$

Using these latter quantities, the estimates of $a_i(p_1,p_2, \ldots, p_r) = \alpha_i$ can be found by solving a system of equations with $l$ unknowns analogous to system 6 (with $n - m + 1 > mk$). The $\alpha_i$ thus obtained can be used to give an estimate of the expected value of $y(n + 1)$ with the given $z_i(n + 1)$ $(i = 1, \ldots, mk)$.

It is obvious that for fixed $\Delta t$ the accuracy of these estimates increases as $n$ increases.

Before, we began from the assumption that the regression coefficients were constant. In real processes occurring in technical operations, the process parameters $(p_1, p_2, \ldots, p_r)$ are not strictly constant, but depend on changes in the surrounding conditions, on wear of the apparatus, and so on. Hence the coefficients $a_i(p_1, p_2, \ldots, p_r)$ should be thought of as functions of time. However, it is assumed in our division of the quantities affecting $Y(t)$ into arguments and parameters that the quantities $a_i(p_1, p_2, \ldots, p_r)$ have considerably less relative variation with time than have $\psi_i[z_1(t), z_2(t), \ldots, z_{mk}(t)]$.

Next, assuming that $a_i(i = 1, \ldots, l)$ vary with time, we consider the problem of obtaining estimates of the sequential value of $a_i$ for $\bar{t} = n$. The values of $y(j)$ $(j = m, \ldots, n)$ obtained at time $\bar{t} = n$ are in this case not of equal value for calculating the estimate of $a_i(n)$, and this must be taken into account in Eq. 4 by introducing an additional factor $g = g(n - j)$ into each of the terms of

$$Q = \sum_{j=m}^{n} g(n - j)\left[y(j) - \sum_{i=1}^{l} \alpha_i\psi_i(j)\right]^2 \quad [13]$$

The function $g(n - j)$, which we shall call the reliability function of the $j$th reading with respect to the moment $n$, must be defined beforehand on the basis of the known statistical properties of the process $Y(t)$ in such a way that the estimates obtained give the best fit. It is obvious that the reliability function can always be normalized so that $g(0) = 1$. Then $g(n - j) \leqslant 1$ for $(n - j) > 0$.

Both theoretical and practical difficulties arise in the determination of the reliability function. However, by taking into account the slow variation of $a_i$ over time, we can select a time interval $T = N\Delta t$ which is large enough from the point of view of the variation in $\psi_i$ during which $a_i$ can be taken as constant to an accuracy which is sufficient in practice.

With these conditions, $g(n - j)$ can be of the form

$$\begin{aligned} h(n - j) &= 1 \text{ for } j > n - N \\ h(n - j) &= 0 \text{ for } j \leqslant n - N \\ &\ldots\ldots\ldots\ldots\ldots\ldots\ldots\ldots\ldots\ldots\ldots\ldots [14] \end{aligned}$$

The system of equations giving the estimates of $a_i$ then reduces to the form

$$\begin{aligned} &\alpha_1 \sum_{j=n-(N-1)}^{n} \psi_1^2(j) + \alpha_2 \sum_{j=n-(N-1)}^{n} \psi_1(j)\psi_2(j) + \ldots + \\ &\qquad \alpha_l \sum_{j=n-(N-1)}^{n} \psi_1(j)\psi_l(j) = \sum_{j=n-(N-1)}^{n} \psi_1(j)y(j) \\ &\alpha_1 \sum_{j=n-(N-1)}^{n} \psi_2(j)\psi_1(j) + \alpha_2 \sum_{j=n-(N-1)}^{n} \psi_2^2(j) + \ldots + \\ &\qquad \alpha_l \sum_{j=n-(N-1)}^{n} \psi_2(j)\psi_l(j) = \sum_{j=n-(N-1)}^{n} \psi_2(j)y(j) \\ &\ldots\ldots\ldots\ldots\ldots\ldots\ldots\ldots\ldots\ldots\ldots\ldots\ldots\ldots\ldots\ldots \\ &\alpha_1 \sum_{j=n-(N-1)}^{n} \psi_l(j)\psi_1(j) + \alpha_2 \sum_{j=n-(N-1)}^{n} \psi_l(j)\psi_2(j) + \\ &\ldots + \alpha_l \sum_{j=n-(N-1)}^{n} \psi_l^2(j) = \sum_{j=n-(N-1)}^{n} \psi_l(j)y(j) \quad [15] \end{aligned}$$

When continuous tests of the process $Y(t)$ are made, i.e., as $\Delta t \to 0$, system 15 will be transformed in accordance with the relations

$$\lim_{\Delta t \to 0} \sum_{j=n-(N-1)}^{n} \psi_m(j)\,\psi_i(j) = \frac{1}{T}\int_{t-T}^{t} \psi_m(\theta)\psi_i(\theta)d\theta \quad (i, m = 1 \ldots l)$$

$$\lim_{\Delta t \to 0} \sum_{j=n-(N-1)}^{n} \psi_i(j)y(j) = \frac{1}{T}\int_{t-T}^{t} \psi_i(\theta)y(\theta)d\theta$$

.....[16]

The uniqueness condition for the solution of system 15 then means that the segment of the trajectory which the process describes in $l$-dimensional space $\psi$ over the time interval $t - T \leqslant \theta \leqslant t$ does not lie completely on a hyperplane of the $(l-1)$th order.

We note two particular cases of $Y(t)$.

1 For a linear dynamic system with one input variable $x(t)$, Eq. 9 reduces to the form

$$f(j) = \sum_{i=j-l}^{j} h(j-i)x(i) \qquad [17]$$

as a result of formula 6′ of the Appendix and using dimensionless time.

The unknown values of the weight function $h(0), h(1), \ldots, h(l)$ can be estimated from the results of a sufficiently large number $N(N \geqslant l)$ of observations of the process, using the solution of system 15, here of the form

$$h(0)\sum_{j=n-(N-1)}^{n} x^2(j) + h(1)\sum_{j=n-(N-1)}^{n} x(j)x(j-1) + \ldots + h(l)\sum_{j=n-(N-1)}^{n} x(j)x(j-l) = \sum_{j=n-(N-1)}^{n} x(j)y(j)$$

$$h(0)\sum_{j=n-(N-1)}^{n} x(j-1)x(j) + h(1)\sum_{j=n-(N-1)}^{n} x^2(j-1) + \ldots +$$

$$h(l)\sum_{j=n-(N-1)}^{n} x(j-1)x(j-l) = \sum_{j=n-(N-1)}^{n} x(j-1)y(j)$$

.....

$$h(0)\sum_{j=n-(N-1)}^{n} x(j-l)x(j) + h(1)\sum_{j=n-(N-1)}^{n} x(j-l)x(j-1) + \ldots +$$

$$h(l)\sum_{j=n-(N-1)}^{n} x^2(j-l) = \sum_{j=n-(N-1)}^{n} x(j-l)y(j) \qquad [18]$$

where $x(j-i) = 0$ when $(j-i) \leqslant 0$ $(i = 1, \ldots, l)$.

When $X(t)$ and $Y(t)$ are stationary random functions with zero expectation, as the number of observations $N$ increases we have

$$\lim \frac{1}{N}\sum_{j=n-(N-1)}^{n} x(j-i)x(j-m) = \varphi_{xx}(|i-m|) \quad (i, m = 1 \ldots l)$$

$$\lim \frac{1}{N}\sum_{j=n-(N-1)}^{n} y(j)x(j-i) = \varphi_{xy}(i)$$

.....[19]

for $n < N$ where $\varphi_{xx}$ is the autocorrelation function of $x(t)$ and $\varphi_{xy}$ is the correlation function of the random variables $X(t)$ and $Y(t)$.

Using 19, system 18 can then be transformed into a well-known form which is used in the experimental determination of the transfer function of a system during normal operation (3).

2 For a nonlinear static system with one input variable Eq. 9 reduces to the form

$$f(j) = \sum_{i=0}^{l} a_i[x(j)]^i$$

System 15, determining the estimates of the unknown $a_i$, becomes

$$\alpha_0 N + \alpha_1 \sum_{j=n-(N-1)}^{n} x(j) + \alpha_2 \sum_{j=n-(N-1)}^{n} x^2(j) + \ldots + \alpha_l \sum_{j=n-(N-1)}^{n} x^l(j) = \sum_{j=n-(N-1)}^{n} y(j)$$

$$\alpha_0 \sum_{j=n-(N-1)}^{n} x(j) + \alpha_1 \sum_{j=n-(N-1)}^{n} x^2(j) + \alpha_2 \sum_{j=n-(N-1)}^{n} x^3(j) + \ldots + \alpha_l \sum_{j=n-(N-1)}^{n} x^{l+1}(j) = \sum_{j=n-(N-1)}^{n} x(j)y(j)$$

.....

$$\alpha_0 \sum_{j=n-(N-1)}^{n} x^l(j) + \alpha_1 \sum_{j=n-(N-1)}^{n} x^{l+1}(j) + \alpha_2 \sum_{j=n-(N-1)}^{n} x^{l+2}(j) + \ldots + \alpha_l \sum_{j=n-(N-1)}^{n} x^{2l}(j) = \sum_{j=n-(N-1)}^{n} x^l(j)y(j)$$

[20]

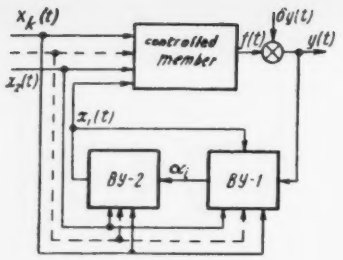


Fig. 1

Sequential regression analysis can be carried out with special, sufficiently fast, computing units, which receive at their input the data of successive experiments on the process being studied. These units must include memory blocks for storing the results of the last $N$ experiments as well as the functional transforms for calculating the given functions $\psi_i$, and a unit for solving the system of Eqs. 15. An analog computer is sufficient for problems involving one or two unknown coefficients, but in more complicated cases it is necessary to use digital electronic machines.

## Some Applications of Sequential Regression Analysis to Problems of Automatic Inspection and Control

Automatic sequential regression analysis can be used to solve a number of problems in the field of automatic control. We will not spend time on the obvious applications of this method to the study of object and process parameters, but shall consider some other problems.

### (a) Application to Control Systems With a Disturbance

Consider the control object $OP$ (Fig. 1), at whose input act the disturbances $x_1(t)$, $x_2(t)$, . . . , $x_k(t)$, causing the reaction $f(t)$. This reaction, together with the action $\delta y(t)$, means that there will be a disturbance of the output coordinate of the object $y(t)$. Let $x_1(t)$ be a corrective action, and let $x_i(t)$ $(i = 2, \ldots, k)$ be the disturbances to be measured. We are required to find a law for the corrective action $x_1(t)$ which stabilizes the output coordinate of the object $y(t)$ from the effect of the disturbances $x_i(t)$.

If the equation of the object is known and its parameters do not vary with time, this problem can only be solved when the corrective action $x_1(t)$ is a function of the disturbances $x_i(t)$ $(i = 2, \ldots, k)$. As we know (4), control as a function of disturbance can completely stabilize $y(t)$ from the effect of the disturbances $x_i(t)$, i.e., can make the reaction $f(t)$ identically equal to zero. Regulation in terms of disturbance has a special role in problems where the output coordinate of an object with a pure lag equal to $\tau$ has to be freed from variable disturbances with components whose period of change is less than $\tau$. The usual methods of control proportional to deviation have proved ineffective in solving problems of this type. However, an essential defect in systems of control by a disturbance is the absence of feedback control, which causes output errors when the parameters of the object or of the regulator change.

Because of this, it has been suggested (5,6) that for objects with large position lags, a combined regulation should be used, consisting of a control system as a function of disturbance, whose control parameters are corrected with the help of special computing units which receive information from both the input and the output ends of the process. In (7) a system operating according to this principle was developed for the control of a memoryless linear object with one measurable disturbance at the input.

Using the relations established previously, combined control can be applied, in the more general case, to the stabilization of $y(t)$ from the effect of disturbances $x_i(t)(i = 2, \ldots, k)$ in the control object, described by Eqs. 8 and 9. The control system in this case consists of two computing units, BY-1 and BY-2 (Fig. 1). BY-1, which receives the data of discrete or continuous readings of the quantities $y(t)$, $x_1(t)$, $x_2(t)$, . . . , $x_k(t)$ calculates the sequential estimates of the coefficients $a_i$ in Eq. 9 by solving the system of Eqs. 15. The results which are obtained by BY-1 are sent to BY-2, in which the equation $f(t) = 0$ is solved with respect to $x_1(t)$, and the necessary sequential value of $x_1(t)$ is determined and sent to the input of the object.

### (b) Application to Extremal Control

A similar method can be used to solve problems in extremal control. For in many such problems the dependence of the optimized function $y$ on the controlled arguments $x_1$, $x_2$, . . . , $x_k$ can be given theoretically in the form of an equation with unknown or slowly varying coefficients. If this dependence satisfies Eqs. 8 and 9, then computers BY-1 and BY-2 can be used to find the extremal value of $y$. In BY-1, just as in the previous case, is calculated the estimate of the sequential value of the coefficients $a_i$ in the equation of the process, and these quantities are sent to BY-2, in which are computed the values of $x_i(i = 1, \ldots, k)$ which will give $y$ an extremal value, using the process equations. When noise $\delta y$ is present, the estimates of the coefficients $a_i$ which have been calculated will vary within definite limits, thus making the value of $y$ deviate from its extremum. These deviations are used by the system as test steps.

### (c) Application to Automatic Inspection

In a number of problems in automatic inspection the exact value of the controlled quantity $x$ can be obtained only by special discrete control measurements, which may take a long time to obtain (for example, chemical analysis for each test). However, it is possible to obtain a continuous estimate of the sequential value of $x$ by means of approximate indirect methods which measure some other quantity $y$ which is connected with $x$ by the regression equation 9.

If the coefficients $a_i$ in this equation are known, then for any given measurement of $y$ the best estimate of the value of $x$ which corresponds to it can be found. If the regression coefficients change sufficiently slowly in comparison with the possible intervals between exact control measurements of $x$, then the estimates of $a_i$ can be found by using sequential regression analysis on the difference between the exact measurements of $x$ and the measurements of $y$ which correspond to them.

## Appendix

We wish to show that in a dynamic nonlinear system without feedback, consisting of stages which satisfy conditions 10 and 11, or condition 12, the dependence of the output quantity $f(t)$ on the disturbances $x_1(t)$, $x_2(t)$, . . . , $x_k(t)$ can be put in the form of Eq. 9 to the necessary accuracy.

Consider the system of Fig. 2, where the static (memory-

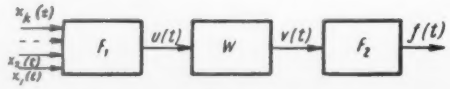


Fig. 2

less) nonlinear stages $F_1$ and $F_2$ are described by the equations

$$u(t) = F_1[x_1(t), x_2(t), \ldots, x_k(t)] \qquad [1']$$

$$f(t) = F_2[v(t)] \qquad [2']$$

and where $F_1$ and $F_2$ are single valued continuous functions which can be expanded in a convergent power series in the neighborhood of any point lying within the region of possible changes in their arguments.

The linear dynamic stage $W$ is described by the equation

$$v(t) = \int_{-\infty}^{t} u(t)h(t - \tau)d\tau \qquad [3']$$

where the pulse transfer function $h(t - \tau)$ is continuous and satisfies condition 11.

It is obvious that if the stage $W$ is stable, then condition 11 can always be satisfied by a suitable choice of the corresponding values of the quantities $A$ and $a$.

Expanding $F_1$ in the neighborhood of the point $x_1, x_2, \ldots, x_k = 0$ in a finite power series with enough terms for the required accuracy, we have

$$u(t) = a_0 + \sum_{i=1}^{J} a_i\varphi_i[x_1(t), x_2(t), \ldots, x_k(t)] \qquad [4']$$

where $a_0$ and $a_i$ are values of the function $F_1$ and its first and higher partial derivatives at the point $x_1, x_2, \ldots, x_k = 0$, and $\varphi_i[x_1(t), x_2(t), \ldots, x_k(t)]$ is the product of corresponding integral and zero powers of $x_1(t), x_2(t), \ldots, x_k(t)$.

It is easy to see that when condition 11 is satisfied and the functions $h(t - \tau)$ and $u(\tau)$ are continuous, the integral in Eq. 3′ can be replaced to the necessary degree of accuracy by the finite sum

$$v(t) = \sum_{m=0}^{M-1} h(m\Delta t)u(t - m\Delta t)\Delta t \qquad [5']$$

where the quantities $\Delta t$ and $M$ are chosen to give the necessary accuracy.

Transforming to relative time $\bar{t} = t/\Delta t$, when $\bar{t} = j$ we have

$$v(j) = \sum_{m=0}^{M-1} h(m)u(j - m) \qquad [6']$$

Putting Eq. 4′ in Eq. 6′, we obtain

$$v(j) = \sum_{m=0}^{M-1} h(m)\left\{a_0 + \sum_{i=1}^{J} a_i\varphi_i \times [z_1(j - m), z_2(j - m), \ldots, x_k(j - m)]\right\} \qquad [7']$$

Introducing the $Mk$ new variables $z_i(j)$ $(i = 1, \ldots, Mk)$

$$z_1(j) = x_1(j), z_2(j) = x_2(j), \ldots, z_k(j) = x_k(j)$$

$$z_{k+1}(j) = x_1(j - 1), \quad z_{k+2}(j) = x_2(j - 1), \ldots, z_{2k}(j) = x_k(j - 1)$$

. . . . . .

$$z_{(M-1)k+1}(j) = x_1[j - (M - 1)], z_{(M-1)k+2}(j) = x_2[j - (M - 1)], \ldots, z_{Mk}(j) = x_k[j - (M - 1)] \qquad [8']$$

and putting Eqs. 8′ in 7′, we have

$$v(j) = b_0 + \sum_{i=1}^{J} b_{1i}\varphi_i[z_1(j), z_2(j), \ldots, z_k(j)] + \sum_{i=1}^{J} b_{2i}\varphi_i[z_{k+1}(j), z_{k+2}(j), \ldots, z_{2k}(j)] + \ldots + \sum_{i=1}^{J} b_{Mi}\varphi_i[z_{(M-1)k+1}(j), z_{(M-1)k+2}(j), \ldots, z_{Mk}(j)] \qquad [9']$$

where

$$b_0 = \sum_{m=0}^{M-1} h(m)a_0$$

$$b_{mi} = h(m - 1)a_i \qquad (m = 1 \ldots M, i = 1 \ldots J)$$

Relation 9′ can be put in the form

$$v(j) = b_0 + \Delta v(j) \qquad [10']$$

where $\Delta v(j) = 0$ when $z_1(j), z_2(j), \ldots, z_{Mk}(j) = 0$.

Further, expanding $F_2$ in a power series in the neighborhood of the point $v = b_0$, and taking sufficient terms of the expansion to give the required accuracy, we obtain

$$y(j) = c_0 + \sum_{q=1}^{Q} c_q[\Delta v(j)]^q \qquad [11']$$

where $c_0$, $c_q$ are corresponding coefficients in the expansion. Putting the value of $\Delta v$ from relation 9′ into 11′ and simplifying, we find

$$y(j) = c_0 + \sum_{l=1}^{L} \alpha_l\psi_l[z_1(j), z_2(j), \ldots, z_{Mk}(j)] \qquad [12']$$

where $\psi_l$ is the product of corresponding integral and zero powers of $z_1(j), z_2(j), \ldots, z_{Mk}(j)$ and $\alpha_l$ is a polynomial in the coefficients $c_q$ and $b_{mi}$.

It is easy to see that Eqs. 4′, 9′ and 12′ correspond to condition 9. Moreover, the functions $\varphi_i$ and $\psi_i$ in Eqs. 4′, 9′ and 12′ are of the same nature; i.e., they are products of integral and zero powers of the input variables $z(j)$.

Thus we have seen that when a disturbance, described by Eq. 9, is supplied to the output of the stage $F$ or $W$, the reaction at the output of stage $F$ or $W$ can be expressed with an arbitrary accuracy in the form of Eq. 9. Quantities $\psi_i$ in Eq. 9 are finite products of zero and integral powers of the variables $x_1, \ldots, x_k$ corresponding to the given as well as to some previous discrete moments of time.

It is clear therefore that the reaction at the output of a nonlinear dynamic system without feedback, and consisting of a finite number of stages $F$ and $W$, which satisfy the conditions given, can be expressed arbitrarily accurately in the form of Eq. 9.

*—Submitted December 2, 1959*

## References


1 Dunin-Barkovsky, I. V. and Smirnov, N. V., *Teoriya veroyatnostyay i matematicheskaya statistika v tekhnikye* (*Theory of Probability and Mathematical Statistics in Technics*), Gostekhteorizdat, 1955.

2 Smirnov, V. I., *Kurs visshey matematiki* (*Course of Higher Mathematics*), vol. 3, 1, Gostekhteorizdat, 1954.

3 Goodman, T. P. and Reswick, J. B., "Determination of System Characteristics from Normal Operating Records," Trans. ASME, Feb. 1956.

4 Kulyebakin, V. S., "O primenimosti printsipa absolyutnoy invariantnosti v fizicheskikh realnikh sistemakh" (Application of the Principle of Absolute Invariance in Real Physical Systems), *Doklady Akad. Nauk SSSR*, 1948, vol. 10, no. 2.

5 Fossberg, K., "The Use of New Techniques in Automatic Mill Control," *Control Engineering*, Oct. 1955.

6 Feldbaum, A. A., "Primenyeniye vichislitelnikh ustroystv v avtomaticheskikh sistemakh" (Use of Computers in Automatic Systems), *Avtomatika i Telemekhanika* (*Automation and Remote Control*), 1958, no. 11.

7 Chelyutsky, A. B., "Primenyeniye vichislitelnoy tekhniki v prokatnom proizvodstvye" (Use of Computing Techniques in the Rolling Mill), *Bull. Central Sci. Res. Inst. of Ferrous Metallurgy*, 1958, no. 10, p. 342.

# Some Guidance Problems in Interplanetary Space

B. V. RAUSHENBACH
and E. N. TOKAR'

THIS article examines several problems related to the control of an interplanetary missile. By an interplanetary missile we mean an apparatus moving outside the limits of the atmosphere. This may be an artificial Earth satellite, a stage of a space rocket, etc. The control system for such a missile must permit it to change the motion of the center of mass of the missile and execute arbitrary rotations about the center of mass; it must also be possible to keep the axis of the missile in a given position.

To move the missile about the center of mass, Tsiolkovsky proposed two methods: Creation of a reactive force for which the line of action does *not* pass through the missile's center of mass, and the use of reactive flywheels. Control of the missile by means of reactive engines can be analyzed relatively simply. However, analysis of the control with the aid of reactive flywheels cannot.

For purposes of generalization, let us suppose that the number of stabilizing flywheels in the body of the missile is equal to $n$. Use of an arbitrary number of flywheels does not introduce any complications in writing the equations of motion. We will consider the positions of the flywheels and the orientations of their axes within the body of the missile as arbitrary, but fixed with respect to time; let us also suppose that the flywheels are statically and dynamically balanced upon their axes; in other words, their axes of rotation are the main central axes of inertia. This assumption is obviously correct for flywheels with axial symmetry.

## 1 Equations of Motion About the Center of Mass

In order to set up the equations of motion, we introduce two coordinate systems, taking as the general starting point for the calculations the point $O$, the center of mass of the material system consisting of the body of the missile and the reactive flywheels. In Fig. 1, $OX_0Y_0Z_0$ is the coordinate system whose axes always remain parallel to the axes of a certain inertial system; $OXYZ$ is the coordinate system which is rigidly fixed with respect to the body of the missile. The problem of orientation of the $OX$, $OY$ and $OZ$ axes within the body of the missile will be left open for now. The instantaneous angular velocity of system $OXYZ$ relative to system $OX_0Y_0Z_0$ will be designated by $\omega$; the projections of this angular velocity on the $OX$, $OY$ and $OZ$ axes will be designated respectively by $p$, $q$ and $r$.

Let positive directions along the axes of suspension of each of the flywheels be given; we will designate the orientation of the flywheel axes by the cosines of the angles formed by the positive directions of the flywheel axes with the positive directions of axes $OX$, $OY$ and $OZ$. Then for the $i$th flywheel, this direction cosine will be $a_{ix}$, $a_{iy}$ and $a_{iz}$. The angular velocity of the $i$th flywheel relative to the $OXYZ$ system will be designated as $\boldsymbol{\omega}_i$, and the projection of this vector on the axis of rotation of the flywheel by $\omega_i$. The projection of vector $\boldsymbol{\omega}_i$ on the $OX$, $OY$ and $OZ$ axes in the foregoing notation will be respectively $\omega_i a_{ix}$, $\omega_i a_{iy}$ and $\omega_i a_{iz}$.

The angular momentum of the material system under consideration in its relative motion about the center of mass reduced to the point $O$ will be

$$\mathbf{K} = \int_S [\mathbf{r} \times \mathbf{v}]dm$$

where

$\mathbf{v}$ = velocity of an element of mass $dm$ with respect to the $OX_0Y_0Z_0$ system
$\mathbf{r}$ = radius vector of the observed element of mass $dm$

Integration is carried out over the entire system S.

Let us represent the vector $\mathbf{K}$ as the sum of the angular momentum of the body of the missile and the angular momenta of the reactive flywheels. The angular momenta of the flywheels can be divided into the angular momenta arising from translational velocities of points on the flywheels in the $OX_0Y_0Z_0$ system and the angular momenta arising from the intrinsic rotational motions of the flywheels relative to the $OXYZ$ system

$$\mathbf{K} = \int_C [\mathbf{r} \times \mathbf{v}]dm + \sum_{i=1}^{n} \int_{M_i} [\mathbf{r} \times \mathbf{v}_{trans}]dm + \sum_{i=1}^{n} \int_{M_i} [\mathbf{r} \times \mathbf{v}_{rel}]dm$$

where in the first integral, integration is carried out over the body of the missile C, and in the other integrals it is carried out over the $i$th flywheel $M_i$.

The velocity of any point of the body $\mathbf{v}$ (including the translational velocity of every point of the flywheel $\mathbf{v}_{trans}$) is expressed by the angular velocity of the $OXYZ$ system in accordance with the Euler equation $\mathbf{v} = [\boldsymbol{\omega} \times \mathbf{r}]$. This makes it possible to group the first $n + 1$ addends

$$\int_C [\mathbf{r} \times \mathbf{v}]dm + \sum_{i=1}^{n} \int_{M_i} [\mathbf{r} \times \mathbf{v}_{trans}]dm = \int_S [\mathbf{r} \times (\boldsymbol{\omega} \times \mathbf{r})]dm$$

Consequently

$$\mathbf{K} = \int_S [\mathbf{r} \times (\boldsymbol{\omega} \times \mathbf{r})]dm + \sum_{i=1}^{n} \int_{M_i} [\mathbf{r} \times \mathbf{v}_{rel}]dm$$

Now let us examine the second term of the expression obtained.

As a result of the fact that the axes of suspension of the flywheels in the body of the missile coincide with their principal axes, the angular momenta of relative motion of the flywheels in the $OXYZ$ system—if we assume that they are

Translated from *Artificial Earth Satellites*, 1960, no. 5, pp. 41–53. Translated by Research Information Service, New York.

reduced to centers which are the centers of mass of the flywheels—will be $\omega_1 J_1, \omega_2 J_2, \ldots, \omega_n J_n$. Here $\omega_1, \omega_2, \ldots, \omega_n$ denote the angular velocities of the flywheels relative to the $OXYZ$ system, and $J_1, J_2, \ldots, J_n$ are their axial moments of inertia. Relative to the $OXYZ$ system, the velocities of the centers of mass of the flywheels are equal to zero (the flywheels are balanced on their axes of suspension within the body of the missile), which results in independence of the corresponding angular momenta from the centers to which they are reduced. Taking point $O$ as the general center of reduction for all the flywheels, we obtain

$$\int_{M_i} [\mathbf{r} \times \mathbf{v}_{rel}] dm = \boldsymbol{\omega}_i J_i$$

from which the expression for $\mathbf{K}$ will be

$$\mathbf{K} = \int_S [\mathbf{r} \times (\boldsymbol{\omega} \times \mathbf{r})] dm + \sum_{i=1}^{n} \boldsymbol{\omega}_i J_i \qquad [1]$$

By representing the angular momentum of the system in this form, we can select the orientation of the $OX$, $OY$ and $OZ$ axes in the body of the missile in such a way that the expression for the projection of the angular momentum on the axis of the $OXYZ$ system will appear in its simplest form. The determination of such a system of axes is important not only from the point of view of simplifying the writing of the equations of motion, but also from the point of view of improving the dynamics of the stabilized missile. Locating planes in which the signals from the sensitive elements of the stabilization system are produced parallel to the coordinate planes of the $OXYZ$ system, selected in the manner described, and situating the axes of the reactive flywheels parallel to the axes of the very same system, gives us the minimum cross coupling between oscillations of the missile about its three axes of stabilization.

It is easy to see that first term in Eq. 1 represents the angular momentum which a system would have if its flywheels were stopped, were fastened rigidly to the missile's body, and rotated with it as a single rigid unit. Let us choose $OX$, $OY$ and $OZ$ as the principal central axes of inertia for such a hypothetical body; and let the moments of inertia of this body about these axes be $A$, $B$ and $C$, respectively. The first term in Eq. 1 would then be written with maximum simplicity as

$$\int_S [\mathbf{r} \times (\boldsymbol{\omega} \times \mathbf{r})] dm = Ap\mathbf{e}_x + Bq\,\mathbf{e}_y + Cr\,\mathbf{e}_z$$

where $\mathbf{e}_x$, $\mathbf{e}_y$ and $\mathbf{e}_z$ are unit vectors along the $OX$, $OY$ and $OZ$ axes. Using the expression for the projection of vectors $\boldsymbol{\omega}_i$ on the axes of the $OXYZ$ system, we write the second term of Eq. 1 in the form

$$\sum_{i=1}^{n} \boldsymbol{\omega}_i J_i = \mathbf{e}_x \sum_{i=1}^{n} \omega_i a_{ix} J_i + \mathbf{e}_y \sum_{i=1}^{n} \omega_i a_{iy} J_i + \mathbf{e}_z \sum_{i=1}^{n} \omega_i a_{iz} J_i$$

Grouping according to unit vectors $\mathbf{e}_x$, $\mathbf{e}_y$ and $\mathbf{e}_z$, we finally obtain for $\mathbf{K}$

$$\mathbf{K} = \left(Ap + \sum_{i=1}^{n} \omega_i a_{ix} J_i\right) \mathbf{e}_x + \left(Bq + \sum_{i=1}^{n} \omega_i a_{iy} J_i\right) \mathbf{e}_y + \left(Cr + \sum_{i=1}^{n} \omega_i a_{iz} J_i\right) \mathbf{e}_z \qquad [2]$$

Let us apply the angular momentum theorem to the motion of the system with respect to its center of mass; since the center of mass of the system $O$ is taken as the point to which the angular momentum vector is reduced, we may write

$$d\mathbf{K}/dt = \mathbf{M} \qquad [3]$$

where

$d\mathbf{K}/dt$ = total derivative of the vector $\mathbf{K}$ with respect to time

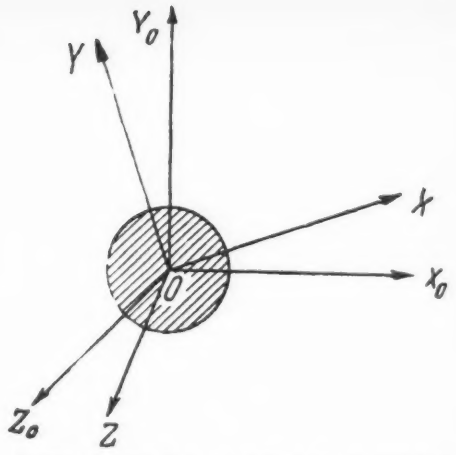


**Fig. 1 Mutual orientation of the missile and reference systems $OXYZ$ and $OX_0Y_0Z_0$**

$\mathbf{M}$ = sum of moments due to all external forces acting on the system

The external moments acting on the system are the moment of external perturbation $\mathbf{M}_{ex}$ acting on the missile and the control moment of the reaction engines $\mathbf{M}_r$ (for the case where reaction engines[1] are used as auxiliaries in conjunction with reactive flywheels for stabilization of the missile), and

$$\mathbf{M} = \mathbf{M}_{ex} + \mathbf{M}_r$$

Calculating the total derivative of vector $\mathbf{K}$ as the sum of the relative and translational velocities of the end of vector $\mathbf{K}$ in the $OXYZ$ system, we obtain

$$d\mathbf{K}/dt = \dot{K}_x \mathbf{e}_x + \dot{K}_y \mathbf{e}_y + \dot{K}_z \mathbf{e}_z + [\boldsymbol{\omega} \times \mathbf{K}]$$

Here, $\dot{K}_x$, $\dot{K}_y$ and $\dot{K}_z$ are derivatives with respect to time of the projection of vector $\mathbf{K}$ on the $OX$, $OY$ and $OZ$ axes

$$\dot{K}_x = A\dot{p} + \sum_{i=1}^{n} \dot{\omega}_i a_{ix} J_i$$

$$\dot{K}_y = B\dot{q} + \sum_{i=1}^{n} \dot{\omega}_i a_{iy} J_i$$

$$\dot{K}_z = C\dot{r} + \sum_{i=1}^{n} \dot{\omega}_i a_{iz} J_i$$

Equating the corresponding projection of the vectors $d\mathbf{K}/dt$ and $\mathbf{M}$ along the axes of the $OXYZ$ system, we obtain (we will omit summation subscripts 1 to $n$ from here on)

$$A\dot{p} + \sum \dot{\omega}_i a_{ix} J_i + q\left(Cr + \sum \omega_i a_{iz} J_i\right) - r\left(Bq + \sum \omega_i a_{iy} J_i\right) = M_{exx} + M_{rx}$$

$$B\dot{q} + \sum \dot{\omega}_i a_{iy} J_i + r\left(Ap + \sum \omega_i a_{ix} J_i\right) - p\left(Cr + \sum \omega_i a_{iz} J_i\right) = M_{exy} + M_{ry}$$

$$C\dot{r} + \sum \dot{\omega}_i a_{iz} J_i + p\left(Bq + \sum \omega_i a_{iy} J_i\right) - q\left(Ap + \sum \omega_i a_{ix} J_i\right) = M_{exz} + M_{rz}$$

[1] If the reaction engines are introduced into the problem, then the mass of the system and all its other inertial parameters—moments of inertia, principal inertial axes, etc.—ought to be considered as variables; however, the expenditure of mass necessary for the control of the missile's position about its center of mass is small, and the change in mass can be ignored in the calculations.

We then transform the system obtained as follows

$$A\dot{p} - \sum a_{ix}(a_{ix}\dot{p} + a_{iy}\dot{q} + a_{iz}\dot{r})J_i + \sum a_{ix}(\dot{\omega}_i + a_{ix}\dot{p} + a_{iy}\dot{q} + a_{iz}\dot{r}) + qr(C - B) = M_{exx} + M_{rx} - q\sum\omega_i a_{iz}J_i + r\sum\omega_i a_{iy}J_i$$

$$B\dot{q} - \sum a_{iy}(a_{ix}\dot{p} + a_{iy}\dot{q} + a_{iz}\dot{r})J_i + \sum a_{iy}(\dot{\omega}_i + a_{ix}\dot{p} + a_{iy}\dot{q} + a_{iz}\dot{r})J_i + rp(A - C) = M_{exy} + M_{ry} - r\sum\omega_i a_{ix}J_i + p\sum\omega_i a_{iz}J_i$$

$$C\dot{r} - \sum a_{iz}(a_{ix}\dot{p} + a_{iy}\dot{q} + a_{iz}\dot{r})J_i + \sum a_{iz}(\dot{\omega}_i + a_{ix}\dot{p} + a_{iy}\dot{q} + a_{iz}\dot{r})J_i + pq(B - A) = M_{exz} + M_{rz} - p\sum\omega_i a_{iy}J_i + q\sum\omega_i a_{ix}J_i \quad \ldots\ldots [4]$$

Let us clarify the meaning of the third terms in the left-hand portions of the foregoing equations. We will examine the motion of the $i$th wheel in the coordinate system whose axes are connected with the flywheel. As one of these axes, let us select the suspension axis of the wheel. Let the positive direction be the same as that defined earlier; the origin is taken at the center of mass of the wheel. Let us then arbitrarily locate the other two axes in the plane perpendicular to the first axis. Owing to the axial symmetry of the wheel, the moments of inertia about these two axes will be equal to each other. Let us designate them as $J_{ie}$ (the equatorial moment of inertia of the $i$th gyro).

Since the chosen system of axes represents a system of principal central axes of inertia with respect to the wheel in question, we are able to use the dynamic equations of Euler as the equations of motion.

The projection of the total angular velocity of the flywheel on the first coordinate axis (axis of suspension) is determined by the equation

$$p' = \omega_i + a_{ix}p + a_{iy}q + a_{iz}r$$

The projection of the total angular velocity of the flywheel on the other two coordinate axes will be designated as $q'$ and $r'$. In this notation, the first of the dynamic equations of Euler (the equation referring to the projections on the first coordinate axis) may be written as

$$J_i(\dot{\omega}_i + a_{ix}\dot{p} + a_{iy}\dot{q} + a_{iz}\dot{r}) = M'_i$$

Here $M'_i$ is the projection of the total moment applied to the flywheel along the positive direction of its axis. It is obvious that $M'_i$ is equal in absolute value to the axial moment at the shaft of the wheel and has a positive sign if the axial moment acting on the wheel forms a right-handed screw with the positive direction of the axis, or a negative sign if the axial moment acts in the opposite direction. The axial moment at the shaft of the wheel depends only on the active moment of the mechanism driving the wheel $M'_{ai}$ and on the frictional moment at the shaft of the gyro $M'_{ci}$

$$M'_i = M'_{ai} + M'_{ci}$$

Here $M'_{ai}$ and $M'_{ci}$ are algebraic quantities calculated exactly in the same way as the value for $M'_i$. Thus

$$J_i(\dot{\omega}_i + a_{ix}\dot{p} + a_{iy}\dot{q} + a_{iz}\dot{r}) = M'_{ai} + M'_{ci}$$

Multiplying this equation by $a_{ix}$ and summing with respect to $i$ from 1 to $n$, we obtain the expression for the third term in the first equation of system 4

$$\sum a_{ix}(\dot{\omega}_i + a_{ix}\dot{p} + a_{iy}\dot{q} + a_{iz}\dot{r})J_i = \sum a_{ix}(M'_{ai} + M'_{ci})$$

It is easy to obtain analogous expressions for the corresponding terms in the other two equations as well

$$\sum a_{iy}(\dot{\omega}_i + a_{ix}\dot{p} + a_{iy}\dot{q} + a_{iz}\dot{r})J_i = \sum a_{iy}(M'_{ai} + M'_{ci})$$

$$\sum a_{iz}(\dot{\omega}_i + a_{ix}\dot{p} + a_{iy}\dot{q} + a_{iz}\dot{r})J_i = \sum a_{iz}(M'_{ai} + M'_{ci})$$

Replacing the active moments and the frictional moments $M'_{ai}$ and $M'_{ci}$ applied to the shafts of corresponding wheels, by moments $M_{ai}$ and $M_{ci}$ directly opposing these and applied to the body of the missile, we obtain finally

$$A\dot{p} - \sum a_{ix}(a_{ix}\dot{p} + a_{iy}\dot{q} + a_{iz}\dot{r})J_i + qr(C - B) = M_{exx} + M_{rx} + \sum a_{ix}(M_{ai} + M_{ci}) - q\sum\omega_i a_{iz}J_i + r\sum\omega_i a_{iy}J_i$$

$$B\dot{q} - \sum a_{iy}(a_{ix}\dot{p} + a_{iy}\dot{q} + a_{iz}\dot{r})J_i + rp(A - C) = M_{exy} + M_{ry} + \sum a_{iy}(M_{ai} + M_{ci}) - r\sum\omega_i a_{ix}J_i + p\sum\omega_i a_{iz}J_i$$

$$C\dot{r} - \sum a_{iz}(a_{ix}\dot{p} + a_{iy}\dot{q} + a_{iz}\dot{r})J_i + pq(B - A) = M_{exz} + M_{rz} + \sum a_{iz}(M_{ai} + M_{ci}) - p\sum\omega_i a_{iy}J_i + q\sum\omega_i a_{ix}J_i \quad \ldots\ldots [5]$$

The last two terms in the right-hand sides of Eqs. 5 represent projections of the gyroscopic moments applied to the body of the missile and arising from the induced precession of the wheels in the missile. The terms $M_{rx}$, $\sum a_{ix}\ M_{ai}$ and so forth, represent projections of the control moments produced by the output members of the stabilization system; these moments depend on the angular coordinates of the missile and their derivatives, and may also be determined by a special control program for controlling the attitude of the missile or by guidance signals from Earth.

Let us now examine the case of stabilization of a missile with the aid of three reactive flywheels. We will assume that the rotational axes of the first, second and third flywheels are parallel to axes $OX$, $OY$ and $OZ$, respectively, of a connected system $OXYZ$, selected in the body of the missile in the manner described. The positive directions of the rotational axes coincide with the positive directions of the respective axes of the $OXYZ$ system. Then for the direction cosines we have

$$\begin{Vmatrix} a_{1x} & a_{1y} & a_{1z} \\ a_{2x} & a_{2y} & a_{2z} \\ a_{3x} & a_{3y} & a_{3z} \end{Vmatrix} = \begin{Vmatrix} 1 & 0 & 0 \\ 0 & 1 & 0 \\ 0 & 0 & 1 \end{Vmatrix}$$

Designating further

$$\begin{array}{lll} \omega_1 = \omega_x & \omega_2 = \omega_y & \omega_3 = \omega_z \\ M_{a1} = M_{ax} & M_{a2} = M_{ay} & M_{a3} = M_{az} \\ M_{c1} = M_{cx} & M_{c2} = M_{cy} & M_{c3} = M_{cz} \end{array}$$

and setting the axial moments of inertia of the wheels equal to each other ($J_1 = J_2 = J_3 = J$), we obtain the equations of motion for the stabilized missile in this case

$$(A - J)\dot{p} + (C - B)qr = M_{exx} + M_{rx} + M_{ax} + M_{cx} - \omega_z qJ + \omega_y rJ$$

$$(B - J)\dot{q} + (A - C)rp = M_{exy} + M_{ry} + M_{ay} + M_{cy} - \omega_x rJ + \omega_z pJ$$

$$(C - J)\dot{r} + (B - A)pq = M_{exz} + M_{rz} + M_{az} + M_{cz} - \omega_y pJ + \omega_x qJ \quad \ldots\ldots [6]$$

The equations obtained are similar to the ordinary dynamic equations of Euler for the body of a missile. In fact, the only difference between the left-hand portions of these equa-

tions and the left-hand portions of the Euler equations is the presence of the correcting factor $J$ in the first terms of the equations; by introducing the same corrections in the second terms of the equation in the following manner

$$(C - B)qr = [(C - J) - (B - J)]qr$$

and so forth, it would be easy to obtain complete similarity of the left-hand portions of Eqs. 6 with the left-hand portions of the Euler equations. The difference would consist only in that, instead of factors $A$, $B$ and $C$, we would everywhere encounter the differences $(A - J)$, $(B - J)$, $(C - J)$. The right-hand portions of Eqs. 6 are entirely similar to the right-hand portions of the Euler equations written for the body of the missile; they contain the projections of all moments which can be considered as external with respect to the body. In addition to moments $\mathbf{M}_{ex}$ and $\mathbf{M}_r$, such moments for the body of the missile would be, obviously, the active moments and frictional moments at the wheel shafts transmitted to the body, and also the gyroscopic moments of the wheels, the projections of which $\omega_y rJ$, $\omega_z qJ$ and so forth, are also contained in the right-hand portions of the derived equations.

However, the noted similarity is only superficial, and is a result of the circumstance that both the Euler equations and Eqs. 6 represent equations of motion of a system consisting of one or four rigid bodies, written with respect to a reference system in which the expressions for the projection of the angular momentum on the coordinate axes have maximum simplicity. One should not forget that, unlike in the case of the Euler equations, axes $OX$, $OY$ and $OZ$ (Eqs. 6 are written in terms of projections on these axes) are neither the principal nor the central axes of inertia of the missile's body, and that neither the factors $A$, $B$ and $C$ nor the differences $(A - J)$, $(B - J)$ and $(C - J)$ which appear in Eqs. 6 coincide with the moments of inertia of the missile's body about these axes.

## 2 Conclusions From the Law of Conservation of Angular Momentum

In order to refer the nonrotating system $OX_0Y_0Z_0$ to the system $OXYZ$ connected with the body of the missile, we will introduce three angles $\vartheta$, $\psi$ and $\varphi$ (Fig. 2).

We will designate angle $\vartheta$ as the angle between $OX'$—the projection of the axis $OX$ on the plane $X_0OY_0$—and axis $OX_0$. Angle $\psi$ is designated as the angle between axis $OY$ and the line of intersection between planes $X_0OY_0$ and $YOZ$. In the given instance, the following succession of rotations of the body of the missile holds during transition from a position where the systems $OXYZ$ and $OX_0Y_0Z_0$ coincide, to the given position of the system $OXYZ$. First, a rotation about axis $OZ_0$ through the angle $\vartheta$, then a rotation about the new position of axis $OY_0$ (see $OY'$ in Fig. 2) through the angle $\psi$, and then finally, a rotation through angle $\varphi$ about axis $OX$. The table shows the direction cosines for the axes connected with the missile and the nonrotating coordinate system.

Let us express the projections of the angular velocities of the body of the missile in terms of angles $\vartheta$, $\psi$ and $\varphi$

$$\begin{aligned} p &= \dot{\varphi} - \dot{\vartheta}\sin\psi \\ q &= \dot{\psi}\cos\varphi + \dot{\vartheta}\sin\varphi\cos\psi \\ r &= \dot{\vartheta}\cos\varphi\cos\psi - \dot{\psi}\sin\varphi \end{aligned} \qquad \ldots\ldots\ldots\ldots\ldots\ldots\ldots\ldots\ldots\ldots [7]$$

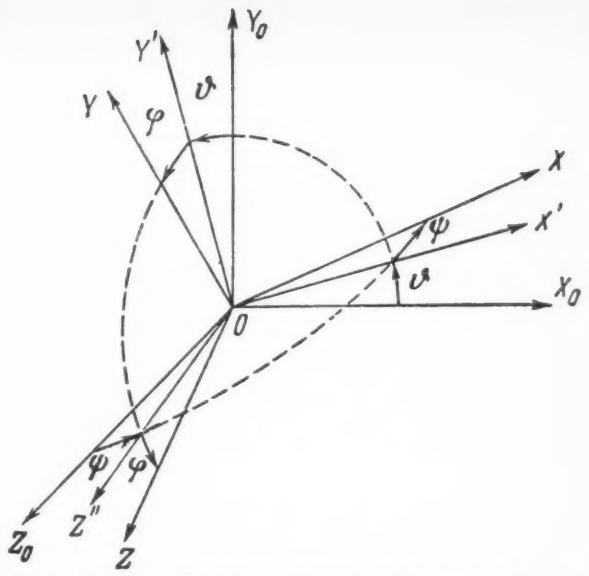


Fig. 2 Sequence of rotations through angles $\vartheta$, $\psi$ and $\varphi$ for transferring system $OX_0Y_0Z_0$ into $OXYZ$

The motion of the missile with respect to its center of mass is expressed by Eq. 3. If no external moments are applied to the missile ($\mathbf{M} = 0$), then from Eq. 3 we obtain an obvious consequence, which is known in mechanics as the law of conservation of angular momentum

$$\mathbf{K} = \mathbf{C}$$

where $\mathbf{C}$ is a constant vector.

Based on this law, we can draw a series of interesting conclusions, for the case of the problem of rotation of the missile about its center of mass.

Let the projections of vector $\mathbf{K}$ on the axis of a coordinate system which is nonrotating in inertial space, be $C_{x0}$, $C_{y0}$, $C_{z0}$. Then its projections in the $OXYZ$ system of coordinates are connected with $C_{x0}$, $C_{y0}$, $C_{z0}$ by the equations

$$\begin{aligned} C_{x0} &= K_x\cos\psi\cos\vartheta + K_y(\sin\varphi\sin\psi\cos\vartheta - \\ &\quad \cos\varphi\sin\vartheta) + K_z(\cos\varphi\sin\psi\cos\vartheta + \sin\varphi\sin\vartheta) \\ C_{y0} &= K_x\cos\psi\sin\vartheta + K_y(\sin\varphi\sin\psi\sin\vartheta + \\ &\quad \cos\varphi\cos\vartheta) + K_z(\cos\varphi\sin\psi\sin\vartheta - \sin\varphi\cos\vartheta) \\ C_{z0} &= -K_x\sin\psi + K_y\sin\varphi\cos\psi + K_z\cos\varphi\cos\psi \end{aligned} \qquad \ldots\ldots\ldots\ldots\ldots\ldots\ldots\ldots\ldots\ldots [8]$$

Moreover, the following obvious equation is true

$$C_{x0}^2 + C_{y0}^2 + C_{z0}^2 = K_x^2 + K_y^2 + K_z^2$$

Quantities $K_x$, $K_y$ and $K_z$ are easily obtained from Eqs. 2.

Let us examine the motion of the missile characterized by the fact that its control system, with the aid of flywheels, keeps a certain plane (connected with the missile) continuously parallel to a given plane in the inertial space. Without loss of generality, we can assume that axes $OX$ and $OY$ of the moving coordinate system lie in a given plane parallel to the

| Axes of the nonrotating system | Axes of the body system | | |
|---|---|---|---|
| | $X$ | $Y$ | $Z$ |
| $X_0$ | $\cos\psi\cdot\cos\vartheta$ | $-\cos\varphi\cdot\sin\vartheta + \sin\varphi\cdot\sin\psi\cdot\cos\vartheta$ | $\cos\varphi\cdot\sin\psi\cdot\cos\vartheta + \sin\varphi\cdot\sin\vartheta$ |
| $Y_0$ | $\cos\psi\cdot\sin\vartheta$ | $\cos\varphi\cdot\cos\vartheta + \sin\varphi\cdot\sin\psi\cdot\sin\vartheta$ | $\cos\varphi\cdot\sin\psi\cdot\sin\vartheta - \sin\varphi\cdot\cos\vartheta$ |
| $Z_0$ | $-\sin\psi$ | $\sin\varphi\cdot\cos\psi$ | $\cos\varphi\cdot\cos\psi$ |

plane $OX_0Y_0$. Then, in unperturbed motion, $\psi = \varphi = 0$, and Eqs. 8 take the form

$$C_{x0} = K_x \cos \vartheta - K_y \sin \vartheta$$
$$C_{y0} = K_x \sin \vartheta + K_y \cos \vartheta$$
$$C_{z0} = K_z$$
$$\ldots\ldots\ldots\ldots\ldots\ldots\ldots\ldots\ldots\ldots\ldots\ldots [9]$$

In Eqs. 9, angle $\vartheta$ may be a given function of time. For example, let the missile fly around some heavenly body along a plane orbit, and let it be required of the control system that the missile axis lying in the plane $XOY$ remain pointed constantly to the center of the heavenly body while plane $XOY$ itself be parallel to the plane of the orbit. Then, in one revolution, angle $\vartheta$ will change by $2\pi$, since the body of the missile will complete one revolution about axis $OZ$.

The first two equations of 9 show that under such conditions of motion about a heavenly body the quantities $K_x$ and $K_y$ as well as angle $\vartheta$ will be periodic functions of time.

It is easy to see that

$$K_x = C_{xy} \sin [\vartheta(t) + \theta]$$
$$K_y = C_{xy} \cos [\vartheta(t) + \theta]$$
$$\ldots\ldots\ldots\ldots\ldots\ldots\ldots\ldots\ldots\ldots\ldots\ldots [10]$$

where

$$C_{xy} = \sqrt{C_{x0}^2 + C_{y0}^2}$$
$$\theta = \arctan (C_{x0}/C_{y0})$$

In the unperturbed motion assumed here, angles $\psi = \varphi = 0$, and the angular velocities of the body of the missile, as can be seen from Eq. 7, will be

$$p = 0 \qquad q = 0 \qquad r = \dot{\vartheta}$$

In this case, as follows from Eq. 2, projections of the angular momentum $K_x$ and $K_y$ which differ from zero can be connected only with the rotation of flywheels which have attained certain angular velocities over a time period preceding the moment in question. In the given instance, this permits us to consider $K_x$ and $K_y$ projections of the angular momenta of the flywheels. Consequently, the rotational speed of the wheels whose axes are motionless with respect to the body of the missile, must, in general, vary periodically. In the simplest case, where the missile has three flywheels whose rotational axes are parallel to axes $OX$, $OY$ and $OZ$, those wheels whose axes are parallel to $OX$ and $OY$ will have a periodically varying rotational speed. Using the notation adopted previously for the case where the projection of the angular momentum of the body of the missile on the $OX$ and $OY$ axis is equal to zero, we obtain

$$K_x = \omega_x J_x \qquad K_y = \omega_y J_y \qquad [11]$$

where

$J_x, J_y$ = moments of inertia of wheels set parallel to axes $OX$ and $OY$, respectively
$\omega_x, \omega_y$ = their angular velocities

(subscripts $i$ and $\omega$ are omitted, since there is no possibility of confusion in this case).

From Eqs. 10 and 11 it follows that $\omega_x$ and $\omega_y$ are periodic functions of time. Over the time period of a single revolution of the missile about the central body, the angular velocity of each wheel attains a maximum value, drops to zero, changes its sign, and attaining in absolute magnitude the very same maximum value, again falls to zero and then returns to its initial value. This behavior of the wheels is understandable if we consider that for $r \neq 0$ the angular velocities of wheels $\omega_x$ and $\omega_y$ produce gyroscopic moments which differ from zero in the first two equations of 6; these moments can be eliminated by suitable acceleration or deceleration of the wheels. It appears, indeed, that damping of the gyroscopic moments is necessary for fulfillment of the requirements that $p = 0$ and $q = 0$.

It is important to note that these accelerations and decelerations, which are unavoidably connected with an expenditure of energy, are not at all necessary for orderly motion in orbit. In fact, if at the initial moment the projections of vector $\mathbf{K}$ on the plane of the orbit were equal to zero, i.e., $C_{x0} = C_{y0} = 0$, then, as can be seen from Eqs. 10 and 11, $\omega_x = \omega_y = 0$ during the entire time of motion in the given orbit. Thus, if one is aiming for a reduction in the expenditure of energy, then the reactive wheels whose axes lie in the plane of the orbit should be slowed down (for example, by employing moments created by reaction motors).

Such braking of the wheels is not always possible; for this reason let us examine more closely the problem of expenditure of energy on the periodic speeding up of wheels.

The kinetic energy of the wheels is expressed by the equations

$$\frac{1}{2} J_x \omega_x^2 = \frac{1}{2J_x} C_{xy}^2 \sin^2 [\vartheta(t) + \theta]$$

$$\frac{1}{2} J_y \omega_0^2 = \frac{1}{2J_y} C_{xy}^2 \cos^2 [\vartheta(t) + \theta]$$

Comparing these two equations term by term, it is easy to see that where $J_x \neq J_y$ the total kinetic energy of the wheels is a periodic function of time. Consequently, in the general case, part of the mechanical energy of the wheels must periodically be transformed into another form of energy (for example, electrical energy), which must then once again undergo transformation into rotational energy. It is to be noted, that even when $J_x = J_y$, the braking of one wheel and the simultaneous speedup of another is practically always convenient to achieve by means of the transformation of the kinetic energy of the braked wheel into another form of energy and the speedup of the second wheel by some motor which is set into motion as a result of the application of nonmechanical energy. Thus, in the general case, the operation of wheels is inescapably related to the transformation of energy, and this, in turn, means additional losses. We will now evaluate these losses.

Let the efficiency of transformation of mechanical energy into some other form of energy which can then be retransformed into mechanical energy be $\eta_1$, and the efficiency of retransformation be $\eta_2$. The quantity of mechanical energy transformed into the new form of energy when the wheel is braked completely will be equal to $(1/2J)\eta_1 C_{xy}^2$, and the irreversible losses of mechanical energy will be $(1/2J) \times (1 - \eta_1) C_{xy}^2$. Upon acceleration of the wheel, an expenditure of energy amounting to $(1/2J\eta_2) C_{xy}^2$ takes place, which exceeds the achieved kinetic energy by $(1/\eta_2 - 1)(1/2J) C_{xy}^2$. Thus, the total loss of energy over the time period from braking to acceleration of the wheel will be

$$\Delta E = \frac{1}{2J} \left( \frac{1}{\eta_2} - \eta_1 \right) C_{xy}^2$$

The equation obtained shows that for given $C_{xy}$, $\eta_1$ and $\eta_2$, it is possible to obtain a reduction in losses only by increasing the moment of inertia of the wheel.

An increase in $J$ is however connected with an increase in the dimensions or the mass of the wheel or a simultaneous increase in both. Let us therefore examine the problem of the optimum values of $J$ for two wheels, with the condition that the total mass of these wheels will be limited. The total loss of energy of both wheels over a single cycle of deceleration and acceleration will be

$$\Delta E = \frac{1}{2} \left( \frac{1}{J_x} + \frac{1}{J_y} \right) \left( \frac{1}{\eta_2} - \eta_1 \right) C_{xy}^2$$

In view of the given construction of the wheel, its mass $m$ can usually be approximated by an exponential function of its moment of inertia, $m = aJ^n$, where $a$ is a constant and $n > 0$. The condition that $n > 0$ is entirely natural, since with an increase in $J$ the mass of the wheel also increases.

The condition of constancy of the overall mass of the two wheels is expressed by the equation

$$J_x{}^n + J_y{}^n = b \qquad [12]$$

where $b$ is a constant.

Let us find the minimum $\Delta E$ satisfying the conditions of Eq. 12. Using the Lagrange method, we will seek an extremum of a function $Z$ of two variables $J_x$ and $J_y$

$$Z = \frac{1}{2}\left(\frac{1}{J_x} + \frac{1}{J_y}\right)\left(\frac{1}{\eta_2} - \eta_1\right) C_{xy}{}^2 + \lambda(J_x{}^n + J_y{}^n - b)$$

where $\lambda$ is the Lagrange multiplier. After elementary computations, we obtain the condition for an extremum $J_x = J_y$. It is easy to see that it is the condition for a minimum.

Thus, to reduce losses of energy in a control system, it is necessary, as far as possible, to brake the wheels, and if this is not possible, then to increase their moments of inertia. In so doing, it is necessary to select equal moments of inertia for wheels which interact during motion in orbit.

## 3 Example of Application of the Derived Equations to the Case of Small Deflections of the Missile From a Given Attitude

As an example, let us examine the case of stabilization of a missile about a given, unvarying position in space. Let the stabilization system be required to maintain the missile's position, and during this let coordinate system $OXYZ$ always coincide with a certain nonrotating coordinate system $OX_0Y_0Z_0$.

The mutual positions of systems $OXYZ$ and $OX_0Y_0Z_0$ will be characterized as before by the angles $\vartheta$, $\psi$, $\varphi$. As for the orientation of the wheel axes in the body of the missile and the magnitudes of their axial moments of inertia, we will make the same assumptions we made previously in deriving Eqs. 6. We will neglect the magnitude of the axial moment of inertia of the wheels $J$ relative to the moments of inertia $A$, $B$ and $C$. We will assume further that $\mathbf{M}_{ex} = \mathbf{M}_r = 0$ and will neglect the magnitudes of the gyroscopic moments and frictional moments relative to the magnitudes of the control moments $M_{ax}$, $M_{ay}$, $M_{az}$. We will limit ourselves to the case of small deviations of the missile from the given position. Eqs. 7 then are simplified

$$p = \dot{\varphi} \qquad q = \dot{\psi} \qquad r = \dot{\vartheta}$$

If we suppose further that the derivatives of the projections of the angular velocity $\dot{p}$, $\dot{q}$, $\dot{r}$ are of the same order of smallness as the projections $p$, $q$, $r$ themselves, then the second terms of the left-hand sides of Eqs. 6 can be eliminated, since they are small terms of higher orders, and the equations take the form

$$A\ddot{\varphi} = M_{ax} \qquad B\ddot{\psi} = M_{ay} \qquad C\ddot{\vartheta} = M_{az}$$

Let us suppose that the moment at the shaft of the reactive wheel mounted in the direction of axis $OX$ is a function of the angular velocity it develops, and, in addition, depends (through some control system) on angle $\varphi$ and its derivative $\dot{\varphi}$

$$M_{ax} = -M'_{ax}(\omega_x, \varphi, \dot{\varphi})$$

If we can write analogous expressions for $M_{ay}$ and $M_{az}$, we obtain

$$A\ddot{\varphi} = -M'_{ax}(\omega_x, \varphi, \dot{\varphi})$$
$$B\ddot{\psi} = -M'_{ay}(\omega_y, \psi, \dot{\psi})$$
$$C\ddot{\vartheta} = -M'_{az}(\omega_z, \vartheta, \dot{\vartheta})$$

From this it follows that the oscillations of the missile about axes $OX$, $OY$ and $OZ$ will become independent.

Let us consider the first of these equations in greater detail. We expand the function $M'_{ax}$ into a Taylor series near the point $(\omega_{x0}, 0, 0)$, corresponding to an unperturbed program. Retaining the first members of the expansion, we obtain

$$M'_{ax}(\omega_x, \varphi, \dot{\varphi}) = M'_{ax}(\omega_{x0}, 0, 0) + \frac{\partial M'_{ax}}{\partial \omega}\delta\omega_x + \frac{\partial M'_{ax}}{\partial \varphi}\varphi + \frac{\partial M'_{ax}}{\partial \dot{\varphi}}\dot{\varphi}$$

where the partial derivatives are evaluated at point $(\omega_{x0}, 0, 0)$. The motion of the missile in plane $YOZ$ will be described by the equation

$$A\ddot{\varphi} + \frac{\partial M'_{ax}}{\partial \dot{\varphi}}\dot{\varphi} + \frac{\partial M'_{ax}}{\partial \varphi}\varphi + \frac{\partial M'_{ax}}{\partial \omega}\delta\omega_x = M_{ax}(\omega_{x0}, 0, 0)$$

In order to eliminate $\delta\omega_x$, we use the first equation of 8. For the case of the small angles $\vartheta$, $\psi$, $\varphi$— neglecting terms of the first and higher orders of smallness—we obtain $C_{x0} = K_x$ or $C_{x0} = A\dot{\varphi} + J\omega_x$. Variation in the neighborhood of the point of interest yields

$$\delta\omega_x = -(A/J)\dot{\varphi}$$

Consequently, the final equation for motion of the missile in plane $YOZ$ will have the form

$$A\ddot{\varphi} + \left(\frac{\partial M'_{ax}}{\partial \dot{\varphi}} - \frac{A}{J}\frac{\partial M'_{ax}}{\partial \omega_x}\right)\dot{\varphi} + \frac{\partial M'_{ax}}{\partial \varphi}\varphi = M_{ax}(\omega_{x0}, 0, 0)$$

The term $M_{ax}(\omega_{x0}, 0, 0)$ on the right-hand side of the equation represents the forcing function determining the static error of the system

$$\varphi_{static} = \frac{M_{ax}(\omega_{x0}, 0, 0)}{\partial M'_{ax}/\partial \varphi}$$

It is interesting to note that the dependence of the moment $M_{ax}$ on the angular velocity of the wheel for $\partial M'_{ax}/\partial \varphi < 0$ facilitates damping of the disturbance. For a sufficiently strong dependence of the moment $M_{ax}$ on the angular velocity $\omega_x$, it is not necessary to introduce the derivative of the angle in the control program.

## Reviewer's Comment

The problem of controlling the orientation of a rocket in space is related to a more general problem in mechanics, i.e., the dynamics of rigid bodies. The usual problem in mechanics prescribes the external forces and constraints and requires a solution for the subsequent motion. In the present case, the objective is to specify the desired motion and then to determine the control forces and moments, so that the desired result is obtained. A very thorough survey of the past work on the dynamics of rigid bodies can be found in the book by Lemanis and Minorsky (1). In the case of a spinning body, the analysis of the control by reaction engines is not relatively simple. An analysis of this problem is contained in a recent note by Suddath (2). A detailed account of the attitude control problem for space vehicles can be found in a paper by Roberson (3). This article contains an extensive bibliography. An account of a NASA study of attitude control for space vehicles is also available (4).

—Bernard Paiewonsky
Aeronautical Research Associates of Princeton


1 Lemanis and Minorsky, N., *Dynamics and Non-Linear Mechanics, Surveys in Applied Mathematics, II*, John Wiley and Sons, Inc., N. Y., 1958.
2 Suddath, J. H., "A Theoretical Study of the Angular Motions of Spinning Bodies in Space," NASA TR R-83.
3 Roberson, R. E., "Attitude Control of Satellites and Space Vehicles," in *Advances in Space Science*, Vol. 2, Ordway, F. I., III, Ed., Academic Press, Inc., N. Y., 1960, pp. 351–436.
4 Gillespie, W., Jr., Eide, D. G. and Churgin, A. B., "Some Notes on Attitude Control of Earth Satellite Vehicles," NASA TN D-40.


# Aerodynamic Interaction in a Free Molecular Flow


**E. LARISH**

**Institute of Applied Mechanics**
**Rumanian Academy of Sciences**
**Bucharest**



MOLECULAR flow conditions are considered for bodies of any shape (not necessarily convex). The problem is found to be that of solving an integral equation, which in form is the same as one in the theory of illumination; the problem may be solved by means of photometric measurements. A solution is given for the interior of a spherical surface, and a use of the solution is discussed.


1. Molecular flow occurs when Knudsen's number $K = \lambda/l$ is large ($\lambda$ is the mean free path and $l$ is a characteristic length); $K \geq 2$ gives effective molecular flow. An isolated simple body having a convex surface at every point presents no problem if the law of molecular reflection is known; Patterson (1)[1] gives a detailed treatment, with references to the literature. It is usual to neglect the effects of reflected molecules on the incident flow (the incident particles are assumed to have an undisturbed Maxwellian velocity distribution). The problem becomes much more difficult if there are several bodies separated by distances comparable to their own dimensions or if the shape is locally concave. Here allowance must be made for repeated reflections, which give rise to interactions. The parameters of the incident flux are among the quantities to be calculated.

The laws of molecular reflection are important. Experiment [see (1), p. 168] shows that 95–98% of the incident molecules are reflected diffusely from ordinary polished surfaces. I shall neglect the few particles that show a correlation between the angles of incidence and reflection. The reflected molecules have a Boltzmann energy distribution whose temperature may be close to (but perhaps not equal to) the temperature of the surface.

2. The number of particles striking an element $d\sigma_P$ per unit time surrounding a point $P$ at a surface with an interior normal $\mathbf{v}_P$ is the sum of the number incident directly and of the number incident after reflection. The first component depends only on the direction of $\mathbf{v}_P$ and is

$$N_1(P)d\sigma_P = n\sqrt{\frac{RT}{2\pi}}\,[e^{-\beta^2} + \sqrt{\pi}\,\beta(1 + erf\beta)]d\sigma_P \qquad [2.1]$$

$$\left(\beta = \frac{v}{c}\,\mathbf{v}_P\right)$$

where

$\mathbf{v}$ = macroscopic speed
$n$ = density (in particles per cm$^3$)
$T$ = temperature of the flow
$R$ = gas constant

The second component is to be deduced by adopting the following device. The particles are reflected diffusely, so the flux originating at any surface is equivalent to a distribution of sources having a density $q$ (particles per cm$^3$). Lambert's


Translated from *Izvestiia Akademii Nauk SSSR, Otdelenie Tekhnicheskikh Nauk, Mekhanika i Mashinostroenie* (*Bulletin of the Academy of Sciences USSR, Div. Tech. Sci., Mechanics and Machine Construction*), 1960, no. 3, pp. 117–120. Translated by Research Information Service, New York.


[1] Numbers in parentheses indicate References at end of paper.

law is obeyed; the reflected molecules behave as though they come from some hypothetical gas on the far side of the surface. The number of impacts on the surface from particles whose directions of motion lie within a solid angle $d\Omega$ whose axis is inclined at an angle $\varphi$ to the normal is proportional to $\cos\varphi d\Omega$. Thus $[q\cos\varphi d\Omega d\sigma/\pi]$ of the particles reflected by the element $d\sigma$ enter that solid angle (Fig. 1). This second component is now to be found as

$$N_2(P)d\sigma_P = d\sigma_P \int_{S(P)} \frac{q(Q)\alpha_{PQ}\alpha_{PQ}}{\pi r_{PQ}^2}\, d\sigma_Q \qquad [2.2]$$

in which

$$\alpha_{PQ} = \frac{\mathbf{v}_P\cdot(\mathbf{r}_P - \mathbf{r}_Q)}{|\mathbf{r}_P - \mathbf{r}_Q|}$$

$$r_{PQ} = |\mathbf{r}_P - \mathbf{r}_Q|$$

The integral is taken over the part $S(P)$ of the surface that is visible from $P$ (Fig. 1).

The main difficulty lies in deducing the distribution of sources; the equation is easily derived from the condition of conservation for a small volume

$$q(P) = N_1(P) + N_2(P) = N_1(P) + \int_{S(P)} \frac{q(Q)\alpha_{PQ}\alpha_{QP}}{\pi r_{PQ}^2} \qquad [2.3]$$

which is a linear integral equation whose solution is essentially the solution to the whole problem.

The temperature of the body and the aerodynamic forces can be calculated if the distribution is known. I shall assume that the accommodation coefficient for the temperature is unity (normal values range from 0.9 to 1), so a reflected molecule has the temperature of the point from which it was reflected. Patterson (1) gives the contributions of the reflected molecules to the energy and momentum fluxes (pp. 159–178). By analogy with Eq. 2.2, the energy flux incident on $d\sigma_P$ is found as

$$d\sigma_P \int_{S(P)} \frac{e(T_Q)q(Q)\alpha_{PQ}\alpha_{QP}}{\pi r_{PQ}^2}\, d\sigma_Q \qquad [2.4]$$

where

$T_Q$ = surface temperature at point $Q$
$e(T)$ = mean molecular energy at temperature $T$

Each reflected molecule carries, on the average, energy $e(T)_P$, so the net energy reaching the body via $d\sigma_P$ is

$$\epsilon_2(P)d\sigma_P = d\sigma_P \int_{S(P)} \frac{[e(T_Q) - e(T_P)]q(Q)\alpha_{PQ}\alpha_{QP}}{\pi r_{PQ}^2}\, d\sigma_Q \qquad [2.5]$$

The incident flux of Eq. 2.1 brings in a momentum

$$d\sigma_P \int_{S(P)} \frac{i(T_Q)q(Q)\alpha_{PQ}\alpha_{QP}\,(\mathbf{r}_P - \mathbf{r}_Q)}{\pi r_{PQ}^3}\, d\sigma_Q \qquad [2.6]$$

in which $i(T)$ is the mean absolute momentum of a molecule at temperature $T$. The reflected molecules make a contribution

$$\tfrac{1}{2}i(T_P)N_2(P)\mathbf{v}_P \qquad [2.7]$$

because they are reflected diffusely. The additional momentum flux is then

$$\mathbf{i}_2(P)d\sigma_P = d\sigma_P \int_{S(P)} \frac{q(Q)\alpha_{PQ}\alpha_{QP}}{\pi r_{PQ}^2} \times \left[ i(T_Q)\frac{\mathbf{r}_P - \mathbf{r}_Q}{r_{PQ}} + \frac{i(T_P)}{2}\mathbf{v}_P \right] \qquad [2.8]$$

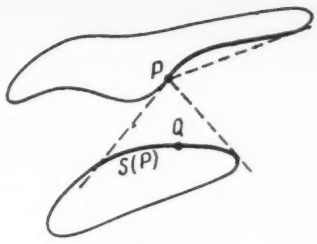


Fig. 1

which produces at $P$ an extra pressure $p_2$ and an extra tangential force $\boldsymbol{\tau}_2$, which are respectively

$$p_2(P) = \mathbf{i}_2(P)\cdot\mathbf{v}_P \qquad \boldsymbol{\tau}_2(P) = \mathbf{i}_2(P) - p_2(P)\mathbf{v}_P \qquad [2.9]$$

**3.** Eq. 2.3 has the same form as the equation describing the illumination in a space having non-absorbing walls which reflect in accordance with Lambert's law. Here the source density is the intensity of illumination produced by unit surface element, and the incident flux is that produced by the external sources. The analogy can be used to produce optical analogs in order to solve Eq. 2.3; the scale of the analog is without significance. Measurements are made of the intensity produced by external sources corresponding to $N_1$, which may be multiplied by any factor. Green's function for Eq. 2.3 can be reproduced in the usual way. The solution for large Mach numbers (Newtonian flow) is particularly easy to find, because the model need only be placed in a parallel beam of light.

It is difficult to solve Eq. 2.3 in general; some exact solutions are given in textbooks on light, but they are of little value here. The interaction between two bodies is governed by the ratio of the areas to the square of the separation; if that ratio is small, successive approximation methods give the result quickly.

**4.** Consider as an example the repeated reflection within a concave spherical surface of radius $R$; here part of the integrand takes the very simple form

$$\frac{\alpha_{PQ}\alpha_{QP}}{r_{PQ}^2} = \frac{1}{4R^2} \qquad [4.1]$$

The integrals may be simplified further if the Mach number is large; then

$$N_1(P) = n(\mathbf{v}\cdot\mathbf{v}_P) \qquad [4.2]$$

and the equation takes the form

$$q(P) = n(\mathbf{v}\cdot\mathbf{v}_P) + \frac{1}{4\pi R^2}\int q(Q)d\sigma_Q \qquad [4.3]$$

and has the solution

$$q(P) = n(\mathbf{v}\cdot\mathbf{v}_P) + \frac{nvS'}{4\pi R^2 - S} \qquad [4.4]$$

where

$S$ = area of the part of the spherical surface exposed to the flow
$S'$ = projection of that area on the flow direction. (It is supposed that the flow strikes the entire surface.)

We can use Eq. 4.4 to consider a spherical molecular flow diffuser, a device that may be of value for air intakes for use at high altitudes. The diffuser has the shape shown in Fig. 2.

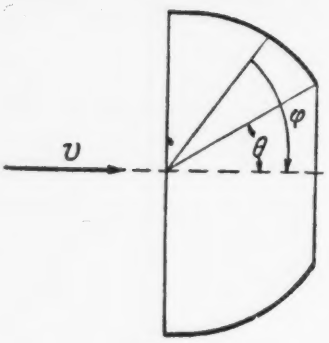


Fig. 2

We have

$$q(P) = nv\cos\varphi + \frac{nv\pi R^2(1 - \sin^2\theta)}{8\pi R^2 - 2\pi R^2\cos\theta} =$$

$$nv\left(\cos\varphi + \frac{\cos^2\theta}{4 - 2\cos\theta}\right) \quad [4.5]$$

and from the small hole there emerge

$$\pi R^2 nv\left[1 - \cos^2\theta + \frac{\cos^2\theta(1 - \cos\theta)}{2 - \cos\theta}\right] \quad [4.6]$$

molecules; then the emergent flux is increased by one half of the incident flux.

—*Received November 20, 1959*

### Reference

1 Patterson, G. N., "Molecular Flow of Gases," 1956.

---

### Reviewer's Comment

The author presents a theoretical analysis of free molecular flows with incident molecules coming from both the free stream and from diffuse reflection from a surface. Perhaps the most interesting part of the paper is the suggested use of the mathematical analogy between aerodynamic flow and illumination. This analogy permits solutions to aerodynamic problems to be obtained from measurements of light intensity. The 50% increase in exit momentum mentioned in Section 4 is obtained as $\theta$ approaches zero.

—Frank W. Barry
Hamilton Standard Div.
United Aircraft Corp.

---

# Luminosity of Matter Confined Within a Finite Volume and Having Arbitrary Absorption and Emission Bands

A. M. SAMSON

SECONDARY processes of absorption and emission which take place in volumes of finite dimensions influence the intensity, yield, shape of the lines, the duration, and other characteristics of the radiation emitted from the volume. It is very important to take this effect into account in astrophysics (1),[1] in the investigation of gas discharges, or in the studies of the luminescent properties of substances with strongly overlapping absorption and emission bands, etc. The following equation (2,3) underlies the investigation of the effect of secondary processes

$$\frac{dy}{d\tau} = -y + \gamma_0\int_{V'} y(\rho)K(|\rho - \rho_0|)dV' + \gamma_0 F(\rho_0, \tau) \quad [1]$$

$$K(\rho) = \frac{f(\rho)}{4\pi\rho^2} = \frac{1}{4\pi\rho^2}\int_{-\infty}^{+\infty}\frac{1}{\gamma_0}\epsilon(\omega)\gamma(\omega)b(\omega)e^{-b(\omega)\rho}d\omega \quad [2]$$

$$\tau_0 = \int_{-\infty}^{+\infty}\gamma(\omega)\epsilon(\omega)d\omega \quad [3]$$

Translated from *Akademiia Nauk BSSR, Doklady*, 1959, vol. 3, no. 12, pp. 479–483. Translated by A. Werner, New York.

[1] Numbers in parentheses indicate References at end of paper.

Here, $y$ is the ratio of density of emitted particles to the density of all particles; $\tau$ is the ratio of time $t$ to the duration of luminescence of the elementary volume $\tau_0$; $\omega$ is the frequency, expressed in terms of the half width of the emission band computed from its maximum [$\omega = (\nu - \nu_0)/\Delta\nu$]; $\gamma(\omega)$ denotes quantum yield of elementary volume; $\epsilon(\omega)$ and $b(\omega)$ the shapes of emission and absorption bands. Also

$$\int_{-\infty}^{+\infty} \epsilon(\omega)d\omega = 1 \qquad b(0) = 1 \qquad [4]$$

Volume $V'$ and radius vector $\rho$ are incorporated in Eq. 1 as dimensionless magnitudes: $\rho$, derivative of radius vector $r$ over absorption coefficient at the maximum of the emission band $k_0$; $V'$, derivative of volume $V$ over $k_0^3$ [total absorption coefficient equals $k_0 b(\omega)$]. Eq. 1 is written without taking the forced emission into account and is valid when the emission band is independent of the frequency of stimulating light.

The free term $\gamma_0 F(\rho, \tau)$ characterizes the possible particle densities at point $\rho$, stimulated without the participation of secondary absorption and emission processes. The analytical form of this term depends on the condition of stimulation.

Eq. 1 for a constant $\gamma(\omega)$ was formulated by Biberman (2). Agranovich (3) assumes the value of $\gamma(\omega)$ dependent on the frequency of stimulating light; however, applicability of Equation [1] is subject to the following restrictions:

1 The law of radiation damping of the elementary volume is identically exponential for all emission band frequencies.

2 The dependence of the quantum yield on the stimulating light frequency is determined by inactive absorption (extinction processes of the first kind), and consequently the duration of luminosity is not dependent on the spectrum composition of light.

Many solutions of a particular kind for Eq. 1 for the coincidence of frequencies of the emitted and absorbed quanta (resonant emission) are given in literature (1,4). Solution 1, in a general case, is extremely complicated owing to the existence of a frequency integral. An attempt is made in the present work to reduce Eq. 1 to a better known equation for resonant radiation.

As a rule, the total density of radiating particles $y(\rho)$ is of the same order of magnitude with the density, which is determined (4) by the magnitude of the free term $\gamma_0 F(\rho, \tau)$. Consequently, the error of solution caused by the approximate kernel, is of the same order of magnitude as the error of kernel.[2] Therefore, if it is possible to substitute the kernel of the integral Eq. 1 with a simpler kernel, incorporated in the integral equation for resonant radiation, the specified problem will be satisfied.

Comparison of Eq. 1 with the corresponding equation of the propagation of resonant radiation (4) shows that they differ only in the kernel, which in the latter case is of the form

$$K_{res}(\rho) = \frac{f_{res}(\rho)}{4\pi\rho^2} = \frac{1}{4\pi\rho^2} e^{-\rho} \qquad [5]$$

Comparison of Eq. 2 with Eq. 5 shows that the kernels differ by the value of $f(\rho)$. In the resonant case ($f_{res}$) has an exponential form. In the case of Eq. 2 it has the form of a sum (integral) of exponentials. Kernels $K$ and $K_{res}$ rapidly decrease with increasing argument $\rho$ and, consequently, solution of Eq. 1 is dependent essentially on the behavior of kernels only for small values of the argument [for sufficiently uniform $y(\rho)$]. This circumstance indicates that substitution of $f(\rho)$ with a simpler function $f_{res}$ must be such that they do not differ too much for small values of $\rho$.

Expanding $f(\rho)$ and $f_{res}(\rho)$ into series in steps of $\rho$, and adjusting the first terms of the expansion to each other, we have for $f(\rho)$ the approximate expression which incorporates only one constant $k_{eff}$

$$f(\rho) \approx f_1(\rho) = k_{eff} e^{-k_{eff}} \qquad [6]$$

where

$$k_{eff} = \int_{-\infty}^{+\infty} \frac{\gamma(\omega)}{\gamma_0} \epsilon(\omega) b(\omega) d\omega \qquad [7]$$

Magnitude $k_{eff}$ is the correction factor for the absorption coefficient. For $\epsilon(\omega) = \delta(\omega)$ or for $b(\omega) = 1$, $k_{eff}$ is equal to 1.

It is clear that Eq. 6 gives values close to the exact ones only for small values of the argument. It is possible to find the formula for $f(\rho)$ which gives a better approximation when two constants are introduced. Comparing the two first terms of the expansion $f(\rho)$ and $f_{res}(\rho)$, we have for $f(\rho)$ an expression which is determined with the aid of two constants

$$f(\rho) \approx f_2(\rho) = \alpha k'_{eff} e^{-k_{eff}} \qquad [8]$$

where

$$\alpha k'_{eff} = k_{eff} \qquad \alpha k'^2_{eff} = \int_{-\infty}^{+\infty} \frac{\gamma(\omega)}{\gamma_0} \epsilon(\omega) b^2(\omega) d\omega \qquad [9]$$

Here $k'_{eff}$ as before, is the correction factor for the absorption coefficient, $\alpha$ is the correction factor for the yield $\gamma_0$. As for $k_{eff}$, the magnitude of $k'_{eff}$ and $\alpha$ equal 1 when the emission band $\epsilon(\omega)$ is much narrower than the absorption band $b(\omega)$.

The foregoing expressions for the multiplicative factor $f(\rho)$ of the kernel of the integral equation give a good approximation to the exact values for small $\rho$. In order to evaluate the nature of the approximation for $\rho$, several concrete calculations for the following $\gamma(\omega)$, $\epsilon(\omega)$ and $b(\omega)$ were made

$$\frac{\gamma(\omega)}{\gamma_0} \epsilon(\omega) = \frac{1}{\sqrt{\pi}} e^{-\omega^2} \qquad b(\omega) = e^{\Delta^2 - (\omega - \Delta)^2} \qquad [10]$$

$$\frac{\gamma(\omega)}{\gamma_0} \epsilon(\omega) = \frac{1}{\pi} \frac{1}{1 + \omega^2} \qquad b(\omega) = \frac{1}{1 + \omega^2} \qquad [11]$$

Magnitude $\Delta$ in Eq. 10 characterizes (for constant $\gamma$) in half widths the distance between maxima of the emission and absorption bands. The values 0 and 0.5 have been selected for the calculation of $\Delta$. The calculated data are compiled in Table 1.

Exact values of $f(\rho)$ were calculated with the aid of quadrature formulas of the Gaussian type (5). If the absorption and emission bands have a dispersional form (Eq. 11) a simple equation is derived for $f(\rho)$

$$f(\rho) = \frac{1}{2} e^{\rho/2} \left[ I_0\left(\frac{\rho}{2}\right) - I_1\left(\frac{\rho}{2}\right) \right] \qquad [12]$$

where $I_0$ and $I_1$ are Bessel functions of the imaginary argument. The values $f(\rho)$ computed in accordance with this formula are also given in Table 1. This table shows that for $\rho < 1$, $f_1$ and $f_2$ only differ slightly from the exact values. The values $f_2(\rho)$, as expected, approximate $f(\rho)$ better than $f_1(\rho)$, even for $\rho > 1$, whereas $f_2(\rho) < f(\rho)$. For example, $f_2(\rho)$ is smaller than $f(\rho)$, on the average, for $\rho = 1.0$ by 1.5–4%; for $\rho = 1.5$ by 5–10%; for $\rho = 2.0$ by 10–20%. For the same $\rho$, the difference between $f_1(\rho)$ and $f(\rho)$ is greater, whereas for a rather considerable range of variation of $\rho$ (to $\rho = 3$–4), $f_1(\rho)$ is greater than $f(\rho)$.

As already pointed out, the kernel of the integral equation decreases considerably more rapidly than $f(\rho)$, and, consequently, the error in the value of the kernel for large values of the argument must not be strongly reflected in the solution of the equation.

In Fig. 1 is shown the behavior of the kernel of the integral equation for a plane parallel layer, when the shape of the absorption and emission bands are given by Eq. 10. The

[2] It can be shown that for a stationary system, if

$$\gamma_0 \int_{V'} \Delta K(|\rho - \rho_0|) y(\rho) dV' \ll \gamma_3 F$$

then $\Delta y \ll y$ ($\Delta K$ is the absolute error of kernel, $\Delta y$ the densities of radiating particles).

**Table 1**

| | Δ=0 | | | Δ=0.5 | | | Scattered from | | |
|---|---|---|---|---|---|---|---|---|---|
| ρ | $f(\rho)$ | $f_1(\rho)$ | $f_2(\rho)$ | $f(\rho)$ | $f_1(\rho)$ | $f_2(\rho)$ | $f(\rho)$ | $f_1(\rho)$ | $f_2(\rho)$ |
| 0.0 | 0.707 | 0.707 | 0.707 | 0.801 | 0.801 | 0.801 | 0.500 | 0.500 | 0.500 |
| 0.2 | 0.601 | 0.614 | 0.601 | 0.656 | 0.683 | 0.655 | 0.431 | 0.452 | 0.430 |
| 0.4 | 0.512 | 0.533 | 0.510 | 0.540 | 0.582 | 0.536 | 0.372 | 0.409 | 0.370 |
| 0.6 | 0.437 | 0.462 | 0.433 | 0.445 | 0.495 | 0.438 | 0.323 | 0.370 | 0.319 |
| 0.8 | 0.373 | 0.402 | 0.368 | 0.369 | 0.422 | 0.358 | 0.280 | 0.335 | 0.274 |
| 1.0 | 0.319 | 0.349 | 0.313 | 0.307 | 0.360 | 0.293 | 0.244 | 0 303 | 0 236 |
| 1.5 | 0.219 | 0.245 | 0.208 | 0.198 | 0.241 | 0.177 | 0.176 | 0.236 | 0.162 |
| 2.0 | 0.152 | 0.172 | 0.138 | 0.132 | 0.161 | 0.107 | 0.129 | 0.184 | 0.112 |
| 3.0 | 0.077 | 0.085 | 0.061 | 0.064 | 0.072 | 0.039 | 0.074 | 0.112 | 0.053 |
| 4.0 | 0.042 | 0.042 | 0.027 | 0.036 | 0.032 | 0.014 | 0.047 | 0.068 | 0.025 |

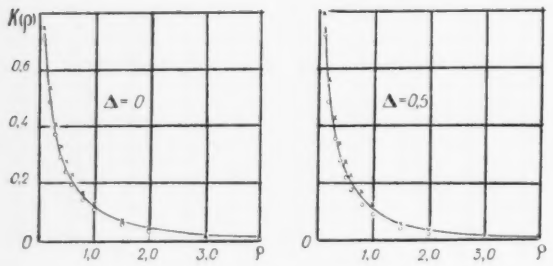


**Fig. 1**

solid curve corresponds to the kernel

$$K(\rho) = \frac{1}{2}\int_{-\infty}^{+\infty} \frac{\gamma(\omega)}{\gamma_0}\, \epsilon(\omega) b(\omega) E_1[b(\omega)\rho]\, d\omega \qquad [13]$$

The crosses and circles correspond to approximate values of kernels according to equations

$$\times \qquad K_1(\rho) = (1/2) k_{eff} E_1(k_{eff}\rho)$$

$$\circ \qquad K_2(\rho) = (\alpha k'_{eff}/2) E_1(k'_{eff}\rho)$$

where $E_1(\rho)$ is the integral exponential function.

The figure shows that the approximate values (crosses and circles) agree well with the exact curve. The agreement is better, the smaller the argument. Values $K_2(\rho)$, for example, in the interval of $\rho$ from 0 to 2, differ from the exact values by one or two units in the second decimal place. The values of $K(\rho)$ vary from $\infty$ to 0.04 in the same interval.

The problem, then, of determining the density of radiating particles of a substance with arbitrary absorption and emission bands confined in a volume of finite dimensions can be reduced to an identical problem for resonant radiation (coincidence of frequencies of emitted and absorbed quanta). Only the kernel of the corresponding integral equation is replaced with a kernel of the equation for resonant radiation by introducing two constants, dependent on the shape of the emission and absorption bands. In this case, inclusion of two constants (in accordance with formula 9) must give satisfactory results:

1 For comparatively small volumes (the optical thickness at the maximum of the emission band is of the order of magnitude of two to three units).

2 In the case when stimulation of particles is concentrated on a comparatively small portion of the volume.

If the stimulated particles are distributed more or less uniformly over a large volume, better results are probably obtained by introducing only one constant $k_{eff}$ determined by formula 11. This can be expected on the basis of the following representations. For small $\rho$, $f_1 < f$, $K_1 < K$; and for large $\rho$, conversely, $f_1 > f$, $K_1 > K$. Thus the error $\Delta K$ is such that the integral of $\Delta K$ over an infinitely large volume equals zero. For a uniform distribution of the density of radiating particles ($y$ = constant), the error $\Delta y$, dependent on such a kernel, is minimal. (See footnote 2.) This implies that in certain instances it is expedient to include $\alpha'$ contained within the following limits instead of magnitude $\alpha$

$$k_{eff} < \alpha' < 1 \qquad [14]$$

In conclusion, I should like to express my appreciation to B. I. Stepanov, Member of the Academy of Sciences BSSR, for his invaluable advice.

*—Submitted September 11, 1959*

## References

1 Sobolev, V. V., *Transfer of Radiant Energy in the Atmospheres of Stars and Planets*, GITTL, 1956.

2 Biberman, L. M., *Zh. Eksper. Teoret. Fiz. (Soviet Phys.-JETP)*, 1947, vol. 17, p. 416.

3 Agranovich, V. M., *Izvestiia Akad. Nauk SSSR, Seriia Fizika (Bull. Acad. Sci. USSR, Physics Series)*, 1959, vol. 23, p. 40.

4 Samson, A. M., *Vestsi Akad. Navuk BSSR, Seriia Tekh. Navuk (Bull. Acad. Sci. BSSR, Technical Sciences Series)*, 1959, no. 3.

5 Krylov, V. I., *Approximate Calculation of Integrals*, Fizmatgiz, Moscow, 1959.

## Reviewer's Comment

In this paper, it is shown that the problem of the secondary absorption and emission processes in a medium with arbitrary spectral bands confined in a finite volume may be reduced to an identical problem for resonance radiation. On replacing the kernel of the corresponding transport equation by the kernel of the diffusion equation of resonance radiation and introducing two constants which depend on the shape of the spectral bands, the transport integral equation appropriate to the numerical analysis is derived.

In what follows, it is of interest to mention some articles concerning the resonance radiation not cited here. Assuming that the escape of resonance quanta can be treated statistically as a decay of atoms in the excited state in a manner similar to that used in the diffusion process, Milne (6) first formulated and solved approximately the equation of transfer for the imprisoned resonance radiation.

Holstein (3,4), who presented a rigorous method for handling the imprisonment by means of the integral equation, investigated the rate of emission of the gases by determining the cessation of the optical excitation for a variety of spectral shapes in plane and cylindrical geometries. With the aid of the method of discrete ordinates, Chandrasekhar (1) and Edmonds (2) have obtained the solutions of the diffusion equation of imprisoned radiation in the first and the second approximations, respectively. Based on the integral method of Holstein, Walsh (8) has computed approximately the density and the imprisonment lifetime of resonance radiation in a gaseous discharge between parallel plates. The particular case with Doppler broadening was investigated.

With the aid of the diffusion treatment of resonance radiation based on the two-fluid theory, Little (5) showed that a linear dependence of the decay time on pressure is in good agreement with experiment in natural mercury, using the measured values of lifetimes and cross sections and assuming Doppler broadening. Recently, Veklenko (7) also treated the diffusion problem of the resonance radiation. Applying the Ambarzumian transform, i.e., the point-to-plane transform, to the transient transport equation for the resonance radiation, a one-dimensional integro-differential equation is obtained. With the aid of the Fourier transform, the source function is given. Then, using the inverse Fourier and Ambarzumian transforms provides a complete solution of the problem for an arbitrary shape of spectral lines.

—Sueo Ueno
Rand Corp.


1 Chandrasekhar, S., *Radiative Transfer*, Clarendon Press, Oxford, 1950.
2 Edmonds, F. N., Jr., *Phys. Rev.*, 1950, vol. 78, p. 424.
3 Holstein, T., *Phys. Rev.*, 1947, vol. 72, p. 1212.
4 Holstein, T., *Phys. Rev.*, 1951, vol. 83, p. 1159.
5 Little, P. F., in *Proc. Fourth Int. Conf. on Ionization Phenomena in Gases*, N. R., Nilsson, Ed., North Holland Pub. Co., 1959, p. 202–205.
6 Milne, E. A., Jr., *J. Math. Soc. London*, 1926, vol. 1, p. 40.
7 Veklenko, V. A., *Zh. Eksper. Teoret. Fiz.* (*Soviet Phys.—JETP*), 1959, vol. 36, p. 138.
8 Walsh, P. J., *Phys. Rev.*, 1957, vol. 107, p. 338.


# Magneto-Vortical Rings


YU. P. LADIKOV



A STUDY is made of the existence and stability of a steady-state plasma torus; the velocity vector $\mathbf{v}$ and the magnetic vector $\mathbf{H}$ are assumed to be collinear

$$\mathbf{H} = \gamma\mathbf{v} = \varkappa\sqrt{4\pi\rho}\,\mathbf{v}$$

in which $\varkappa$ is a scalar constant and $\rho$ is density. Shafranov (1)[1] has detected such formations, but he did not examine the solution in detail; he supposed that such a ring can be stable only if the velocity of the gas in the ring is larger than the corresponding Alfven speed ($v \geqslant H\sqrt{4\pi\rho}$), i.e., if $\varkappa \leqslant 1$. It is found here that such a ring can be stable for $\varkappa > 1$ subject to certain restrictions on the perturbations. Further, the pressure within the ring can exceed the external pressure very greatly, so the temperature can be high. Such a ring may be a model for ball lightning; some of the effects observed with such lightning (motion in closed spaces, magnetization of metal objects) might be explainable in terms of such a model (2).



Translated from *Izvestiia Akademii Nauk SSSR, Otdelenie Tekhnicheskikh Nauk, Mekhanika i Mashinostroenie* (*Bulletin of the Academy of Sciences USSR, Div. Tech. Sci., Mechanics and Machine Construction*), 1960, no. 4, pp. 7–13. Translated by Research Information Service, New York.


[1] Numbers in parentheses indicate References at end of paper.

The precise significance of the model is determined by the lifetimes of such rings and by the possibility of observing them.

### 1 Steady-State Motion of a Magneto-Vortical Ring

1 We assume that the interior of the ring is filled with an incompressible liquid having infinite conductivity. The azimuthally directed vortexes and currents cause the flow and the magnetic field in meridional planes. The equations of magnetohydrodynamics then become

$$(1 - \varkappa^2)(\operatorname{rot}\mathbf{v} \times \mathbf{v}) = -\operatorname{grad}\left(\frac{p}{\rho} + \frac{v^2}{2}\right)$$

$$\operatorname{div}\mathbf{v} = 0 \qquad \operatorname{rot}\mathbf{v} = \Omega \qquad [1.1]$$

which is integrable for the axially symmetric case (3) if $\Omega/r = f(\psi)$. This condition on the current function $\psi$ gives us an equation in polar coordinates $r$, $\theta$, $z$

$$\frac{\partial^2\psi}{\partial r^2} - \frac{1}{r}\frac{\partial\psi}{\partial r} + \frac{\partial^2\psi}{\partial z^2} = r^2 f(\psi) \qquad [1.2]$$

and for the surface of the torus

$$\psi = \text{constant} \qquad [1.3]$$

In what follows toroid coordinates $\xi$, $\theta$, $\eta$ shall be used which are related to $r$, $\theta$, $z$ by

$$r = \frac{a \sinh \eta}{\cosh \eta + \cos \xi} \qquad \theta = \theta \qquad z = \frac{a \sin \xi}{\cosh \eta + \cos \xi} \qquad [1.4]$$

The coordinate surfaces are then: For a torus

$$\eta = \text{constant} \qquad (r - a \coth \eta)^2 + z^2 = (a/\sin \eta)^2$$

for a sphere

$$\xi = \text{constant} \qquad (z - a \cot \xi)^2 + r^2 = (a/\sin \xi)^2$$

for a plane

$$\theta = \text{constant}$$

The square of a line element takes the form

$$ds^2 = [a^2/(\cosh \eta + \cos \xi)^2] \times (d\xi^2 + \sinh^2 \eta \, d\theta^2 + d\eta^2) \qquad [1.5]$$

The radius $c$ of the cross section is small relative to $a$, the radius of the ring (Fig. 1); then the $\eta$ for points near the surface on both sides are very large, so $\chi = \exp(-\eta)$ is very small.

Hicks (4) has solved Eq. 1.2 subject to Eq. 1.3 and $c/a \ll 1$ on the assumption that $f(\psi) = M = \text{constant}$; the approximate form is

$$\psi = \frac{1}{b^2}\left[\frac{Q}{8} + B + Q\chi^2 - \frac{9}{2} Q\chi^2 \cos \xi + \ldots\right] \qquad [1.6]$$

$$(Q = -\Gamma a/4\pi)$$

where

$\Gamma$ = velocity circulation in the external flow
$B$ = constant

The cross section is not assumed to be an exact circle; the equation of the bounding surface is assumed to be

$$\chi = b\left(1 + \sum_{n=1}^{\infty} \beta_n \cos n\xi\right) \qquad [1.7]$$

The condition $\psi = \text{constant}$ gives us that $\beta_1 = 9b/4$; the other $\beta_n$ are smaller quantities. The projections of the velocity are related to the current function by

$$v_\xi = -\frac{\vartheta}{r}\frac{\partial \psi}{\partial \eta} \qquad v_\eta = -\frac{\vartheta}{r}\frac{\partial \psi}{\partial \xi}$$

$$\vartheta^2 = \left(\frac{\partial \xi}{\partial r}\right)^2 + \left(\frac{\partial \xi}{\partial z}\right)^2$$

so

$$v_\xi = -\frac{Q\chi}{a^2b^2} + \frac{11}{4}\frac{Q}{a^2b^2}\chi^2 \cos \xi + \ldots$$

$$v_\eta = \frac{9}{4}\frac{Q}{a^2b^2}\chi^2 \sin \xi, \ldots$$

$$|\mathbf{v}| = \frac{Q}{2a^2b^2}\left(2\chi - \frac{11}{2}\chi^2 \cos \xi\right)$$

$$\ldots\ldots\ldots\ldots\ldots\ldots\ldots\ldots\ldots\ldots\ldots\ldots\ldots\ldots\ldots\ldots\ldots\ldots [1.8]$$

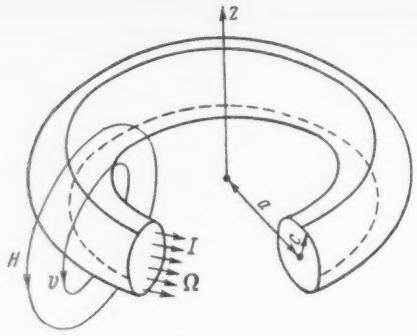


Fig. 1

Now $\mathbf{H} = \varkappa(4\pi\rho)^{1/2}\mathbf{v}$, so

$$H_\xi = -\frac{\varkappa\sqrt{4\pi\rho}Q}{2a^2b^2}\left(2\chi - \frac{11}{2}\chi^2 \cos \xi\right)$$

$$H_\eta = \frac{9}{4}\varkappa\sqrt{4\pi\rho}\,\frac{Q}{a^2b^2}\chi^2 \sin \xi$$

$$|\mathbf{H}| = \frac{\varkappa\sqrt{4\pi\rho}Q}{2a^2b^2}\left(2\chi - \frac{11}{2}\chi^2 \cos \xi\right)$$

$$\ldots\ldots\ldots\ldots\ldots\ldots\ldots\ldots\ldots\ldots\ldots\ldots\ldots\ldots\ldots\ldots\ldots\ldots [1.9]$$

The integral of Eq. 1.1 is

$$\frac{p}{\rho} = c - (v^2/2) + M(1 - \varkappa^2)\psi(\xi, \eta) \qquad [1.10]$$

and $M$ is related to $\Gamma$ by

$$\Gamma = \int_L v ds = \iint \Omega d\sigma = -4\pi M a^3 b^2$$

$$M = -\frac{\Gamma}{4\pi a^3 b^2} = \frac{Q}{a^4 b^2}$$

Substituting into Eq. 1.10, we have

$$\frac{p}{\rho} = \frac{p_0}{\rho} + \frac{u^2}{2b^2}\left(\chi^2 - \frac{7}{2}\chi^3 \cos \xi\right) - \frac{\varkappa^2 u^2}{b^2}\left(\chi^2 - \frac{9}{2}\chi^2 \cos \xi\right) \qquad [1.11]$$

where

$u$ = $Q/a^2b$ is the principal value of the velocity at the surface of the ring
$p_0$ = pressure at the central line for $\chi = 0$

The total pressure at the surface is

$$p + \frac{H^2}{8\pi} = p_0 + (1 - \varkappa^2)\frac{\rho u^2}{2}(1 + b \cos \xi) \qquad [1.12]$$

2 We assign to the whole mass of fluid a velocity $V$, and consider the external flow about a torus having at infinity a velocity $V$ and a given $\Gamma$ at the surface of the ring. A magnetic field (caused by the current in the ring) exists in the external space, but this field is not related to the motion of the medium.

Hick's solution for this $V$ and $\Gamma$ takes the following approximate form for points near the ring

$$\psi = -\frac{1}{2}Va^2(1 - 4\chi\cos\xi) + (1 - \chi\cos\xi)\left\{Q\left[\frac{1}{2}\left(\ln\frac{4}{\chi} - 2\right) + \frac{1}{8}\chi^2\left(\ln\frac{4}{\chi} + 1\right)\right] - \frac{b}{\chi}\left[4Qb\left(\ln\frac{4}{b} - \frac{1}{4}\right) - 4Va^2b\right]\left[\frac{1}{2} - \frac{3}{4}\chi^2\left(\ln\frac{4}{b} - \frac{1}{2}\right)\right]\cos\xi\right\} \quad [1.13]$$

so

$$v_\xi = -\frac{Q}{a^2\chi}\left\{1 - \frac{\chi}{2Q}\left[4Va^2 - 4Q\left(\ln\frac{4}{\chi} - \frac{1}{2}\right)\right]\cos\xi\right\}$$

$$v_\eta = -\frac{1}{2a^2}\left[2Va^2 + 2Q\left(\ln\frac{4}{\chi} - 2\right)\right]\sin\xi$$

$$|\mathbf{v}| = \frac{Q}{a^2\chi}\left\{1 - \frac{\chi}{2Q}\left[4Va^2 - 4Q\left(\ln\frac{4}{\chi} - \frac{1}{2}\right)\right]\cos\xi\right\} \quad [1.14]$$

The external magnetic field satisfies the same equations and boundary conditions, so, putting $V = 0$ and $\Gamma = 4\pi I$ (in which $I$ is current) in Eq. 1.14, we have

$$H_\xi = -\frac{\varkappa\sqrt{4\pi\rho}Q}{a^2\chi}\left\{1 + \frac{\chi}{Q}\left[4Q\left(\ln\frac{4}{\chi} - \frac{1}{2}\right)\right]\cos\xi\right\}$$

$$H_\eta = -\frac{\varkappa\sqrt{4\pi\rho}}{2a^2}2Q\left(\ln\frac{4}{\chi} - 2\right)\sin\xi$$

$$|\mathbf{H}| = \frac{\varkappa\sqrt{4\pi\rho}}{a^2\chi}Q\left[1 + 4\chi\left(\ln\frac{4}{\chi} - \frac{1}{2}\right)\cos\xi\right] \quad [1.15]$$

For $\chi = b[1 + (9b/4)\cos\xi]$ the total external pressure on the ring is

$$p + \frac{H^2}{8\pi} = p_\infty - \rho_1\frac{u^2}{2}\left\{1 - \frac{b}{Q}\left[4Va^2 - 4Q\left(\ln\frac{4}{b} - \frac{1}{2}\right)\right]\cos\xi\right\} + \frac{\rho\varkappa^2u^2}{2}\left[1 + 4b\left(\ln\frac{4}{b} - \frac{1}{2}\right)\cos\xi\right] \quad [1.16]$$

The normal components of the field and velocity are zero at the surface of the ring, so we have the condition

$$\{p + H^2/8\pi\} = 0 \quad [1.17]$$

(Here and in what follows $\{A\}$ denotes the difference in the values of $A$ across the surface of discontinuity.) The coefficients to $\cos n\xi$ ($n = 0, 1$) in Eqs. 1.12 and 1.16 give us

$$p_0 = p_\infty - (\rho_1 + \rho)\frac{u^2}{2} + \rho\varkappa^2u_2 = p_\infty - (\rho_1 + \rho)\frac{u^2}{2} + \frac{I^2}{4\pi a^2b^2}$$

$$V = ub\left[\left(1 - \varkappa^2\frac{\rho}{\rho_1}\right)\ln\frac{4}{b} + \frac{1}{4}\frac{\rho}{\rho_1}(1 + \varkappa^2 - \frac{1}{2}\right]$$

$$V = ub\left[\left(1 - \frac{\varkappa^2}{\nu}\right)\ln\frac{8a}{c} + \frac{1 + \varkappa^2}{4\nu} - \frac{1}{2}\right] \quad [1.18]$$

where

$u$ = speed of the circulation at the surface
$c \approx 2ab$ = mean radius of the cross section
$\nu = \rho_1/\rho$, ratio of the densities

for $\rho_1 = \rho$ we have

$$p_0 = p_\infty - \rho u^2(1 - \varkappa^2)$$

$$V = ub\left(\ln\frac{8a}{c} - \frac{1}{4}\right)(1 - \varkappa^2) \quad [1.19]$$

The first formulas in Eqs. 1.18 and 1.19 show that large pressures (and temperatures) can occur with the ring if the magnetic energy exceeds the kinetic energy. The ring will move in a sense opposed to the sense of the circulation at points lying on the axis of symmetry (an incident flow will compress the ring). In the converse case, the ring can be a region of reduced pressure, in which case it will move in the other sense. The ring will not move ($V$ will be zero) if

$$\varkappa = \left(\frac{\ln\frac{4}{b} - \frac{1}{2} + \frac{1}{4}\frac{\rho}{\rho_1}}{\frac{\rho}{\rho_1}\left(\ln\frac{4}{b} - \frac{1}{4}\right)}\right)^{1/2} \approx \sqrt{\frac{\rho_1}{\rho}}$$

Then the pressure at the center is

$$p_0 = p_\infty + (\rho_1 - \rho)(u^2/2)$$

and will exceed the pressure at infinity if $\rho_1 > \rho$.

## 2 Stability

The foregoing analysis shows that any change in the parameters not accompanied by a change in the ring shape will produce only a change in the speed of the forward motion; it will not produce instability. Therefore we shall examine perturbations to the surface, whose equation in the unperturbed state is

$$\chi = b(1 + \tfrac{9}{4}b\cos\xi) \quad [2.1]$$

As Basset (4), who examined the out-of-plane oscillations of a vortex ring, we shall assume that any perturbation is of the second order of smallness relative to $b = c/2a$, i.e., that the equation for the perturbed state is

$$\chi = b[1 + \beta\exp i(m\xi + n\theta + \sigma t)] \quad [2.2]$$

in which $\beta$ is of the order of $b$. This is equivalent to the assumption that the unperturbed cross section is the perfect circle

$$\chi = \exp(-\eta) = b \qquad \eta = \text{constant} \quad [2.3]$$

Then the unperturbed velocity, field and pressure are: In the internal region

$$v_\xi^\circ = -u\frac{\chi}{b} = -\frac{Q\chi}{a^2b^2} \qquad v_\eta^\circ = v_\theta^\circ = H_\eta^\circ = H_\vartheta^\circ = 0$$

$$H_\xi = -\gamma u\frac{\chi}{b} \qquad p^\circ = p_0 + \rho\frac{u^2}{2}\frac{\chi^2}{b^2} - \rho\varkappa^2\frac{\chi^2}{b^2}u^2 \quad [2.4]$$

in the external region

$$v_\xi^\circ = -u(b/\chi) \qquad v_\eta^\circ = v_\theta^\circ = H_\eta^\circ = H_\theta^\circ = 0$$

$$H_\xi^\circ = -\gamma u \frac{b}{\chi} \qquad p^\circ = p_\infty - \rho_1 \frac{u^2}{2}\frac{b^2}{\chi^2}$$

.....[2.5]

The perturbed values are

$$\mathbf{v} = \mathbf{v}^\circ + \mathbf{v} \qquad \mathbf{H} = \mathbf{H}^\circ + \mathbf{h} \qquad p = p^\circ + p^{(1)}$$

in which the perturbations $\mathbf{v}$, $\mathbf{h}$ and $p^{(1)}$ are high orders of small quantities relative to $\mathbf{v}^\circ$, $\mathbf{H}^\circ$ and $p^\circ$; these perturbations must (after linearization) satisfy these equations: For the internal region

$$\frac{\partial \mathbf{v}}{\partial t} + \operatorname{grad}(\mathbf{v}^\circ \cdot \mathbf{v}) - \mathbf{v}^\circ \times \operatorname{rot}\mathbf{v} - \mathbf{v} \times \operatorname{rot}\mathbf{v}^\circ +$$

$$\frac{1}{4\pi\rho}(\mathbf{H}^\circ \times \operatorname{rot}\mathbf{h} + \mathbf{h} \times \operatorname{rot}\mathbf{H}^\circ) = -\frac{1}{\rho}\operatorname{grad} p^{(1)}$$

$$\partial \mathbf{h}/\partial t = \operatorname{rot}[\mathbf{v}^\circ \cdot \mathbf{h}] + \operatorname{rot}[v \cdot H^\circ]$$

$$\operatorname{div}\mathbf{v} = 0 \qquad \operatorname{div}\mathbf{h} = 0$$

.....[2.6]

and for the external region

$$\frac{\partial \mathbf{v}}{\partial t} + \operatorname{grad}(\mathbf{v}^\circ \cdot \mathbf{v}) = \frac{1}{\rho_1}\operatorname{grad} p^{(1)} \qquad \operatorname{div}\mathbf{v} = 0$$

$$\operatorname{rot}\mathbf{v} = 0 \qquad \operatorname{div}\mathbf{h} = 0 \qquad \operatorname{rot}\mathbf{h} = 0$$

.....[2.7]

The junction between the two solutions at the surface of the perturbed torus is governed by the conditions

$$\frac{\partial F}{\partial t} + \mathbf{v}\cdot\operatorname{grad} F = 0, \quad \{H_n\} = 0, \quad \left\{p + \frac{H^2}{8\pi}\right\} = 0 \qquad [2.8]$$

in which

$$F(\xi, \theta, \chi, t) = b[1 + \beta \exp(im\xi + in\theta + i\sigma t)] - \chi \qquad [2.9]$$

---

We put

$$\mathbf{v} = [v_\xi(\chi)\mathbf{i}_\xi + v_\theta(\chi)\mathbf{i}_\theta + \mathbf{v}_\eta(\chi)\mathbf{i}_\eta]\exp i(m\xi + n\theta + \sigma t)$$

$$\bar{\mathbf{h}} = [h_\xi(\chi)\mathbf{i}_\xi + h_\theta + (\chi)\mathbf{i}_\theta h_\eta(\chi)\mathbf{i}_\eta]\exp i(m\xi + n\theta + \sigma t)$$

$$p^1 = p_1(\chi)\exp i(m\xi + n\theta + \sigma t)$$

.....[2.10]

Transferring to dimensionless quantities by means of

$$v_\xi = uv \qquad v_\eta = uv_3 \qquad v_\theta = uv_2$$

$$h_\xi = \gamma u h_1 \qquad h_\theta = \gamma u h_2 \qquad h_\eta = \gamma u h_3$$

$$p_1 = \rho u^2 \Pi(\chi) \qquad \sigma = -(u/2ab)\lambda$$

.....[2.11]

we have for the internal region that

$$-i(\lambda + m)v_1 + 2v_3 - 2\varkappa^2 h_3 = -(imb/\chi)\Pi(\chi)$$
$$-(\lambda + m)v_2 + \varkappa^2(mh_2 - 2\chi n h_1) = -2bn\Pi(\chi)$$
$$-i(\lambda + m)v_3 - 2v_1 + \varkappa^2(h'_1\chi + 3h_1 + imh_3) = b\Pi'(\chi)$$
$$(\lambda + m)h_i = mv_i \qquad (i = 1, 2, 3)$$
$$imv_1 + 2\chi i n v_2 - v'_3\chi - v_3 = 0$$
$$imh_1 + 2\chi i n h_2 - h'_3\chi - h_3 = 0$$

.....[2.12]

This system gives Bessel's equation for $v_2$

$$y^2\frac{d^2v_2}{dy^2} + y\frac{dv_2}{dy} + (y^2 - m^2)v_2 = 0 \qquad [2.13]$$

in which

$$y = 2\chi n\sqrt{4\tau^2 - 1}$$
$$\tau = [\lambda + m(1 - \varkappa^2)]/[(\lambda + m)^2 - \varkappa^2 m^2]$$

.....[2.14]

The solution bounded at $\chi = 0$ gives us that

$$v_2 = AJ_m(y) \qquad [2.15]$$

whence we have from Eq. 2.8 that

$$A = [2bn\beta(\lambda + m)(1 - 4\tau^2)]/[y_0 J'_m(y_0) + 2m\tau J'_m(y_0)]$$

$$y_0 = 2bn\sqrt{4\tau^2 - 1}$$

.....[2.16]

All other unknowns are expressed as functions of $v_2$

$$v_1 = A\frac{2\tau y J'_m(y) + mJ_m(y)}{2n\chi(1 - 4\tau^2)}$$

$$h_i = \frac{m}{\lambda + m}v_i \qquad v_3 = iA\frac{yJ'_m(y) + 2m\tau J_m(y)}{2n\chi(1 - 4\tau^2)}$$

$$\Pi(\chi) = A\frac{\{[(\lambda + m)^2 - \varkappa^2 m^2](1 - 4\tau^2) + m^2\}J_m(y) + 2m\tau y J'_m(y)}{2bn(\lambda + m)(1 - 4\tau^2)}$$

.....[2.17]

The total pressure from within at the surface is

$$p + \frac{H^2}{8\pi} = \left(p^\circ + \frac{H^{\circ 2}}{8\pi}\right)_{\chi=b} + \left\{b\beta\left[\frac{\partial}{\partial\chi}\left(p^\circ + \frac{H^{\circ 2}}{8\pi}\right)\right]_{\chi=b} + p_1 + \frac{H^\circ h_\xi}{4\pi}\right\}\exp(im\xi + in\theta + i\sigma t) =$$
$$p_0 + (1 - \varkappa^2)\rho\frac{u^2}{2} + \rho u^2\beta\left\{1 - \varkappa^2 + \frac{[(\lambda + m)^2 - m^2\varkappa^2](1 - 4\tau^2)J_m(y)}{y_0 J'_m(y_0) + 2m\tau J_m(y_0)}\right\}\exp i(m\xi + n\theta + \sigma t) \qquad [2.18]$$

---

The projection of the velocity in the external region is to be found by solving Neumann's problem (the boundary conditions of Eq. 2.8 are used). The solutions are

$$v_1 = \frac{m\beta(\lambda + m)}{2\chi n}\frac{K_m(2\chi n)}{K'_m(2bn)} \qquad v_2 = \beta(\lambda + m)\frac{K_m(2\chi n)}{K'_m(2bn)}$$

$$v_3 = \frac{i\beta(\lambda + m)K'_m(2\chi n)}{K'_m(2bn)} \qquad h_1 = \frac{\beta m^2 K_m(2\chi n)}{2\chi n K'_m(2bn)}$$

$$h_2 = \frac{\beta m K_m(2\chi n)}{K'_m(2bn)} \qquad h_3 = \frac{i\beta m K'_m(2\chi n)}{K'_m(2bn)}$$

.....[2.19]

to the accuracy implied by the assumptions; here $K_m(2\chi n)$ are MacDonald functions of $m$th order. From Eq. 2.7 we have

$$\Pi(\chi) = \beta(\lambda + m)^2 K_m(2\chi n)/2bnK'_m(2bn) \qquad [2.20]$$

The total pressure from outside at the surface is

$$p + \frac{H^2}{8\pi} = \left(p^\circ + \frac{H^{\circ 2}}{8\pi}\right)_{\chi=b} + \left\{b\beta\left[\frac{\partial}{\partial\chi}\left(p^\circ + \frac{H^{\circ 2}}{8\pi}\right)\right]_{\chi=b} + p_1 + \frac{H^\circ h_\xi}{4\pi}\right\} \exp i\,(m\xi_1 + n\theta + \sigma t) =$$

$$p_\infty - \rho_1\frac{u^2}{2} + p\varkappa^2\frac{u^2}{2} + u^2\beta\left\{\rho_1 - p\varkappa^2 + [\rho_1(\lambda+m)^2 - \rho\varkappa^2 m^3]\,\frac{K_m(2\chi n)}{K'_m(2bn)\cdot 2bn}\right\} e^{i(m\xi+n\theta+\sigma t)} \quad [2.21]$$

Then from Eqs. 2.18 and 2.21 we have for $\lambda$ the equation

$$\frac{[(\lambda+m)^2 - \varkappa^2 m^2](1-4\tau^2)J_m(y_0)}{y_0 J'_m(y_0) + 2m\tau J_m(y_0)} -$$

$$\frac{[\nu(\lambda+m)^2 - \varkappa^2 m^2]K_m(2bn)}{2bnK'_m(2bn)} + 1 - \nu = 0 \quad [2.22]$$

The motion is stable if the roots do not have positive imaginary parts. Let us assume that $2bn \ll 1$, i.e., that the perturbations are not of very high frequency.

First let us examine the case $m = 0$ (pinch disturbance); Eq. 2.22 then has the form

$$(4 - \lambda^2)J_0(y_0)/y_0 J'_0(y_0) + \nu\lambda^2 \ln bn + \nu - 1 = 0 \quad [2.23]$$

Let us suppose that $|\lambda| \approx 1$; then

$$|y_0| = |2bn\sqrt{4/\lambda^2}| \ll 1$$

and Eq. 2.23 gives us

$$\lambda = bn\sqrt{2(\nu-1)/(1 - 2b^2n^2\nu \ln bn)} \quad [2.24]$$

The motion is stable ($\lambda$ is real) if $\nu = \rho_1/\rho > 1$; if $\lambda$ is very small, $y_0 \approx 4bn/\lambda$, and Eq. 2.23 becomes

$$4J_0(y_0) - (1-\nu)y_0 J'_0(y_0) = 0 \quad [2.25]$$

which has only real roots if $\nu \geq 1$, or two conjugate purely imaginary roots if $\nu < 1$ (5).

Now we shall turn to the cases $m \geq 1$, of which only

$$|y_0| = 2bn\sqrt{4\tau^2 - 1}| \ll 1 \qquad 2bn \ll 1$$

is considered. Here Eq. 2.22 becomes

$$\lambda^2(1+\nu) + 2\lambda[m(1+\nu) - 1] + m(m-1)(1+\nu-2\varkappa^2) = 0 \quad [2.26]$$

Stability is indicated by the condition

$$2\varkappa^2 m(m-1)(1+\nu) + m(\nu^2-1) + 1 > 0 \quad [2.27]$$

Eq. 2.26 is simply the equation for the out-of-plane vibrations of a vortex ring (4) if $\varkappa = 0$. Thus the ring can be stable in every case if the density within the ring does not exceed the density outside it.

I am indebted to L. I. Sedov for guidance in this work.

*—Received February 20, 1960*

## References

1 Shafranov, V. D., "Magnetic Vortex Rings," *Zh. Eksper. Teoret. Fiz.*, 1957, vol. 33, no. 3 (9).
2 Stekol'nikov, I. S., *Physics of Lightning and Lightning Protection*, Moscow-Leningrad, 1943.
3 Lamb, H., *Hydrodynamics*, Gostekhizdat, 1947, p. 165.
4 Basset, A., *A Treatise on Hydrodynamics*, Vol. 2, Cambridge, 1888, chap. XIV.
5 Lebedev, N. N., *Special Functions and Their Uses*, GITTL, 1953.

## Reviewer's Comment

This interesting paper by Ladikov appears to be one of several Russian efforts to understand a relatively simple axially symmetric plasma torous configuration, moving steadily in free space. This configuration lends mathematical simplification but retains the possibility of some interesting physical behavior. The ring current is azimuthal, and it is assumed that the ring plasma velocity is parallel to the magnetic field. The entire ring moves along the axis of symmetry. Thus, the plasma behaves somewhat like a spinning smoke ring in free space. A single fluid, continuum MHD approach is used throughout.

I know of no similar work in Western journals. The problem is reminiscent of plasma toroids experimentally produced by Bostick (*Phys. Rev.*, 1956, vol. 104, no. 2, pp. 292–299), although in these experiments the toroid motion was along the plane of the ring.

Although there is a wealth of analysis and experiments on confined plasma toroids resulting from controlled thermonuclear efforts, the free space plasma toroid seems to have been overlooked. Ladikov mentions some lightning phenomena which behave in a manner similar to the model analyzed.

—Robert A. Gross
Department of Mechanical Engineering
Columbia University

# Magnetic Measurements on the Second Cosmic Rocket

S. SH. DOLGINOV
E. G. EROSHENKO
L. N. ZHUZGOV
N. V. PUSHKOV
and L. O. TYURMINA

MAGNETIC measurements on the second cosmic rocket had the following aims: To discover if a magnetic field (of dipole type) exists on the moon, and if it exists, to find its magnitude; to obtain new data on the magnetic field in the outer corpuscular zone (radiation belt) of Earth. Previous information on the latter was obtained by the measurements on the first cosmic rocket (1).[1]

Solutions to both these problems are of fundamental importance for explaining the magnetism of the Earth and cosmic bodies, and for explaining magnetic disturbances and their relation to solar activity, polar aurorae and cosmic rays.

The rocket container sent to the moon on Sept. 12, 1959 contained three independent single-component magnetometers with saturable-core detectors of even harmonics. The detectors measured the components of the magnetic field along each of three mutually perpendicular axes $X$, $Y$, $Z$ associated with the rocket container.

For measurements of weak fields, the only kind we might expect close to the moon, the sensitivity of the magnetometers in the second rocket was increased by approximately four times over that of the magnetometers in the first rocket. This involved a reduction in the measurement range of the magnetometers, and this was the reason why measurement of Earth's magnetic field by the second rocket did not begin until it was approximately 18,000 km from Earth's center; on the first rocket, measurement of the field began at a distance of approximately 14,700 km.

The magnetometers used were relative instruments. The values of magnetometer zeros were determined first of all from the results of measurements at great distances (outside Earth's field). The degree of stability of the zeros of magnetometers $X$, $Y$ and $Z$ is illustrated by the graphs in Fig. 1. Each of the points represents the mean reading during 20 min of flight.

As the graphs show, the zeros of channels $Z$ and $Y$ remained constant to within $\pm 20\ \gamma$ close to Earth. The zero of channel $X$ varied a little. For the part of the trajectory near Earth, it may be said that the zero shifted at a constant rate of around $7\ \gamma$ per hr. On the part of the trajectory outside Earth's magnetic field, the mean error in determining the zeros of the magnetometer channels was $\pm 30\ \gamma$.

In addition, it was possible to check the zeros of the magnetometer channels in parts of the trajectory within Earth's magnetic field from the measured values of the field components and the total vector $T$ calculated on the basis of these measurements.

Let us consider the rotation of a detector set at a constant angle $\psi$ to the horizon and rotating round a vertical axis with angular velocity $\dot{\varphi}$. The detector is at a point where the vector $T_0$ is inclined at angle $\alpha$ to the horizon. The detector readings will vary periodically

$$H_{\text{det. 1}} = T_0(\sin\alpha \sin\psi + \cos\alpha \cos\psi \sin\varphi)$$

The mean value is given by the first term of this expression.

The readings of another detector lying in the same plane as the first, but at an angle of 90 deg to it, will be

$$H_{\text{det. 2}} = T_0(\sin\alpha \sin\psi + \cos\alpha \cos\psi \cos\varphi)$$

i.e., they will also be periodic functions of $\varphi$ with the same mean value, but for each position there will be a phase shift of $\pi/2$ between $H_{\text{det. 1}}$ and $H_{\text{det. 2}}$.

The difference in levels relative to which the readings of two such detectors vary (i.e., the variation in the mean values of $H_{\text{det. 1}}$ and $H_{\text{det. 2}}$) indicates the zero shift in one of the channels. In the coordinate system associated with vector $T_0$ the readings on the detectors of a three-component magnetometer will be

$$Z = T_0 \cos\theta \qquad X = T_0 \sin\theta \sin\varphi$$
$$Y = T_0 \sin\theta \cos\varphi$$

where

$\theta$ = angle between the axis of detector $Z$ and vector $T_0$
$\varphi$ = angle of inclination of the axis of detector $X$ to the plane of the meridian

It is obvious that the square of the modulus $T_0$ ($T_0^2 = X^2 + Y^2 + Z^2$) does not depend on the orientation. However, if the zeros in channels $Z$, $X$, $Y$ shift through values $a$, $b$, $c$, respectively, then the expression for the square of the total vector will contain two additional terms

$$T^2 = T_0^2 + (a^2 + b^2 + c^2) + 2T_0(a\cos\theta + b\sin\theta\sin\varphi + c\sin\theta\cos\varphi)$$

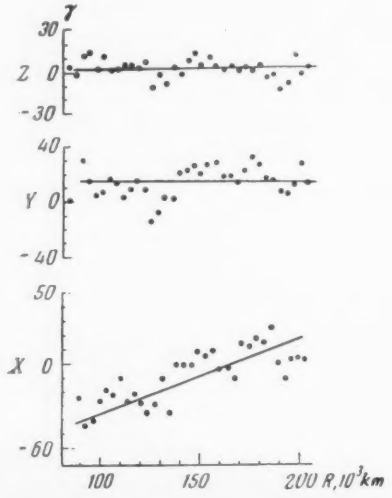


Fig. 1 Readings of magnetometers $Z$, $Y$ and $X$ at 75–200 × $10^3$ km from Earth, showing stability of zeros

Translated from *Artificial Earth Satellites*, 1960, no. 5, pp. 16–23. Translated by Research Information Service, New York.

[1] Numbers in parentheses indicate References at end of paper.

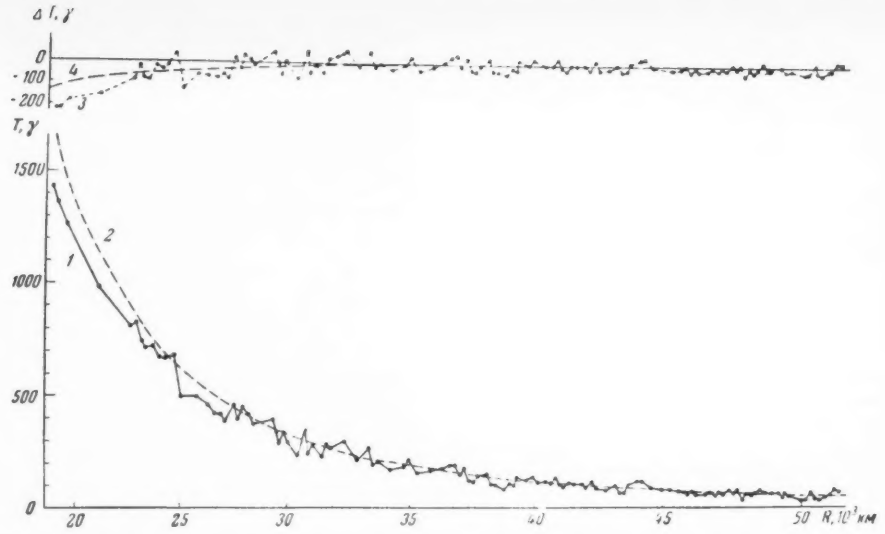


**Fig. 2** Magnitude of total vector of Earth's magnetic field as function of distance from center. 1: Measurements; 2: calculated dependence for dipole field; 3: difference $\Delta T = T_{meas} - T_{calc}$ between measured and calculated intensity; 4: smoothed curve for difference $\Delta T$

The second term in this expression reduces to the total shift of the experimental curve and does not depend on the orientation.

The third term depends on the magnitude of the field and on the orientation of the container. It may be found on the experimental curve of the total vector of the field $T$ from the modulation of the amplitude with a period equal to the period of rotation of the container. From the results it is possible to determine the magnitude and sign of the zero shifts of the detectors which are affected by the container rotation.

Thus, the container rotation provides an additional opportunity to exclude the effects of the zero shifts, and this, to a large extent, overcomes the limitations imposed by the relative nature of the apparatus used.

The errors due to nonsimultaneity of interrogation of the magnetometer channels attain magnitudes of about 30 $\gamma$ only in the initial region of the measurements. The error in determining the total vector was approximately 50 $\gamma$.

## Measurements of Earth's Magnetic Field

The results of the field measurements are shown in Fig. 2. The values of $T$ calculated from the measured values of $X$, $Y$, $Z$ are shown here by points. The continuous curve 2 gives the values of Earth's total magnetic field intensity, calculated from the results of a spherical harmonic analysis of magnetic field measurements at Earth's surface.

From analysis of the results of measurements in the region near Earth and the differences between the measured and calculated values of the total field intensity, we can draw the following conclusions.

The measured and calculated values of the total component of the field agree fairly well with one another at distances of more than 23,000 km from Earth's center. At shorter distances, we find discrepancies similar to those observed in measurements on the first rocket, but of much smaller magnitude.

The intensity of corpuscular radiation in the outer radiation zone was measured by American scientists with the Pioneer III and IV rockets (2,3), and by Soviet scientists with the first and second cosmic rockets (4–6).

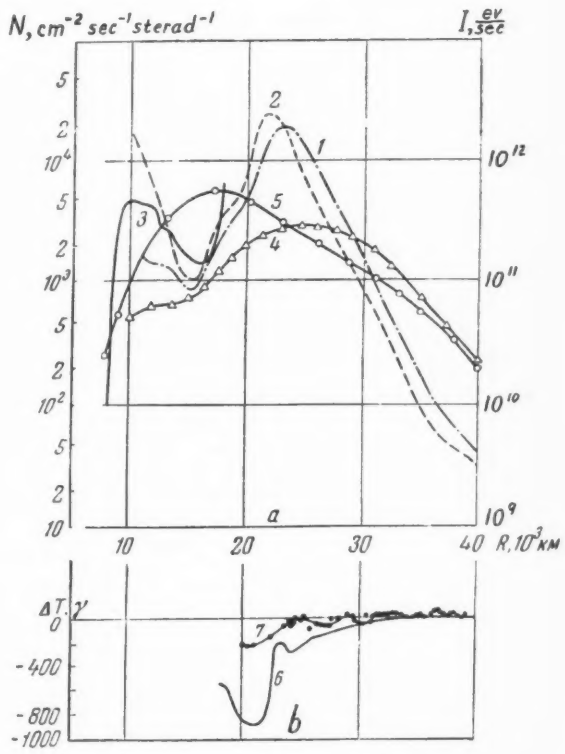


**Fig. 3** Radiation intensity (Fig. 3a) and difference (Fig. 3b) $\Delta T = T_{meas} - T_{calc}$ in region of outer radiation belt in relation to distance from Earth's center. 1,2: Radiation measurements on rocket Pioneer III (ascending and descending legs); 3: measurements on rocket Pioneer IV; 4,5: measurements of total ionization on first and second cosmic rockets (from scintillation counter data); 6,7; differences $\Delta T$ from magnetometer measurements on first and second cosmic rockets

**Table 1**

| Rocket | Distance from Earth's center to zone maximum, $10^3$ km | Decrease in mean diurnal value of horizontal component $\Delta H, \gamma$ |
|---|---|---|
| 1st Cosmic (USSR) | 25 | 50 |
| Pioneer III (U. S.) | 22–24 | 70 |
| 2nd Cosmic (USSR) | 18 | 78 |

When the rocket Pioneer III returned to Earth it had made two sets of measurements in the radiation belt: One on its way out from the Earth and one on its return. The results of the measurements (2–5) are shown in Fig. 3a. Curves 1, 2 and 3 show the intensity of corpuscular radiation in relation to the distance from Earth's center, as recorded in (2 and 3) (the radiation intensity is characterized by the number of particles incident on 1 cm² in 1 sterad per 1 sec). Curves 4 and 5 are plotted from the data of (4 and 5) (the radiation intensity is characterized by the total energy evolution in the crystal of the scintillation counter). The ascending and descending legs of the trajectory of Pioneer III intersected the corpuscular zone at different distances from the geomagnetic equator, which explains the difference in the position of the radiation maximum recorded on ascent and descent of Pioneer III.

The magnetic field in the outer radiation zone has been measured twice—on the first and second cosmic rockets. Curves 6 and 7 on Fig. 3b show the differences between the values of the total intensity of Earth's magnetic field, as measured on the first and second cosmic rockets, and the theoretically calculated values from the results of spherical harmonic analysis.

An examination of the available data shows that the dimensions of the outer zone, the intensity of radiation in it, and the distance of the region of maximum radiation intensity from Earth varies with time (from measurement to measurement)(2,5,6). These changes are correlated with magnetic storms and polar aurorae, indicating that the outer corpuscular region is formed by solar corpuscles trapped by the magnetic field. The analysis reveals a definite relationship between the position of radiation maxima and magnetic activity.

Table 1 shows the distances, taken from Fig. 3a, of the corpuscular radiation maxima from Earth's center and the diminution in the mean diurnal values of the horizontal component ($\Delta H$). As Table 1 reveals, the greatest radiation intensity occurs closer to Earth, the more violent the magnetic storm preceding the formation of the corpuscular region.

The variation of the mean diurnal values of the horizontal component is shown in Fig. 4. Comparing the graphs in Figs. 3 and 4, Dolginov suggested that the radiation maximum is probably located farther from Earth, the greater the number of calm days preceding the experiment. The following model of the effect seems possible. Under the action of the corpuscular stream, the zone is pushed toward Earth. When the main phases of the magnetic storm are completed, the zone is repelled by the inhomogeneous magnetic field of Earth into the region of smaller fields and gradients (like the ionized gases of a burner in the inhomogeneous field of an electromagnet). Thus, we can postulate that the outer zone of corpuscular radiation possesses diamagnetic properties. This last hypothesis does not contradict the fact of the noncoincidence of the cosmic radiation maximum and the maximum depression of the magnetic field, a feature discovered in the flight of the first cosmic rocket.

A comparison of the intensity variations of the corpuscular radiation and magnetic field with distance, as recorded during the flight of the first cosmic rocket, shows that the region where magnetic effects associated with the outer radiation zone were observed was located several thousands of kilometers closer to Earth than the maximum intensity of corpuscular radiation. If a similar relationship had occurred during the flight of the second cosmic rocket and, what is more, if this time the region of magnetic effects had been located closer to the maximum of the corpuscular radiation intensity, such magnetic effects could still not have been recorded, since they lay in that region where the field intensity was high and was outside the measurement range of the magnetometer.

The pattern noted suggests that the outer corpuscular region acts as a special intermediate reservoir of solar corpuscles, which fills up during magnetic disturbances and gradually loses them in the period between disturbances. This, in fact, explains why aurorae are observed at high latitudes every day, and not only in days of magnetic disturbances.

In the first communication on the experimental discovery of the magnetic field of the outer corpuscular region (1), it was suggested that one of the most probable causes of the magnetism of the radiation zone might be electric drift-currents, created by the drift of charged particles in Earth's magnetic field. The possibility of a drift of charged particles in Earth's magnetic field was confirmed by observations of high altitude atomic explosions conducted in the U. S. (7).

As in modern theories of the origin of magnetic storms and aurorae, we can assume that the outer corpuscular zone is formed by the entry of solar corpuscular streams, consisting of neutral particles and different numbers of positive and negatively charged particles (protons, positive ions and electrons), into Earth's magnetic field. When such streams flow around Earth, some of the charged particles will be trapped by the magnetic field and become part of the outer corpuscular zone of Earth.

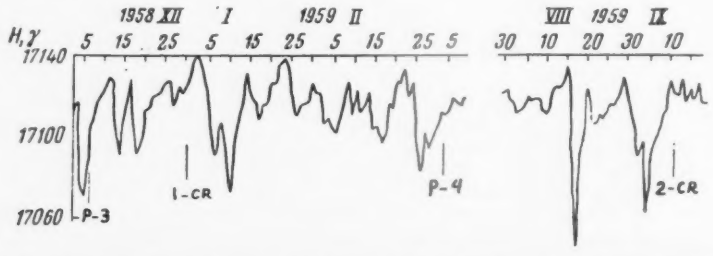


**Fig. 4 Time variation of mean diurnal values of $H$ from ground station measurements during flights of cosmic rockets. Launching times: P-3, Pioneer III; 1-CR, first cosmic rocket; P-4, Pioneer IV; 2-CR, second cosmic rocket**

Charged particles in the radiation zone complete numerous passages from one hemisphere to the other, spiraling around the field lines, and at the same time drifting in a direction perpendicular to the field and its gradient. Positive particles move toward the west, and negative particles toward the east. It can be shown (8) that, owing to the small radius of curvature of the electron tracks, their contribution to the magnetic field of drift-currents in the corpuscular zone will be insignificant. Hence, the magnetic effects recorded by magnetometers on rockets must be attributed to drift-currents of protons and positive ions.

The possibility of the existence of protons in the outer corpuscular region is indicated also by observations of aurorae, the spectrum of which reveals hydrogen lines. At present there are no other experimental data on the presence of protons with energies of several tens of kiloelectron-volts, but indirect evidence of the presence of such protons in the corpuscular zone can be obtained from the results of magnetic measurements in this region and from the recording of hydrogen lines in auroral spectra.

From the data of the magnetic measurements on the first cosmic rocket Pushkov put forward the hypothesis that the two regions of magnetic field reduction, recorded by the magnetometers on this rocket (one at a distance of 23,000 km, and the other at a distance of 25,000 km, from Earth's center), were associated with two maxima of proton intensities, one of which was formed during the great magnetic storm of Dec. 3–6, 1958, and the other during the two moderate magnetic storms observed during the period Dec. 12–20, 1958.

An analysis of the variations of the field components showed that during flight, the container precessed in such a way that the magnetometers $X$ and $Y$ rotated round the $Z$ axis, and the $Z$ axis itself rotated round another axis, the axis of precession, the spatial orientation of which remained constant. The angle of nutation (the angle between the axis of precession and the $Z$ axis) was about 89 deg. The container's natural rotation period, manifested in the periodical changes of the $X$ and $Y$ components, was approximately 900 sec, and the period of precession, manifested in the periodic variation of the $Z$ component, was approximately 86 sec.

The values of the $X$, $Y$ and $Z$ components varied periodically in Earth's magnetic field, owing to the rotation of the container and the magnetometer detectors rigidly attached to it. This rotation continued after the container had left Earth's magnetic field, and it could provide an additional criterion for a decision as to the existence of a field close to the moon and in interplanetary space. If a field exists in these regions, we should observe the same periodic variations of the field components as we observe close to Earth.

## Measurements of the Moon's Magnetic Field

The magnetometers on the second cosmic rocket were also intended for detecting the moon's magnetic field. They functioned normally right up until the container struck the moon. The last measurement was made approximately 50 km from the moon's surface. The measurements did not reveal a magnetic field near the moon.

From an analysis of the precision of measurement of Earth's magnetic field and the accuracy of the telemetric records of the measurements, we can conclude that if the moon had a magnetic field of intensity more than 50–100 $\gamma$ at the moon's surface, this field would have been detected.

Table 2

| Distance from moon's center, km | $T$, $\gamma$ | Distance from moon's center, km | $T$, $\gamma$ | Distance from moon's center, km | $T$, $\gamma$ |
|---|---|---|---|---|---|
| 5150 | **30** | 4000 | 70 | 2800 | 50 |
| 5100 | **80** | 3800 | **70** | 2700 | 110 |
| 4950 | **50** | 3700 | 30 | 2600 | 40 |
| 4850 | **50** | 3400 | 90 | 2290 | 40 |
| 4700 | **20** | 3300 | 40 | 2160 | 170 |
| 4550 | **50** | 3200 | 70 | 2055 | **60** |
| 4400 | 70 | 3100 | 70 | 1935 | **50** |
| 4300 | 40 | 3000 | 60 | 1795 | 120 |

Note: The values are rounded off to tens of gammas. The most reliable values, gaged from the quality of the telemetric traces, are given in bold face.

Table 2 gives the measured values of the total magnetic field intensities at different distances from the moon's center.

As Table 2 reveals, the measured values of the field lie within the limits of measurement errors, and do not show any noticeable increase of field with approach to the moon. We know that if the moon possessed a general field like Earth's, similar to that of a homogeneously magnetized sphere, then, with approach to the moon, there would have been an increase in field inversely proportional to the cube of the distance from the moon's center. In view of the data given, we can conclude that either the moon possesses no magnetic field at all, or its field, even at the surface, is so small that it lies wholly within the limits of measurement error. The greatest possible value of the mean intensity of magnetization of the moon is about 0.0002 cgs units. In any case, we can state that the intensity of the lunar magnetic field at the moon's surface is no more than 1/400 of the magnetic field intensity at Earth's surface (the mean value of the moon's magnetism is not more than 0.25% of the mean value of Earth's magnetism).

## References


1 Dolginov, S. Sh. and Pushkov, N. V., *Doklady Akad. Nauk SSSR (Bull. Acad. Sci. USSR)*, 1959, vol. 127.

2 Van Allen, J. A. and Frank, L. A., *Nature*, 1959, vol. 183, p. 430.

3 Van Allen, J. A., "The Geomagnetically Trapped Corpuscular Radiation," paper presented at conference on cosmic rays in Moscow, July 6–11, 1959.

4 Vernov, S. N., Chudakov, A. E., Vakulov, P. V. and Logachev, Yu. I., *Doklady Akad. Nauk SSSR (Bull. Acad. Sci. USSR)*, 1959, vol. 125, p. 305.

5 Vernov, S. N., Chudakov, A. E., Vakulov, P. V., Logachev, Yu. I. and Nikolayev, A. G., *Artificial Earth Satellites*, 1960, no. 5.

6 Kurnosova, L. V., Logachev, V. I., Razorenov, L. A. and Fradzhin, M. I., *Artificial Earth Satellites*, 1960, no. 5.

7 Singer, S. F., *Missiles and Rockets*, 1959, vol. 5, nos. 13–16.

8 Singer, S. F., Trans. Amer. Geophys. Union, 1957, vol. 38, p. 175.


## Reviewers' Comments

This paper is highly significant. The Russian scientists are to be congratulated for a pioneering effort and for making a prompt report on their work available to scientists all over the world. The measurements themselves deal with one of the fundamental physical parameters of space science and at least set limits on the magnitude of magnetic fields in space and near the moon, estimates of which have been varied and highly controversial.

Although the instrumentation used by the Russians in the measurement of weak magnetic fields was crude by present technology, the instrumentation operated as part of a complex device which achieved a spectacular success. The Russians very honestly reported on the limitations of their instrumentation, and the fact that the experiment was simple probably

insured success. Probably the most significant criticism in regard to the instrumentation is that the range of zero instability in their experiment is approximately equal to the range of actual field variations observed by Explorer X, which contained a sophisticated magnetometer, in traversing the same range of distance from Earth.

The paper reports on both measurements in space and measurements in the vicinity of the moon. These will be commented on separately.

A significant result of the Russian experiment was that it measured a low field value near 23,000 km. These data are controversial. The Russians attribute this phenomenon to an actual field disturbance due to particles in the outer belt. However, such a measurement can also result from an inaccurate representation of Earth's field in their spherical harmonic analysis or trajectory errors in which the spacecraft was actually at a slightly greater altitude or lower latitude than computed. This combination could easily lead to large discrepancies. If one accepts the Russian interpretation, it implies a highly accurate and sophisticated tracking system.

On the other hand, it is possible that the Russian result is entirely correct. At 23,000 km, the spacecraft was apparently located near the inner edge of the outer Van Allen belt, or the outer edge of the slot, depending upon its latitude in geomagnetic coordinates. There is recent supporting evidence from a NASA Javelin sounding rocket, which carried a rubidium vapor magnetometer and was fired at Wallops Island, and there was a diamagnetic type of field disturbance of around 200 $\gamma$ in the horn of the outer belt near its inner edge at the time of this flight. Vanguard III also showed disturbances, mainly next to the slot. This satellite, however, did not reach the outer belt. Finally, preliminary interpretations of Explorer X data show that the field is depressed in intensity over the entire range of the outer part of the inner belt, the slot, and the inner part of the outer belt in the region traversed over South Africa. If this is not found to be the result of an error in trajectory computation, there will be additional reason to believe that the radiation belts are magnetically active in the vicinity of the slot. The result of these indications is that the Russian data may be valid. Future experiments should resolve this problem, and NASA magnetometers are scheduled for flight on S-3 spacecraft in the near future that should cover the region of interest.

Concerning the moon's magnetic field, we accept the Russian measurements as showing the lunar field to be less than 50 $\gamma$. However, this is not too surprising, since the moon's field may be quite weak and influenced greatly by the magnetic field of the sun. Perturbations of the lunar field by the solar "wind" would be expected. In fact, the magnetic field of the moon, if present at all, may be blown out into a teardrop shape by solar influence.

In making their measurement of the lunar magnetic field, the Russians have pioneered and have set an upper limit which will be of considerable value to space scientists in understanding the nature of the lunar body.

—James P. Heppner and
John W. Townsend Jr.
NASA Goddard
Space Flight Center

---

# Propagation and Interaction of Compression and Rarefaction Waves in Elastic-Plastic Media

G. M. LIAKHOV and
N. I. POLIAKOVA

**Rakhmatulin (1,2)[1] was the first to examine the propagation of compression and unloading waves in elastic-plastic media. He obtained an analytical solution for loads which instantaneously increase and then decrease, according to the power law, when the relationship $\sigma = f(\epsilon)$ was linear. The solution to a series of problems connected with the propagation and interaction of waves was provided by Shapiro (3), Lebedev (4), and Biderman (5) employing a method of plotting grid characteristics. Lee (6), Kaliski and Osiecki (7), and others have examined the propagation and interaction of waves where there is an infinitely large unloading velocity. B. A. Olisov, C. Lempson, N. V. Zvolinsk, S. S. Grigoryan and others have examined the application of elastic-plastic medium models to a ground.**

**This article will examine the propagation, reflection and refraction of fixed plane compression and rarefaction waves in elastic-plastic media, employing the Lagrangian mass-time coordinate system, when the law for the compressibility and unloading of media is linear. This made it possible, on the basis of (8), to obtain a formula defining the propagation and interaction of waves.**

Translated from *Izvestiia Akademii Nauk SSSR, Otdel. Tekh. Nauk, Mekhanika i Mashinostroenie* (*Bull. Acad. Sci. USSR, Div. Tech. Sci., Mechanics and Machine Construction*), 1960, no. 3, pp. 99–108. Translated by Primary Sources, New York.

[1] Numbers in parentheses indicate References at end of paper.

## 1 Compression and Unloading of Media

LET US examine a medium in which compression and unloading to some stress $\sigma_s$ occurs elastically, i.e., in accordance with a single law; when $\sigma > \sigma_s$, it occurs according to various laws (Fig. 1). When the load in the medium is removed (if $\sigma_r > \sigma_s$), residual deformation $\epsilon$ is preserved; its magnitude depends on the maximum stress $\sigma_r$ which is achieved during compression. A secondary load takes place according to the unloading law to the stress reached with the first compression.

The $\sigma = f(\epsilon)$ relationship can be made linear, both during loading and unloading of the medium, but with different straight lines.

In the future, the system of magnitudes $p$, $\rho$, used in gasdynamics, will be used. In addition

$$\sigma = -p \qquad \epsilon = \frac{V - V_0}{V_0} = \frac{\rho_0 - \rho}{\rho}$$

where $\rho$ is the medium's density.

If the $\sigma = f(\epsilon)$ relationship were linear, then the connection of pressure $p$ and specific volume $V$ would also be linear. Let us assume that when loading

$$p - p_0 = -A_0^2(V - V_0) \quad \text{when} \quad p < p_s \qquad [1.1]$$

$$p - p_s = -A_1^2(V - V_s) \quad \text{when} \quad p_s < p < p_k \qquad [1.2]$$

$$p - p_k = -A_0^2(V - V_k) \quad \text{when} \quad p > p_k \qquad [1.3]$$

where

$A_0 = c_0\rho$
$A_1 = c_1\rho_1$
$c_0, c_1$ = propagation speeds of elastic and elastic-plastic deformations, respectively
$\rho_0, \rho_1$ = media densities, when $p = p_0$ and $p = p_s$

During unloading of a medium

$$p - p_r = -A_0^2(V - V_r) \qquad [1.4]$$

$p_s$, $V_s$ correspond to a state to which compression and unloading occur plastically. Quantities $p_r$, $V_r$ correspond to a state at which unloading begins. Secondary loading occurs according to the law of Eq. 1.4, where $p < p_r$, and, where pressures are greater, according to a corresponding loading law.

## 2 Propagation of Plane Compression Waves

The solution is effected with the aid of the method stated (8); the Lagrangian coordinate system $h,t$ is employed, where $h$ is the mass of the substance contained within the examined and the initial cross section, and $t$ is the time

$$h = \int_{x(0,t)}^{x(h,t)} \rho dx$$

The main gasdynamic equations in coordinates $h,t$ have the form

$$\frac{\partial u}{\partial t} + \frac{\partial p}{\partial h} = 0 \qquad \frac{\partial u}{\partial h} - \frac{\partial V}{\partial t} = 0 \qquad [2.1]$$

According to Eqs. 1.1 to 1.4, there is a linear connection between the pressure and the volume, i.e.

$$p = -A^2V + B \qquad [2.2]$$

When loading, magnitudes $A$ and $B$ are constant within each section of the compression diagram; when unloading, $A = A_0$ (constant magnitude), and $B = B(h)$.

The magnitude $B$ does not depend on $t$; therefore, from Eqs. 2.1 and 2.2, we obtain

$$\frac{\partial u}{\partial t} + \frac{\partial p}{\partial h} = 0 \qquad \frac{\partial u}{\partial h} + \frac{1}{A^2}\frac{\partial p}{\partial t} = 0 \qquad [2.3]$$

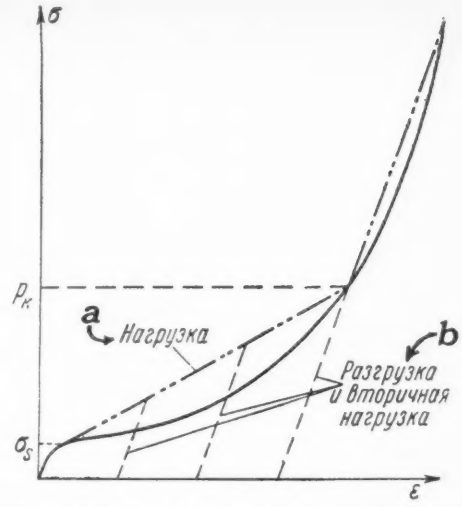


**Fig. 1** [a]Loading; [b]unloading and secondary loading

and the system reduces itself to a homogeneous wave equation

$$\frac{\partial^2 p}{\partial h^2} = \frac{1}{A^2}\frac{\partial^2 p}{\partial t^2} \qquad [2.4]$$

whose solution is

$$p = F_1(h - At) + F_2(h + At)$$
$$u = (1/A)[F_1(h - At) - F_2(h + At)] \qquad [2.5]$$

Discontinuity conditions at coordinates $h,t$ have the form

$$p_2 - p_1 = h_f'^2(V_1 - V_2) \qquad u_2 - u_1 = h_f'(V_1 - V_2) \qquad [2.6]$$

where $h_f'$ is the rate of the discontinuity propagation.

If both states—before discontinuity and during it—lie on a single straight line of the linear compression diagram, i.e.

$$p_2 - p_1 = -A^2(V_2 - V_1)$$

then the first of the conditions in Eq. 2.6 determines the discontinuity rate

$$h_f' = \pm A \qquad [2.7]$$

the second provides

$$p_2 \pm Au_2 = p_1 \pm Au_1 \qquad [2.8]$$

Thus, in passing through a discontinuity (weak or strong) one of the expressions $p \pm Au$ did not experience a jump.

Let the pressure in the initial cross section of medium $h = 0$ grow instantly to $p_m (p_k > p_m > p_s)$ and then drop, according to the given law $p = p(t)$. Then, two fronts would propagate along the medium (Fig. 2). The first, corresponding to a pressure jump from $p_0 = 0$ to $p_s$, moves at velocity $A_0$; the second (which we designate $S$), corresponding to a pressure jump from $p_s$ to a maximum pressure (in a given cross section) moves at velocity $A_1$.

In region 1 (elastic wave) the solution takes the form

$$p = p_s \qquad u = p_s/A_0 \qquad [2.9]$$

In region 2, the medium is unloaded. We seek the flow in region 2, in the form of Eq. 2.5, where $A = A_0$.

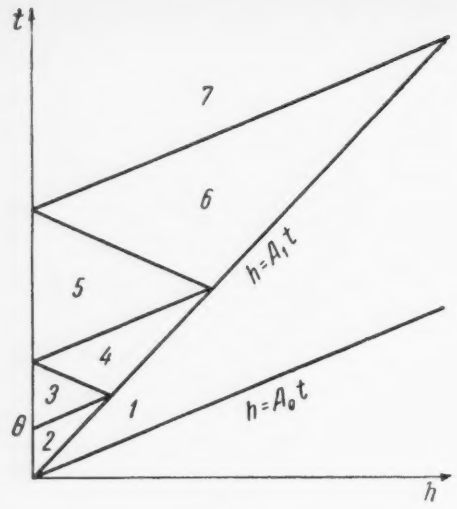


Fig. 2

Let the pressure in section $h = 0$ drop according to the linear law

$$p = p_m(1 - t/\theta) \qquad [2.10]$$

where $\theta$ is the operating time of the wave.

Let us obtain functions $F_1$ and $F_2$ in region 2 in a linear form

$$F_1(h - A_0t) = a_1 + b_1(h - A_0t)$$
$$F_2(h + A_0t) = a_2 + b_2(h + A_0t) \qquad [2.11]$$

Two boundary conditions

$$p = p_m(1 - t/\theta) \quad \text{when} \quad h = 0$$
$$p - A_1u = p_s - A_1u_s \quad \text{when} \quad h = A_1t \qquad [2.12]$$

provide four linear equations for determining the four constants $a_1$, $b_1$, $a_2$ and $b_2$. As a result, we obtain a solution in region 2 in the form

$$p = p_m\left(1 + \frac{A_0^2 + A_1^2}{2A_0^2A_1}\frac{h}{\theta} - \frac{t}{\theta}\right)$$

$$u = \frac{p_m}{A_0}\left(\frac{A_0}{A_1} + \frac{h}{A_0\theta} - \frac{A_0^2 - A_1^2}{2A_0A_1}\frac{t}{\theta}\right) - \frac{p_s}{A_0}\frac{(A_0 - A_1)}{A_1} \qquad [2.13]$$

The particle velocity and pressure, in each section, drop in the course of time. At each moment of time, the maximum values of these magnitudes lie on the line $h = A_1t$. In addition

$$p = p_m - \frac{A_0^2 - A_1^2}{2A_0^2A_1}\frac{p_mh}{\theta}$$

$$u = \frac{p_m}{A_1} - \frac{A_0 - A_1}{A_0A_1}p_s - \frac{A_0^2 - A_1^2}{2A_0^2A_1^2}\frac{p_mh}{\theta} \qquad [2.14]$$

At the moment of time $t = \theta$, when the pressure in section $h = 0$ drops to value $p = 0$, a new wave front will proceed at velocity $A_0$. Making calculations, analogous to those carried out, we obtain a solution in region 3

$$p = \frac{(A_0 - A_1)^2}{2A_0^2A_1}\frac{p_mh}{\theta}$$

$$u = \frac{A_0 - A_1}{A_1A_0}p_m - \frac{A_0 - A_1}{A_1A_0}p_s - \frac{(A_0 - A_1)^2}{2A_0^2A_1}\frac{p_mt}{\theta} \qquad [2.15]$$

The pressure in each section does not change with time; particle velocity is identical in the entire region 3, at each moment of time.

The wave front, reflecting from $S$, begins to move in the opposite direction. A region 4 emerges, in which the solution has the form

$$p = \frac{A_0 - A_1}{A_0 + A_1}p_m + \frac{(A_0 - A_1)^2(A_0^2 + A_1^2)}{2A_0^2A_1(A_0 + A_1)^2}\frac{p_mh}{\theta} - \frac{(A_0 - A_1)^2}{(A_0 + A_1)^2}\frac{p_mt}{\theta}$$

$$u = \frac{A_0 - A_1}{A_1(A_0 + A_1)}p_m + \frac{(A_0 - A_1)^2}{A_0^2(A_0 + A_1)^2}\frac{p_mh}{\theta} - \frac{(A_0 - A_1)^2(A^2 + A_1)^2}{2A_0^2A_1(A_0 + A_1)^2}\frac{p_mt}{\theta} + \frac{(A_0 - A_1)^2p_s}{(A_0 + A_1)A_1A_0} \qquad [2.16]$$

On line $h = A_1t$ in region 4, we have

$$p = \frac{A_0 - A_1}{A_0 + A_1}p_m - \frac{(A_0 - A_1)^3}{2A_0^2A_1(A_0 + A_1)}\frac{p_mh}{\theta}$$

$$u = \frac{A_0 - A_1}{A_1(A_0 + A_1)}p_m + \frac{(A_0 - A_1)^2}{A_0A_1(A_0 + A_1)}p_s - \frac{(A_0 - A_1)^3}{2A_0^2A_1(A_0 + A_1)}\frac{p_mh}{\theta} \qquad [2.17]$$

Reflecting from plane $h = 0$, the wave front will again move toward an increase in $h$. Under repeated reflections, there emerge regions 5, 6, 7 . . .

The solution in region 5 is

$$p = \frac{(A_0 - A_1)^4}{2A_0^2A_1(A_0 + A_1)^2}\frac{p_mh}{\theta}$$

$$u = \frac{(A_0 - A_1)^2p_m}{A_0A_1(A_0 + A_1)} + \frac{(A_0 - A_1)^2p_s}{(A_0 + A_1)A_0A_1} - \frac{(A_0 - A_1)^4}{2A_0^2A_1(A_0 + A_1)^2}\frac{p_mt}{\theta} \qquad [2.18]$$

The solution in region 6 is

$$p = \frac{(A_0 - A_1)^2}{(A_0 + A_1)^2}p_m + \frac{(A_0 - A_1)^4(A_0^2 + A_1^2)}{2(A_0 + A_1)^4A_0^2A_1}\frac{p_mh}{\theta} - \frac{(A_0 - A_1)^4}{(A_0 + A)^4}\frac{p_mt}{\theta}$$

$$u = \frac{(A_0 - A_1)^2}{A_1(A_0 + A_1)^2}p_m - \frac{2(A_1 - A_0)}{(A_0 + A_1)^2}p_s - \frac{(A_0 - A_1)^4(A_0^2 - A_1^2)}{(A_0 + A_1)^42A_0^2A_0^2A_1^2}\frac{p_mt}{\theta} + \frac{(A_0 - A_1)^4}{(A_0 + A_1)^4}\cdot\frac{p_mh}{A_0^2\theta} \qquad [2.19]$$

At the point of intersection $(t_3,h_3)$ of the boundaries between regions 6 and 7 and lines $h = A_1t$, we have

$$p = \frac{(A_0 - A_1)^3}{2A_0(A_0 + A_1)^2}p_m \qquad h_3 = \frac{(A_0 + A_1)^2A_0A_1}{(A_0 - A_1)^3}\theta$$

Similar computations can be made as well for succeeding regions. However, in a series of cases, this has no practical significance, inasmuch as the pressure in region 7 is already small. Actually, if $A_1 = \frac{1}{2}A_0$, then $p = \frac{1}{36}p_m$ when $h = h_3$; if $A_1 = \frac{1}{3}A_0$, then $p = \frac{1}{12}p_m$ when $h = h_3$.

The operating time of waves, as follows from the calculations given, grows with separation from the initial cross section. If the operating time $\theta$ of pressure $p > p_s$ is considered, then when the distance is increased there is a growth in $\theta$ from the beginning; then, when the maximum is reached, it is reduced. The time and place for the maximum to be reached depend on the value of $p$ used.

Fig. 3 shows pressure changes, with time, in some sections of the media.

We have examined the case when the pressure in the initial section $h = 0$ was set in the form of Eq. 2.10. In this section, let the pressure be given as

$$p = p_m(1 - t/\theta)^n \qquad [2.20]$$

Let us represent this function in the form

$$p = a_0 + a_1 t + \ldots + a_n t^n$$

We seek functions $F_1$ and $F_2$ in region 2 in the form of polynomials of the power $n$

$$F_1 = \alpha_0 + \alpha_1(h - A_0 t) + \ldots \alpha_n(h - A_0 t)^n$$
$$F_2 = \beta_0 + \beta_1(h + A_0) + \ldots p_n(h - A_0 t)^n \qquad [2.21]$$

Conducting appropriate calculations, we obtain

$$\alpha_k = \frac{a_k(-1)^k(A_0 + A_1)^{k+1}}{A_0{}^k[(A_0 + A_1)^{k+1} - (A_0 - A_1)^{k+1}]}$$

$$\beta_k = \frac{-a_k(A_0 - A_1)^{k+1}}{A_0{}^k[(A_0 + A_1)^{k-1} - (A_0 - A_1)^{k-1}]} \qquad [2.22]$$

Having determined all the $\alpha_i$ and $\beta_i$, we can find the pressure and the velocity of particles in accordance with Eq. 2.5. Thus, a solution in region 2 was obtained. Solutions to subsequent regions may be found similarly.

## 3 Reflection of Compression Waves

When the compression wave in an elastic-plastic medium is reflected from boundary $T$ with another elastic-plastic or elastic medium, reflected compression or rarefaction waves emerge, from a free surface or obstacle, which move along the disturbed medium.

If the state in front of and on the wave front lies on one line of the compression diagram, then, as was shown, the front velocity is $h_f' \pm A$.

The conditions on the front are

$$p_2 + Au_2 = p_1 + Au_1 \quad \text{if} \quad h_f' = -A$$
$$p_2 - Au_2 = p_1 - Au_1 \quad \text{if} \quad h_f' = A \qquad [3.1]$$

If the front velocity coincides with the velocity of the weak disturbances behind the front, then functions $F_2(h + At) = \frac{1}{2}(p - Au)$, or $F_1(h - A_0 t) = \frac{1}{2}(p - Au)$ behind the front remain the same as on the front and in the region before the front.

If the states before and behind the wave front lie on different straight lines of the compression diagram, then the pressure discontinuity is broken down on two fronts. Behind the first front, which is the discontinuity moving with the velocity of elastic deformations, a pressure growth occurs in each particle to the value reached with the first compression. On the second front, appearing as a strong discontinuity which is propagated with the velocity of elastic-plastic deformations, a pressure jump takes place to the maximum value.

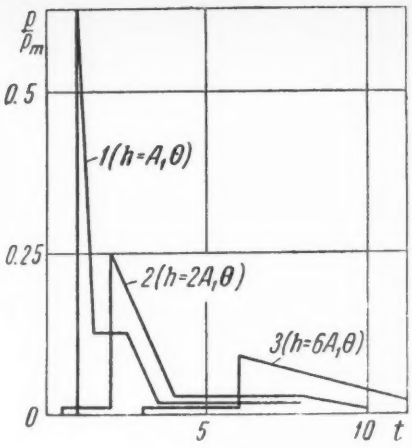

Fig. 3

Let us consider the reflection of compression waves, determined by Eqs. 2.9 and 2.13, from boundary $T$ with another elastic-plastic medium having a greater compressibility.

The coordinate of the medium boundary is $h^*$.

All magnitudes, belonging to the second medium, will henceforth be designated by a prime. Let us assume that $A'_0 < A_0$, $A'_1 < A_1$ and $p'_s > p_s$.

At the moment $t^* = h^*/A_0$, the elastic wave front reaches $T$. The elastic compression wave begins to propagate along the second medium and the rarefaction wave along the first medium (regions 1 and 3 on Fig. 4). The equation for the compression wave front is

$$h = A'_0 t + [(A_0 - A'_0)/A_0]h^* \qquad [3.2]$$

The equation for the rarefaction wave front (boundary of regions 1 and 3) is

$$h = -A_0 t + 2h^* \qquad [3.3]$$

This line is a continuity, since all states are propagated with an identical velocity where there is a linear relationship $p = p(V)$.

The flow in regions 1′ and 3 is determined from the following conditions: It is equal on the boundary of media $p$ and $u$, in both regions; on the compression wave front $p - A'_0 u = 0$; on the boundary of regions 3 and 1, by virtue of Eq. 2.3, $p + A_0 u = p_s + A_0 u_s = 2p_s$.

Hence, the solution in regions 1′ and 3 have the form

$$p = \frac{2A'_0}{A_0 + A'_0}p_s \qquad u = \frac{2p_s}{A_0 + A'_0} \qquad [3.4]$$

The relationship of the pressure in reflected wave 3 and in incident wave 1 (reflection coefficient) is

$$\eta = 2A'_0/(A_0 + A'_0) \qquad [3.5]$$

When the rarefaction wave front encounters the elastic-plastic wave front $S$, regions 4 and 5 form. In region 4, $p = p_s$, and the function $F_2$ is the same as in region 3.

The solution in region 4 is

$$p = p_s \qquad u = [(3A_0 - A'_0)/A_0(A + A'_0)]p_s \qquad [3.6]$$

The particle velocity in region 4 is greater than in regions 1 and 3.

The expression $p + A_1 u$ is maintained on the boundary of regions 2 and 5, while the expression $p - A_1 u$ is maintained

on the boundary of regions 5 and 4. Hence, the solution in region 5 is

$$p = p_m - \frac{2A_1(A_0 - A'_0)p_s}{(A_0 + A_1)(A'_0 + A_0)} + \frac{A_0^2 + A_1^2}{2A_0^2A_1}\frac{p_m h}{\theta} - \frac{p_m t}{\theta}$$

$$u = \frac{p_m}{A_1} + \frac{A_0^3 + A_0A_1^2 - 3A_1^2A'_0A_0^2A'_0}{(A_0 + A_1)(A_0 + A'_0)A_0A_1}p_s + \frac{p_m h}{A_0^2\theta} - \frac{A_0^2 + A_1^2}{2A_0^2A_1}\cdot\frac{p_m t}{\theta} \quad [3.7]$$

The pressure and velocity in regions 5 and 2 differ only by the constant terms. The pressure is greater and the particle velocity smaller in region 2 than it is in region 5. This is manifested by the influence of elastic wave reflection from $T$ on the flow behind the elastic-plastic wave front. Jumps in pressure and velocity occur on the boundary of 2 and 5.

When there is a reflection of the elastic compression wave, determined by the equations in 3.6, from $T$ a new rarefaction wave emerges which proceeds in the opposite direction and once more reflects from the elastic-plastic wave front $S$. Wave reflection would continue until $S$ approaches $T$. When there are numerous reflections, a series of regions form 6, 7, 2' . . ., which adjoin front $S$ or boundary $T$. Their solutions are found as are the solutions in regions 3, 4 and 1'.

At the moment front $S$ approaches boundary $T$, elastic and elastic-plastic compression waves emerge in the second medium (regions $C$ and $B$ in Fig. 4), and a rarefaction wave in the first medium (region $A$). It is assumed that the pressure on the medium boundary exceeds $p'_s$.

The solution in region $C$ would be

$$p = p'_s \qquad u = p'_s/A'_0 \quad [3.8]$$

The equation for the rarefaction wave front (discontinuity) has the form

$$h = -A_0t + [(A_0 + A_1)/A_1]h^*$$

We seek the solution in region $B$ in the form

$$\Phi_1 = \alpha_1 + \beta_1(h - A'_0t) \qquad \Phi_2 = \alpha_2 + \beta_2(h + A'_0t)$$

and in the region $A$ in the form

$$F_1 = a_1 + b_1(h - A_0t) \qquad F_2 = a_2 + b_2(h + A_0t)$$

The first boundary condition is: When $h = h^*$, the pressure and the particle velocity in both media are equal

$$\Phi_1 + \Phi_2 = F_1 + F_2 \qquad \frac{1}{A'_0}(\Phi_1 - \Phi_2) = \frac{1}{A_0}(F_1 - F_2) \quad [3.9]$$

The second boundary condition is: On the elastic-plastic compression wave front in the second medium

$$\Phi_1 + \Phi_2 - (A'_1/A'_0)(\Phi_1 - \Phi_2) = p'_s - A'_1u_s \quad [3.10]$$

The third boundary condition is: Function $F_1(h - A_0t)$ passes through the rarefaction wave front in the first medium without any changes. Inasmuch as $F_1(h - A_0t)$ does not change at all discontinuities which move with velocity $A_0$, $F_1(h - A_0t)$ must be the same in region $A$ as in region 2. Thus, $a_1$ and $b_1$ are known.

Equating the coefficients in Eqs. 3.9 and 3.10 with identical powers of $t$, we obtain another six equations for determining the six coefficients $a_2$, $b_2$, $\alpha_1$, $\alpha_2$, $\beta_1$ and $\beta_2$. The solutions in regions $A$ and $B$ are, correspondingly

$$p = F_1 + F_2 \qquad u = (1/A_0)(F_1 - F_2)$$

$$p = \Phi_1 + \Phi_2 \qquad u = (1/A'_0)(\Phi_1 - \Phi_2) \quad [3.11]$$

The pressure in regions $A$ and $B$ drops in the course of time.

When the rarefaction waves (regions 5, 8, etc.) reflect from section $h = 0$, compression waves form which, in their turn, reflect from section $h = h^*$ in the form of rarefaction waves. In all of the formed regions, the solutions can be obtained similarly.

If the pressure on boundary $T$ does not exceed $p'_s$ when the elastic-plastic wave front $S$ approaches, then the elastic-plastic wave $B$ does not form. As before, function $F_1(h - A_0t)$ in region $A$ is the same as in region 2. Let us designate $\Phi_1$ and $\Phi_2$ as arbitrary functions which determine $u$ and $p$ in region $C$. It follows, from performance curve conditions, bounding region $C$ in the second medium, that

$$\Phi_2 = \tfrac{1}{2}(p - A'_0u) = 0$$

In order to determine the four constants in two functions

$$F_2 = a_2 + b_2(h + A_0t) \qquad \Phi_1 = \alpha_2 + \beta_2(h - A'_1t)$$

we have two equations, expressing the equality of $u$ and $p$ at boundary $T$. Having equated the coefficients where there are identical powers of $t$, we obtain four equations. Thus, the problem was solved completely. In Fig. 5, the relationship $p = p(h)$ is shown for the moments of time, designated as $t_1$ and $t_2$ on Fig. 4.

When $h = h^*$, let the examined medium border on the other elastic-plastic medium, in which $A'_0 > A_0$, $A'_1 > A_1$ and $p'_s > p_s$.

When the elastic wave front reaches $T$, compression waves begin to propagate from the boundary on both sides (in the first medium, with a velocity of $A_1$ and in the second medium

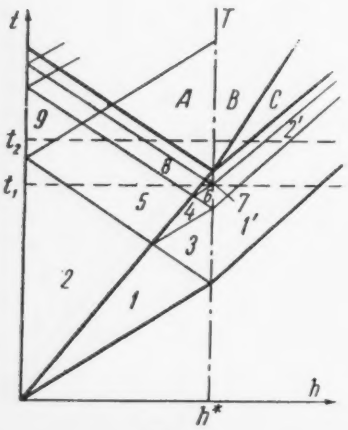


Fig. 4

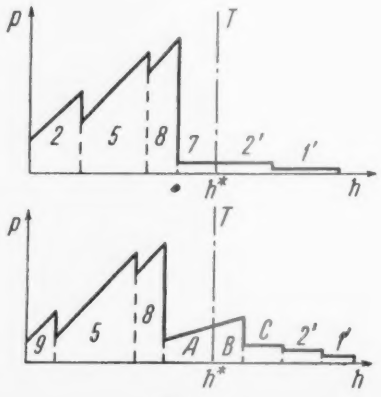


Fig. 5

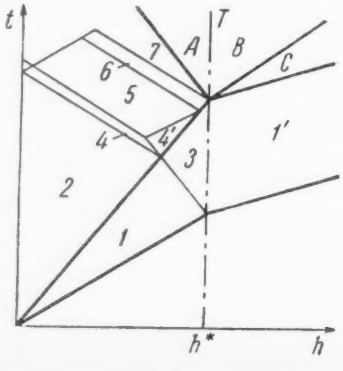


Fig. 6

with a velocity of $A'_0$). The pressure and particle velocity in regions 3 and 1′ (Fig. 6) are equal and constant and are determined from the conditions on these wave fronts

$$p - A'_0 u = 0 \quad \text{when} \quad h = A'_0 t + h^* \left(1 - \frac{A'_0}{A_0}\right)$$

$$p + A_1 u = p_s \left(1 + \frac{A_1}{A_0}\right) \quad \text{when} \quad h = -A_1 t + h^* \left(1 + \frac{A_1}{A_0}\right)$$

Hence, the solutions in regions 3 and 1′ are

$$p = \frac{(A_0 + A_1)A'_0}{(A'_0 + A_1)A_0} p_s \qquad u = \frac{A_0 + A_1}{A_0(A'_0 + A_1)} \qquad [3.12]$$

At point

$$h = \frac{A_0 + A_1}{2A_0} h^* \qquad t = \frac{A_0 + A_1}{2A_0 A_1} h^*$$

the reflected wave front encounters the front $S$. Two discontinuities emerge. Behind the first (weak), moving at velocity $A_0$, a pressure growth occurs to the elastic limit for each particle. On the second discontinuity, moving at velocity $A_1$, a pressure jump occurs for the elastic limit. The flow in region 4 is determined from the conditions that the expression $p + A_0 u$ is maintained on the boundary with region 2 while on the boundary with region 4′ the pressure reaches the elastic limit for each particle

$$p = p_m[1 - (A_0^2 - A_1^2)h/2A_0^2 A_1\theta]$$

Hence, the solution in region 4 is

$$p = p_m \left[1 + \frac{(A_0 + A_1)^2 h^*}{A_0 A_1 (A_0 - A_1)\theta} + \frac{(A_0 + A_1)(A_0^2 + 2A_0 A_1 - A_1^2)h}{2A_0^2 A_1 (A_0 - A_1)\theta} + \frac{A_0 + A_1}{A_0 - A_1} \cdot \frac{t}{\theta}\right]$$

$$u = \frac{p_m}{A_0}\left[\frac{A_0}{A_1} + \frac{(A_0 + A_1)^2 h^*}{A_0 A_1 (A_0 - A_1)\theta} - \frac{(A_0 + A)h}{A_0(A_0 - A_1)\theta} - \frac{(A_0 + A_1)(A_0^2 + 2A_0 A_1 - A_1^2)t}{2A_0 A_1 (A_0 - A_1)\theta}\right] - \frac{A_0 - A_1}{A_0 A_1} p_s \qquad [3.13]$$

The medium is unloaded in region 4′; expression $p - A_1 u$ is maintained on the boundary with region 3, and the expression $p + A_1 u$ on the boundary with region 4. Hence, the solution in region 4′ is

$$p = p_m \left[1 + \frac{(A_0^2 - A_1^2)h^*}{4A_0^2 A_1 (A_0^2 + A_1^2)\theta} + \frac{(A_0 + A_1)h}{2A_0^2 \theta} - \frac{(A_0 + A_1)A_1 t}{(A_0^2 + A_1^2)\theta}\right] + \frac{A_1(A'_0 - A_0)}{A_0(A'_0 + A_1)} p$$

$$u = \frac{p_m}{A_0}\left[\frac{A_0}{A_1} - \frac{(A_0^2 - A_1^2)^2 h^*}{4A_0 A_1^2 (A_0^2 + A_1^2)\theta} + \frac{(A_0 + A_1)A_1 h}{(A_0^2 + A_1)^2 A_0 \theta} - \frac{(A_0 + A_1)t}{2A_0\theta}\right] - \frac{A_0 A'_0 - A_1^2}{A_0 A_1 (A'_0 + A_1)} p_s \qquad [3.14]$$

Let the pressure jump become equal to zero at some point of the boundary for regions 4 and 4′. Then, the second discontinuity ceases to exist and region 5 is formed, bound by the two characteristics in which medium unloading takes place. The flow in region 5 is determined from the conditions that here the functions $F_2(h + A_0 t)$ is the same as in 4′, whereas the function $F_1(h - A_0 t)$ is the same as in 2.

When front $S$ reaches the boundary of regions 5 and 4′, a region 6 forms in which the function $F_1(h - A_0 t)$ is the same as in region 2, whereas the expression $p - A_1 u$ is maintained on the boundary with region 3. The solution in region 6 is

$$p = p_m \left[1 + \frac{(A_1^2 + A_0^2)h}{2A_0^2 A_1 \theta} - \frac{t}{\theta}\right] + p_s \frac{2A_1(A'_0 - A_0)}{(A_0 + A_1)(A_1 + A'_0)}$$

$$u = \frac{p_m}{A_0}\left[\frac{A_0}{A_1} + \frac{h}{A_0\theta} - \frac{(A_0^2 + A_1^2)t}{2A_0 A_1 \theta}\right] - \frac{p_s}{A_0}\left[\frac{A_0^2}{(A_0 + A_1)A_0} + \frac{A_1(A'_0 - 2A_0 - A_1)}{(A_0 + A_1)(A_1 + A'_0)}\right] \qquad [3.15]$$

At the moment of time $t = h^*/A_1$, the front $S$ reaches the boundaries of the media $T$. Further, an elastic and elastic-plastic compression wave emerges in the second medium, while two reflected compression waves emerge in the first medium with front discontinuities and moving at velocities of $-A_0$ and $-A_1$ (Fig. 6). The pressure behind the first (weak) discontinuity grows to the elastic limit of each particle. Function $F_1(h - A_0 t)$ in region 7 is the same as in 2, whereas the pressure on the boundary with region $A$ is equal to the elastic limit. The solution in region 7 has the form

$$p = p_m \left[1 + \frac{2(A_1 + A_0)h^*}{(A_1 - A_0)A_1\theta} + \frac{(A_1 + A_0)(A_1^2 - A_0^2 - 2A_0 A_1)}{2A_0^2 A_1 (A_1 - A_0)\theta} h - \frac{(A_1 + A_0)t}{(A_1 - A_0)\theta}\right] + p_s \frac{2A_1(A'_0 - A_0)}{(A_1 + A_0)(A_1 + A'_0)}$$

$$u = \frac{p_m}{A_0}\left[\frac{A_0}{A_1} - \frac{2(A_1 + A_0)h^*}{(A_1 - A_0)A_1\theta} + \frac{(A_1 + A_0)h}{A_0(A_1 - A_0)\theta} - \frac{(A_1 + A_0)(A_1^2 - A_0^2 - 2A_0 A_1)t}{2A_0 A_1 (A_1 - A_0)\theta}\right] - \frac{p_s}{A_0}\left[\frac{A_0 - A_1}{A_1} + \frac{2A_1(A'_0 - A_0)}{(A_1 + A_0)(A'_0 + A_1)}\right] \qquad [3.16]$$

The flow in regions $A$ and $B$ is determined from the conditions: The expression $p + A_0 u$ is maintained on the boundary with region 7; the pressure and particle velocity on boundary $T$, in both media, are equal, and the expression $p - A'_1 u$ is maintained on the elastic-plastic wave front in the second medium.

Where the first medium borders with an incompressible medium, the solution in region $A$ has the form

$$p = p_m \left[2 + \frac{(A_0 + A_1)[(A_0^2 + A_1^2)A_1 - (A_1 - A_0)^2 A_0]h^*}{A_0^2 A_1 (A_0^2 + A_1^2)\theta} - \frac{2A_1(A_0 + A_1)t}{(A_0^2 + A_1^2)\theta}\right] - \frac{(A_1 - A_0)^2 p_s}{A_0(A_0 + A_1)}$$

$$u = p_m \frac{2A_1(A_0 + A_1)(h - h^*)}{A_0(A_0^2 + A_1^2)\theta} \qquad [3.17]$$

The configuration of the reflected wave system depends on the values of magnitudes $\theta$, $h^*$, $A_0$, $A_1$, $p_m$ and $p_s$. For example, if $p_s$ and $\theta$ are relatively large, then the boundary of regions 4′ and 5 intersects directly with the boundary of region 7.

The expressions for the elastic limit of particles in region 2, 4′ and 6 are different. Therefore, discontinuities arise in the density, fixed in the coordinate system $h,t$ and a series of new fields emerge, which were not noted in Fig. 6. Solutions in regions 7 and $A$, determined by Eqs. 3.16 and 3.17, were obtained for particles in direct proximity to the walls, passing through the discontinuities on the boundary of regions 3 and 6.

If $p_s$ is substantially less than $p_m$, the interaction of the reflected elastic wave (region 3) with the incident elastic-plastic wave can be neglected. Then, region 7 borders on

region 2, and the solutions in regions 7 and 4 are determined by expressions 3.16 and 3.17, respectively, in which the terms containing $p_s$ are absent.

In the foregoing, the cases considered were of the propagation and interaction of waves when the pressure had not reached the value of $p_k$ (Fig. 1); above that point the loading, unloading and secondary loading lines of the linear diagram $p(V)$ coincide. If $p_m > p_k$ in section $h = 0$ then, following the elastic wave where $p = p_s$ and $u_s = p_s/A_0$, a shock wave would be propagated; its front velocity changes from $\sqrt{(p_m - p_s)/(V_s - V_m)}$ when $t = 0$ to $\sqrt{(p_k - p_s)/(V_s - V_k)} = A_1$ at that moment of time when the pressure on the front declines to $p_k$. The propagation of a similar wave and its reaction with a fixed obstacle was examined earlier (8).

The authors would like to express their gratitude to B. A. Olisov, Kh. A. Rakhmatulin, and L. I. Sedov for their consideration of this work.

—*Submitted August 31, 1959*

## References

1 Rakhmatulin, Kh. A., "The Propagation of Unloading Waves," *Prikladnaia Matematika i Mekhanika* (*J. Appl. Math. and Mech.*), 1945, vol. 9, no. 1.

2 Rakhmatulin, Kh. A., "The Propagation of Unloading Waves Along a Rod with a Variable Elastic Limit," *Prikladnaia Matematika i Mekhanika* (*J. Appl. Math. and Mech.*), 1946, vol. 10, no. 3.

3 Shapiro, G. S., "Longitudinal Vibrations of Rods," *Prikladnaia Matematika i Mekhanika* (*J. Appl. Math. and Mech.*), 1946, vol. 10, nos. 5 and 6.

4 Lebedev, N. F., "The Propagation of Unloading Waves Where Linear Hardening Exists," *Prikladnaia Matematika i Mekhanika* (*J. Appl. Math. and Mech.*), 1951, vol. 15, no. 5.

5 Ponomarev, S. D., Biderman, V. L. et al., "Bases of Modern Methods of Strength Computations in Machine Construction," Mashgiz (State Scientific and Technical Publishing House of Literature on Machinery), 1950.

6 Lee, E., "A Boundary Value Problem in the Theory of Plastic Wave Propagation," *Quart. Appl. Math.*, 1953, vol. 4, no. 10.

7 Kaliski, S. and Osiecki, J., "Unloading Wave for a Body with Rigid Unloading Characteristic," *Proc. Vibration Problems*, 1959, no. 1, Warsaw.

8 Liakhov, G. M. and Poliakova, N. I., "Method of Approximating Shock Waves and Their Interaction," *Izvestiia Akad. Nauk SSSR, OTN, Mekhanika i Mashinostroenie* (*Bull. Acad. Sci. USSR, Mechanics and Machine Construction*), 1959, no. 2.

## Reviewer's Comment

This paper deals with the propagation of dilatational waves in an elasto-plastic solid. The nature of the propagation, the effect of waves of unloading, and the interaction between compression and unloading waves are considered, and the reflection of plastic waves at the interface between two elasto-plastic solids is also treated. The reviewer believes the main weakness of the paper to lie in the ill-defined physical properties of the medium which are postulated. Thus it is assumed that the material is elastic up to a given stress and above this stress two different linear relations apply, one for loading and the other for unloading. The stresses considered, however, are hydrostatic stresses, and the relations between pressure and volume appropriate to fluid dynamics are employed. This is justifiable for solids at pressures very large compared with the shear strength of the material, but plastic deformations are then not relevant, since the material behaves in a fluid manner for both loading and unloading. The references given to other work in this field are rather inadequate, and for this, reference should be made to the review paper by Cristescu (1) to the book by Goldsmith (2) and to a forthcoming article by Craggs (3).

—Herbert Kolsky
Applied Mathematics Div.
Brown University

## References

1 Cristescu, N., in *Plasticity*, E. H. Lee and P. S. Symonds, Eds., Pergamon Press, 1960, pp. 385–442.

2 Goldsmith, W., *Impact*, Edward Arnold, London, 1960.

3 Craggs, J. W., "Plastic Waves," in *Progress in Solid Mechanics*, Vol. 2, North Holland Publishing Co., 1961.

# Transistor Phase-Sensitive Amplifier

CH. S. AGALAROV

An automatic control system often contains an amplifier in which the plate circuits are fed with an alternating voltage. The mean current in the load is proportional to the input voltage, whereas the direction of the current depends on the phase; the amplifier is phase-sensitive. Such amplifiers are much used, particularly in servo electric drives (2,3);[1] they may be made cheaper and more reliable by substituting transistors for the vacuum tubes. In some cases such an amplifier is required to amplify an a-c signal whose frequency is that of the line and also a d-c (slowly varying) signal. The sense of the load current must bear a definite relation to the phase of the a-c signal and to the sign of the d-c signal, as in a servo whose error detector produces an a-c signal and which has a d-c operated effector stabilized by d-c feedback.

Fig. 1 shows a circuit satisfying these requirements. The diodes $D_1$ to $D_5$ prevent the current from flowing in both directions in the collector circuits. The load receives a current whose direction is controlled by the phase of the a-c signal

Translated from *Izvestiia Akademii Nauk Azerbaidzhanskoi SSR, Seriia Fiziko-Matematicheskikh Nauk* (*Bull. Azerbaijan Acad. Sci., Physico-mathematical and Technical Sciences Series*), 1959, no. 5, pp. 127–134. Translated by Research Information Service, New York.

[1] Numbers in parentheses indicate References at end of paper.

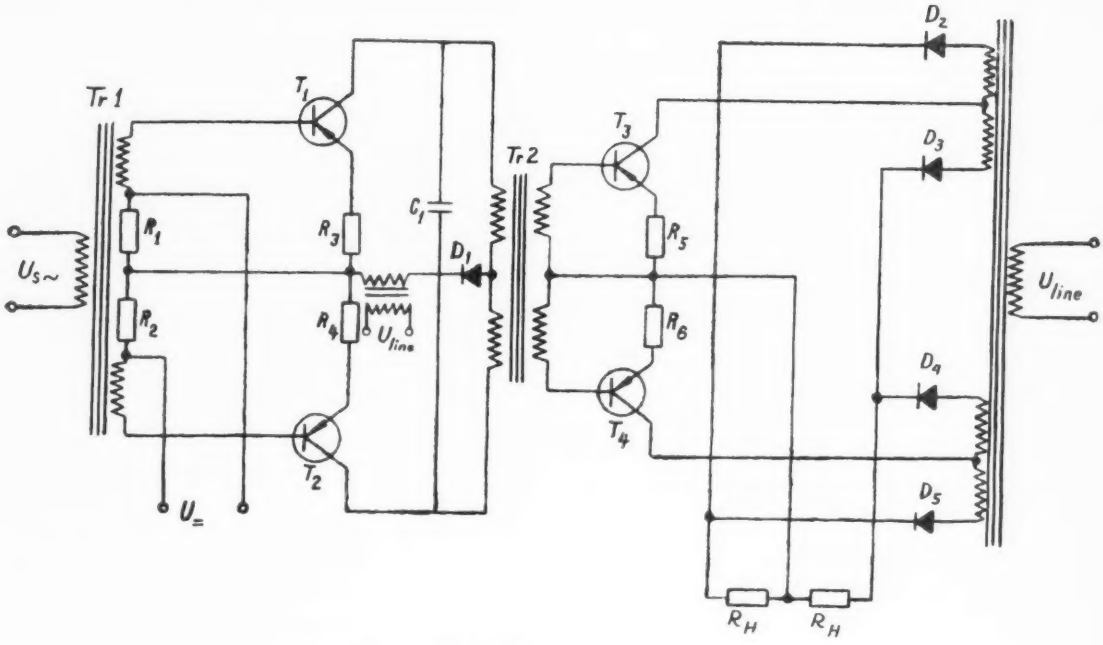


Fig. 1 Circuit of phase-sensitive amplifier

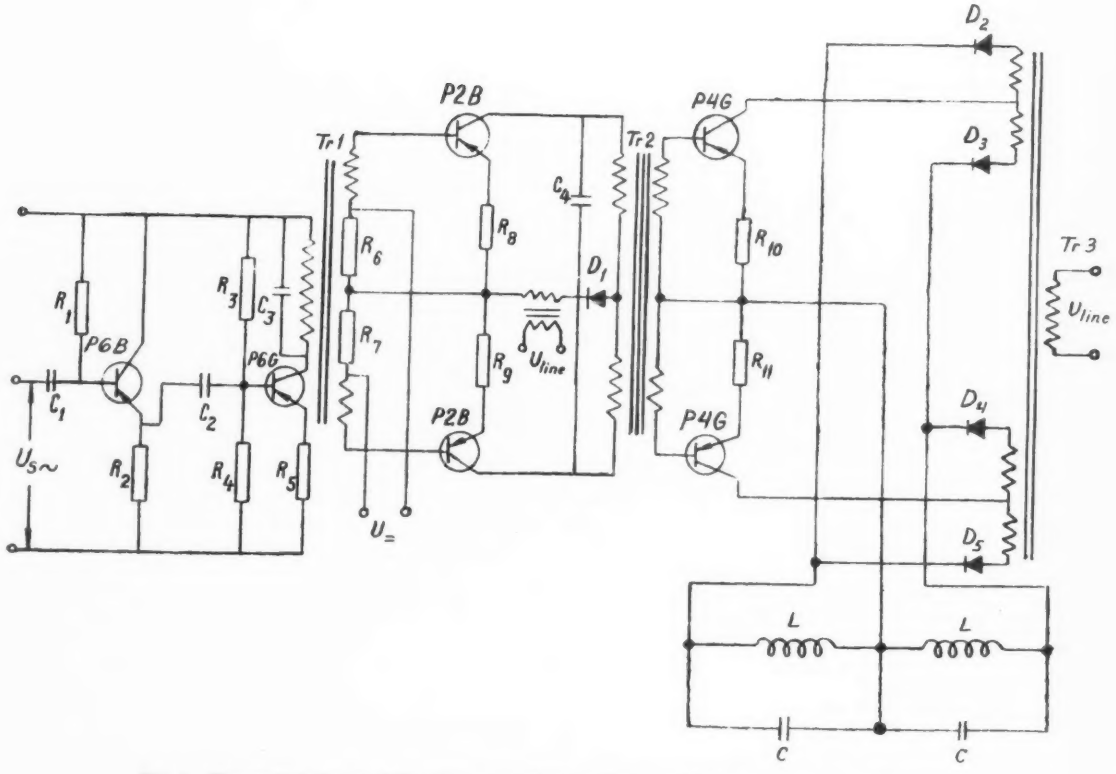


Fig. 2 Theoretical circuit of the phase-sensitive amplifier used in an automatic control system

and by the sign of the d-c signal, and whose magnitude is determined by the algebraic sum of the amplitudes. That current is governed by the difference of the reverse currents in the diodes, not by the initial reverse currents of the collector junctions, when the signals are zero. A proper choice of component values insures that the collector circuit does not become open while the emitter circuit still carries a current. The circuit provides a large power gain.

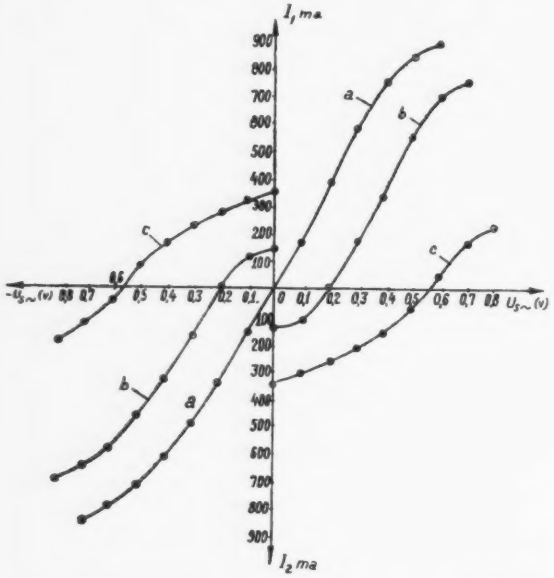


Fig. 3 Output current of the amplifier (Fig. 2) as a function of a-c signal

## Calculation of Phase-Sensitive Amplifiers

The large signal parameters may be used here; Konev (3) gives the basic relationships needed for this purpose. A specified load current can be provided for if we know $R_{ib}$, the input impedance of the transistor in the common-base connection, and $\alpha_T$, the total static current gain, which is the ratio of the total change of collector current (from $I_{c0}$ to $I_c$) to the total change of emitter current (from zero to $I_e$)

$$\alpha_T = (I_e - I_{c0})/I_e$$

It is usual to specify the load resistance and the required difference in the mean currents, $I_1 - I_2$. The line voltage required in one section of the transformer winding in order to provide that difference in a full-wave circuit is

$$U_{line} \approx 1.11(I_1 - I_2)R_L + (R_{ib} + R_e)/\alpha + U_c \qquad [1]$$

where

$R_e$ = external resistance in the emitter circuit
$U_c$ = collector-to-base voltage at maximum collector current

The current is known, as is the reverse voltage on the collector, namely $U_{ct} = U_{line}\sqrt{2}$, so the transistor needed can be selected. The maximum power dissipated at the collector of a transistor is

$$P = 0.16U/R_H \qquad [2]$$

and must not exceed the limit set for that kind of transistor. The signal voltage needed to produce the specified load current is

$$U_s = 0.707I_{ct}(R_{ib} + R_e)/\alpha_T \qquad [3]$$

in which $I_{ct}$ is the amplitude of the collector current. The input impedance of the stage is

$$R_i = (R_{ib} + R_e)/(1 - \alpha_T) \qquad [4]$$

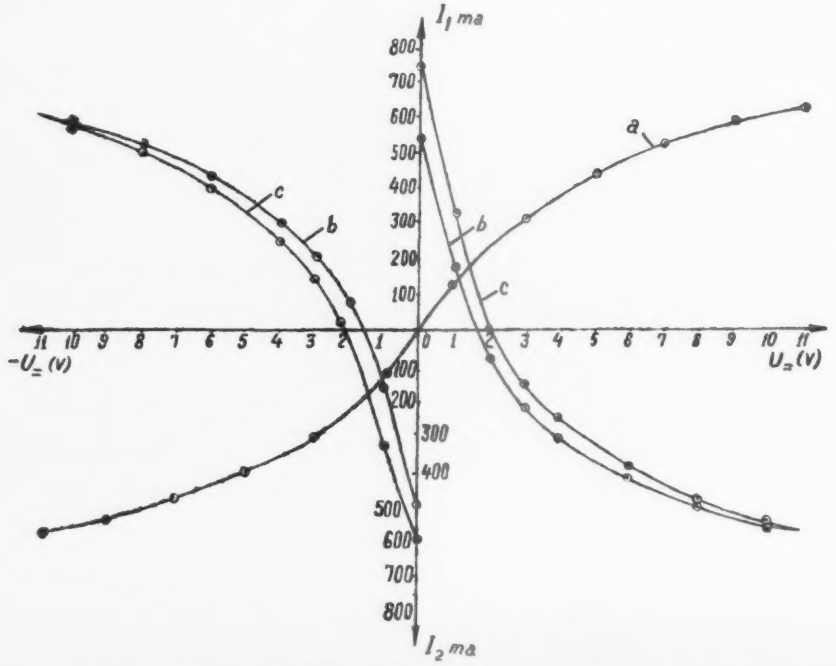


Fig. 4 Output current of the amplifier (Fig. 2) as a function of d-c signal

and the power gain is

$$K_p = 0.81\alpha_T^2 R_H/(1 - \alpha_T)(R_{ib} + R_s) \qquad [5]$$

These equations apply for a load consisting of an inductor whose resistance is $R$, and of a capacitance sufficient to remove a large fraction of the ripple from the load current.

## Experimental Results

The four-stage amplifier (Fig. 2) was designed for use in an automatic load control for a drill used to make oil boreholes. The input stage uses a P6V transistor in the common-collector connection. That connection provides an input impedance of about 60 kΩ, which is fairly high for a transistor a-c amplifier; a high value was needed to match the output impedance of the transducer. The second stage uses a P6G transistor and is a voltage amplifying stage. The third stage contains two P2B transistors and acts as a power preamplifier; it also provides the sensitivity to the sign of the d-c signal. The d-c negative feedback signal is taken to the junction of the two secondaries on transformer *Tr*.1, which couples the second stage to the third. The output stage is a phase-sensitive power amplifier containing two P4G transistors and is fed from the previous stage via transformer *Tr*.2. The amplifier feeds the control windings of an amplidyne, which have a resistance of 18.5 Ω and are shunted by capacitors.

Fig. 3, curve a, shows $I_1 - I_2$ as a function of $U_s\sim$, the a-c input signal, when the phase of that signal is 0 and 180 deg relative to the line voltage. The zero drift at the load is small, which eliminates any steady-state error in the servo. The out-of-balance current corresponding to zero input is 0.1 ma, which is negligible relative to the nominal control current of the amplidyne (220 ma, which is produced by an input of 0.13 v). The response remains linear up to nearly four times the nominal current (880 ma, which is produced as the maximum current by inputs of 0.6 to 65 v). This insures that the transient response of the servo is good. The mutual conductance of the amplifier is 1.3 to 1.45 ma per mv; the maximum power supplied to the load is 14 w.

In Fig. 3, curves b and c show $I_1 - I_2$ as a function of $U_s\sim$ for d-c signals $U_=$ of 1 and 3 v. These signals were applied in the sense such that they reduced $I_1 - I_2$, as would occur in the presence of negative feedback. Fig. 4 shows $I_1 - I_2$ as a function of $U_=$ for $U_s\sim$ of 0, 0.3, and 0.4 v.

This amplifier has been tested in the drill-control system under various conditions; it provided the required performance.

## Thermal Stabilization

Compensation and stabilization are the two methods of providing required performance in the presence of temperature fluctuations. Compensation for temperature changes is produced by including in the circuit of the emitter or base an element whose resistance varies with temperature in such a way that the gain of the stage remains constant. Suitable elements are thermistors, germanium diodes and special ceramic resistors having negative temperature coefficients. The disadvantages here are that circuits utilizing temperature sensitive elements are difficult to analyze analytically and are difficult to adjust.

Stabilization gives satisfactory results for temperature rises of 40 to 50 C above normal. Shea's system is the one most often used; certain specified resistances are included in the circuit in order to stabilize the working point (4). Negative a-c feedback also gives good results; heavy negative feedback insures that the effective parameters are dependent on those of the feedback circuit rather than on those of the transistors. This method of stabilization also provides the advantage that no difficulty will be encountered if a transistor need be replaced. For example, 100% series negative feedback may be introduced into a common-collector stage, in which case the voltage gain of the stage becomes about 1 and is almost independent of the transistor parameters. The input impedance of the stage, subject to the condition $R \gg R_{ib}$, is

$$R_i = R_H/(1 - \alpha)$$

i.e., it depends very little on the parameters of the transistor. Tests show that this is so (1); $R_i$ is almost constant over a wide temperature range.

Further advantages of thermal stabilization are that it is simple to achieve, it permits analytical description, and makes transistors interchangeable; its main disadvantage is that the overall gain is reduced.

All stages in the amplifier were stabilized by negative a-c feedback; the working point of the second stage was stabilized by providing the bias to the base through a divider. The input stage had a constant input resistance by virtue of its common-collector circuit. Fig. 5 shows $I_1 - I_2 = f(U_s\sim)$ for three temperatures. The initial slope (up to $U_s\sim = 0.3$ v) increases with temperature between +10 and +55 C; the increase (relative to the slope at 10 C) is 7% for 30 C and 28% for 55 C. These changes are permissible in an automatic control system. The characteristics are the same for all temperatures for signals larger than 0.3 v. The maximum output current is unaffected; the out-of-balance error increases slightly with temperature (1.4 ma at 55 C) but remains insignificant for the purpose.

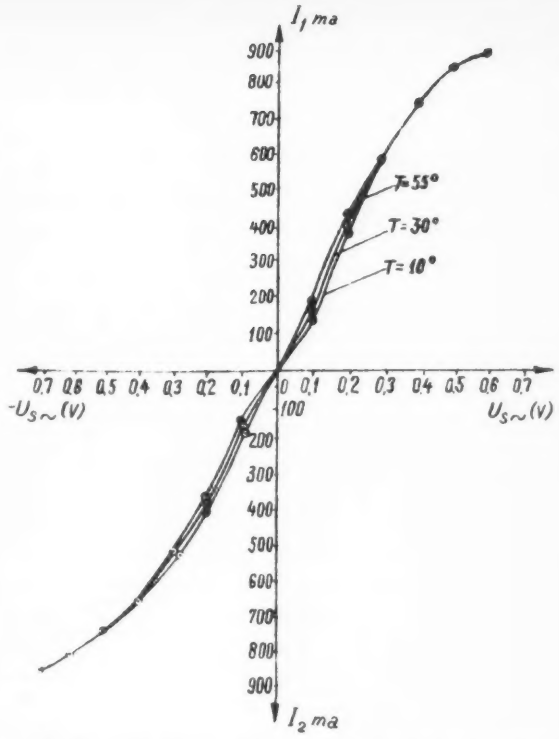


**Fig. 5 Response curves of amplifier for several temperatures**

## Summary

1 A description is given of a phase-sensitive amplifier that can be used in any automatic control system in which the mean values of two rectified currents are controlled as a function of low power a-c and d-c (slowly varying) signals.

2 The amplifier has very little zero drift; its slope is about 1.4 ma per mv, and the maximum power delivered to the load is 14 w.

3 The amplifier is fitted with means of stabilization against temperature changes and operates normally to 55 C.

I am indebted to M. G. Eskin for advice and discussions on this work.

## References

1 Akbulatov, A. Sh., "An Experimental Study of Temperature Compensation," *Semiconductor Devices and Their Uses*, Soviet Radio (Publisher) Moscow, 1956.

2 Konev, Yu. I., "Use of Transistors in Phase-Sensitive Circuits," *ibid.*

3 Konev, Yu. I., *Transistors in Automatic-Control Apparatus*, Soviet Radio (Publisher), Moscow, 1957.

4 Shea, R. F., *Transistors and Their Uses*, Gosenergoizdat, 1957.

## Reviewer's Comment

The output stage is a full-wave power phase detector, quite efficient by the necessary use of rectified a-c on the collectors. The driver stage makes use of half-wave rectified a-c applied to the collectors and the signal is smoothed out into a full sine wave by the associated capacitor and transformer primary. D-c feedback from possibly a tach generator is mixed with the input a-c signal by insertion in the driver base circuit.

The design of the power stages, although quite an efficient method of amplifying at a-c and converting to d-c by phase detection, is not new to American scientists, but does indicate a Russian application of this circuit using transistors. The method of mixing a d-c signal into the base biasing circuit has also been used before and is a convenient and simple way to mix where extreme linearity is not required. Under circumstances where extreme linearity is required, resistive input mixing of the two signals at d-c is usually required.

The schematics seem correct as printed. It would have been better for the author to have spent more time in the explanation of the curves in Figs. 3, 4, and 5, than in the design and stabilization of the first two amplifier stages which are quite straightforward in design.

—William O. Brooks
Space Technology Laboratories, Inc.

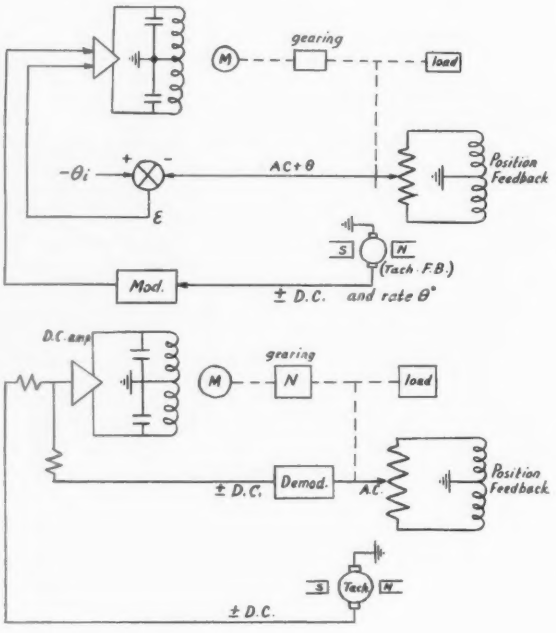

# Digest of Translated Russian Literature

The following abstracts have been selected by the Editor from translated Russian journals supplied by the indicated societies and organizations, whose cooperation is gratefully acknowledged. Information concerning subscriptions to the publications may be obtained from these societies and organizations. Note: Volumes and numbers given are those of the English translations, not of the original Russian.

## *BULLETIN OF THE ACADEMY OF SCIENCES USSR, GEOPHYSICS SERIES (Izvestiia Akademii Nauk SSSR, Seriia Geofizicheskaia).* Published by American Geophysical Union, Washington, D. C.

**No. 9, Sept. 1959.**

**Propagation of Elastic Waves in Layered Media. II,** G. S. Pod'yapol'ski, pp. 913–919.

*Abstract:* The paper continues the analysis of an arbitrary elementary wave begun elsewhere. An exact expression is adduced for an axisymmetric case and a general method is given for the determination of approximate expressions for the individual rapidly changing parts of the displacement field—the seismic waves.

**Intensity of Earth's Magnetic Field in the Historical and Geological Past,** E. Thellier and O. Thellier, pp. 929–949.

*Abstract:* The authors suggest here a method for investigating the remanent magnetization of ancient vases and bricks. These measurements were used for determining the intensity of Earth's magnetic field of times past during which the investigated objects acquired their magnetization. A consistent and steady decrease of Earth's magnetic moment during the past two thousand years becomes evident; in some regions this decrease reaches 65%. The methods proposed by the authors take into consideration all external influences during the magnetization process, and provide in particular, a way for eliminating the effect of repeated heating, the so-called "temperature cleaning" method.

**Problem of an Effective Recombination Coefficient in the Ionosphere,** B. A. Bagaryatsky, pp. 966–968.

*Abstract:* The article discusses the influence exerted by the reaction of an ionomolecular exchange on the magnitude of the effective recombination coefficient in the ionosphere. It is shown that the concentration $[N_2]$ represents a parameter which determines possible changes in the character of the recombination with altitude.

**Application of a Formula of Ostrogradsky to the Approximate Determination of the Mass of a Body,** V. A. Kazinski, pp. 1003–1004.

**Thermodynamics of Earth's Mantle,** B. N. Zharkov, pp. 1005–1009.

**Influence of Parameters of the Free-Molecular Flow of Rarefied Gas on the Instrument Readings During the Rocket Measurements of Density of the Higher Layers of the Atmosphere,** N. G. Belekhova, pp. 1012–1016.

*Introduction:* In this paper the relative movement of the container with the instruments in the free-molecular flow of rarefied gas, is discussed. Such a container furnished with various instruments, including the magnetic and ionizing manometers for measuring the density of the higher layers of the atmosphere, is a hollow cylinder, the hollow of which is connected with the outside medium by means of a number of "windows," uniformly situated along its side surface. In the case discussed, these "windows" are narrow slots parallel to the axis of the container. Obviously such a construction of the container influences the manometer reading to a greater degree than the construction with wide windows, described elsewhere.

*Conclusions:*

1 In the case of a free-molecular flow within the hollow of the container of the discussed construction, a state of balance between the number of flying in and flying out molecules is established quite rapidly (in less than 0.05 sec.).

2 Concentration of the inside molecules within the container can be computed with sufficient accuracy by formula 17, and with the aid of barometric formula 15 it can be simply related with the concentration of molecules $N$ of the surrounding medium.

3 The number of molecules getting into the opening of the manometer, placed inside of the container of described type, in a unit of time, is practically determined by concentration of the inside molecules in the hollow of the container and is computed by formula 27.

**No. 10, Oct. 1959.**

**Some Particular Solutions of the Problem of the Propagation of a Free Tidal Wave in a Channel of Varying Depth,** T. Ya. Sekerzh-Zen'kovich, pp. 1041–1044.

*Abstract:* The propagation of a free tidal wave in an infinite channel of constant width is investigated. It is assumed that the depth of the channel varies linearly from one bank to the other, the depth being zero at one bank and having some finite value at the other. The Coriolis force is taken into account in the solution. Particular solutions are obtained in the form of Tchebycheff-Laguerre polynomials, and these solutions are analyzed.

**Problem of the Speed of Spreading of Small Cosmic Material From the Upper Layers of the Atmosphere Downward,** A. A. Dmitriev, pp. 1045–1047.

*Abstract:* The spreading of very small particles of cosmic origin downward, by means of the turbulent mixing, is discussed. A scheme with the coefficient of turbulence of kinematic viscosity, increasing linearly with height, is used.

**Approximation of Magnetic Anomalies and Reductions by Interpolation Polynomials,** V. A. Kazinski, pp. 1067–1068.

*Introduction:* The polynomial method which has already been applied to the reduction and interpretation of subsurface and surface gravitation measurements can also be instrumental in the testing of models of the elements of a magnetic field.

## *BULLETIN OF THE ACADEMY OF SCIENCES USSR, PHYSICAL SERIES (Izvestiia Akademii Nauk SSSR, Seriia Fizicheskaia).* Published by Columbia Technical Translations, New York.

**Vol. 23, no. 8, 1959.**

**Formation of a High Frequency Discharge at Low Pressures,** G. N. Zastenker and G. S. Solntsev, pp. 925–930.

*Introduction:* In most investigations of electric discharges the fundamental characteristic of initiation of the discharge (breakdown) is assumed to be the ignition voltage. From the standpoint of elucidating the elementary processes involved in the development of discharges, knowledge of this parameter alone is insufficient. This explains a number of attempts to measure another parameter characterizing the onset of discharges, namely, the discharge formation time. Investigation of the discharge formation time involves observation of the time variation of the various parameters characterizing the state of the discharge gap.

The purpose of the present work was to investigate the formation of high frequency (3.3 mc) discharges in argon at pressures from 0.4 to 15 mm Hg.

*Conclusions:*

1 The developed experimental procedure is suitable for in-

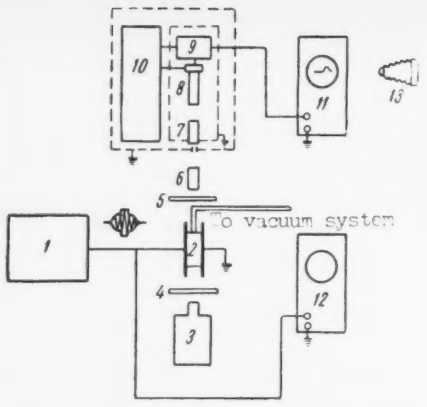


**Fig.1. Diagram of the experimental arrangement: 1) hf pulse generator, 2) discharge tube, 3) mercury tube, 4 & 5) light filters, 6 & 7) lenses, 8) photomultiplier, 9) cathode follower, 10) power supply, 11 & 12) oscillographs, 13) camera.**

vestigating the time variation of different parameters of a high frequency discharge (the voltage on the gap, the discharge current, and the luminous output of the gas) in the process of its formation.

2 The formation time of an hf discharge at low pressure (in the range of our experimental conditions) varies from 300 to 10 microsec with variation of the over-voltage from 5 to 60%.

3 The pressure dependence of the discharge formation time is similar to the pressure dependence of the ignition (breakdown) voltage.

4 Theoretical calculation of the duration of the initial stage of discharge development, during which the role of space charge is minimal, yields satisfactory agreement with the experimental data for pressures exceeding 9 mm Hg.

**Measurement of the Charge Concentration in Plasma by Means of Super-High Frequency Probes,** S. M. Levitskii and I. P. Shashurin, pp. 938–941.

*Introduction:* Within the last decade significant advances have been made in the investigation of gas discharges, owing to the introduction of a new microwave method, namely, the resonant cavity method. Without detracting from the recognized merits of this method, we want to mention some of its disadvantages.

1 To employ the resonant cavity method, the design of the discharge tube must be adapted to the design of the cavity, which may not always be possible or convenient.

2 In its simplest variant the method allows only of measuring relatively low electron concentrations ($\sim 10^9$ cm$^{-3}$). The method yields only the average charge concentration for the volume in which the plasma interacts with the microwave field.

3 Use of the interferometric method which is based on free transmission of radio waves through the plasma, largely eliminates the first two shortcomings, but in this case, too, the electron concentration obtained is an average value.

For local measurement of plasma parameters one can hardly propose any method not based on the introduction of some type of probe into the plasma. In order to retain the advantages of the microwave methods and at the same time obtain local values of charge concentration, the introduced probe must be an shf oscillating system with a locally concentrated electric field penetrating to a limited extent into the surrounding plasma. By immersing such a system into the discharge and observing its behavior, one can judge of the charge concentration in its vicinity.

By way of shf probes one can use such oscillating systems as various types of symmetrical and asymmetrical dipoles, a two-conductor (twin) line, etc. One should, naturally, give preference to systems in which the electric field is more concentrated and which are characterized by low emission.

In our work we used an asymmetrical dipole and a twin line.

**Effect of Disappearance of Negative Ions on Their Concentration in the Discharge Column,** M. V. Konyukov, pp. 960–963.

*Introduction:* The negative component of the plasma in the positive column of a discharge in electronegative gases (or in media with an appreciable admixture of such gases) consists of electrons and negative ions. The latter are apparently responsible for some of the distinctive characteristics of such discharges (anomalous gradients, the formation and subsequent behavior of striations, facilitated contraction of the column, etc.), and hence it may be of interest to calculate their concentration. The purpose of the present work was to evaluate the influence of the decay of negative ions on their concentration.

**Elementary Processes in the Ionization Zone of Corona Discharges at Atmospheric Pressure,** G. N. Aleksandrov, pp. 976–981.

**Broadening and Shift of Spectral Lines in Gas Discharge Plasma,** S. L. Mandel'shtam and M. A. Mazing, pp. 1005–1008.

*Introduction:* Measurement of the spectral line widths is one of the fundamental methods of determining the concentration of charged particles in plasma. Investigation of line broadening is also of independent physical interest inasmuch as in a plasma the radiating atoms are subjected to external influences that cannot be duplicated under other conditions: The atoms are under the influence of strong, inhomogeneous, rapidly varying fields. Theoretical analysis of the interaction of a radiating atom with the ambient fields leads to certain relationships between the line width $\gamma$ and the charged particle concentration $N$, i.e., the relationships that must be used in experimental determination of $N$.

In the present work, we carried out an experimental investigation of broadening under the influence of charged particles of lines exhibiting a quadratic Stark effect.

**Measurements of Electric Fields in a High Frequency Low Pressure Discharge by Means of an Electron Beam,** G. S. Solntsev, A. G. Porokhin and N. M. Chistyakova, pp. 1014–1018.

*Introduction:* The techniques of measuring electric fields in discharges by observing the deflection of an electron beam passing through the discharge has been used in a number of investigations of d-c glow discharges at low pressures. In a low pressure high frequency (hf) discharge the electric field at each point may be represented in the form of a superposition of two fields: the hf field $E_\sim$, produced by the hf oscillator supplying the discharge, and a d-c field $E_-$ due to distribution of space charges in the discharge gap. By shooting an electron beam through the hf discharge one can simultaneously determine $E_\sim$ and $E_-$ and investigate the distribution of the two fields along the discharge axis.

*Conclusions:*

1 The electron beam procedure, which we employed for investigating a high frequency, low pressure $E$ discharge, allows

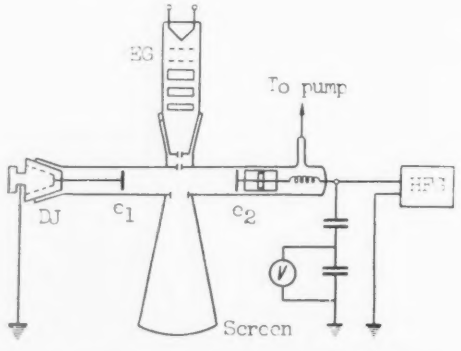


**Fig.1. Discharge tube and electron beam probe: EG - electron gun, $e_1$ & $e_2$ - electrodes, DJ - double joint, HFG - hf generator.**

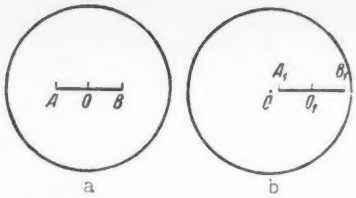


**Fig. 2. Picture observed on the fluorescent screen; a) with an hg voltage on the discharge tube electrodes but no discharge, and b) with a discharge.**

of simultaneous measurement of the hf field and the space charge field at different points in the discharge gap. The procedure has certain limitations and to obtain meaningful results for hf discharges certain specific requirements must be met.

2 In the present work there have been obtained for the first time data on the distribution of the electric field, potential and space charge in a high frequency discharge in argon at a pressure of $10^{-2}$ mm Hg for different instants during the hf voltage cycle.

**Vol. 23, no. 11, 1959.**

**New Data on a Slow Neutron Detector,** T. V. Timofeeva and S. P. Khormushko, pp. 1275–1277.

**Physical-Chemical Nature of Silver Activator in Zinc Sulfide Phosphors,** A. A. Cherepnev, pp. 1321–1327.

*Conclusions:*

1 The formation of luminescent ZnS:Ag is apparently connected with segregation of elemental silver, which is distributed through the system in dispersed form (as was earlier suggested to the case for copper in ZnS:Cu phosphors). Inasmuch as the silver in ZnS is initially present in the form of some compound, the process of its precipitation is accompanied by the separation of an anionic component; thus there are simultaneously formed luminescence centers and traps, characterized by blue emission and the low temperature thermostimulation peak.

2 The process of formation of solid ZnS phosphor proceeds primarily in the gaseous phase: The fluxes NaCl and $H_3BO_3$ are comparatively volatile. This determines the condition of building up of luminescence centers (emission, trapping and quenching centers). Here there occur the effects of precipitation in the solid phase, diffusion of the activators, and formation of their active states through "volatile" components as well as other physical-chemical processes. Owing to the presence of the solid system in all the technological stages, the reactions occurring in the formation of ZnS phosphors are topochemical (localized). Owing to the limited time of the heating operation, equilibrium states are not always attained.

3 Although the final states of the activators silver and copper are identical (dispersed elemental particles), the two activators exhibit differences as well as similarities. The similarity is evinced in the rapid falling off of the absorption curve from the maximum value and in weakening of the zinc band in the luminescence spectrum owing to displacement of the zinc by the activator metal. As regards dispersion and coagulation, however, silver behaves differently: Silver is segregated more easily than copper and is more stable. The difference between the peaks of the blue luminescence bands of zinc and silver is difficult to distinguish.

4 The specific characteristics of the two fluxes, NaCl and $H_3BO_3$, used in our experiments result in differences between the processes of formation of the phosphor crystals and between the behavior of activators (Cu, Ag and others) in the ZnS phosphor system. As a flux, NaCl promotes dispersion, chlorination and desulfurization; $H_3BO_3$ favors vitrification and elimination of ZnO by solution and formation of borates. Intensification of the phosphor formation process in the presence of $H_3BO_3$ with increasing temperature occurs primarily owing to dissociation of the activator sulfide; in the presence of NaCl, as compared with $H_3BO_3$, owing to the reactivity of the chloride such processes occur at lower temperatures.

5 The absence of luminescence when ZnS:Ag is heated in an atmosphere of hydrogen sulfide apparently occurs owing to formation of nonluminescent silver sulfide; in the case of preformation active luminescent centers appear at 1100 deg. The appearance of luminescence is due to the presence of oxidized products. These results are connected with the temperature dependence of the chemical equilibrium in the systems under consideration.

6 Particularly in view of the work of Kynev on ZnS:Cu phosphors, one cannot exclude the possibility that the luminescent agent in ZnS:Ag is silver sulfide in colloidal form. On the basis of our experimental data and the considerations set forth, however, we are inclined to believe that the active agent under the conditions of our experiments is dispersed elemental silver.

**Suitability of the Thiosulfate Procedure for Preparation of Zinc Sulfide for Synthesis of Phosphors,** M. I. Tombak, O. V. Popova, A. F. Komar and A. A. Bundel', pp. 1349–1355.

*Introduction:* At present zinc sulfide for the production of phosphors is prepared by precipitation of the ZnS from a water solution of zinc sulfate with hydrogen sulfide.

Guntz proposed a number of other procedures, not involving the use of $H_2S$, for preparing zinc sulfide; one of these—the thiosulfate procedure—was investigated in detail by Grillot. Investigation of the thiosulfate procedure is of considerable interest and value because the phosphors prepared from the product differ as regards properties from phosphors prepared from ZnS produced by the conventional procedure. Grillot explains this by the fact that the reaction product in the thiosulfate process is zinc disulfide rather than the usual monosulfide. The disulfide sulfur is uniformly distributed through the bulk of the product and is eliminated only at high temperature, which, in the opinion of Grillot, creates conditions favorable for complete reduction of all the oxygen compounds present in the batch.

Thus the distinctive characteristics of ZnS phosphors obtained by heating amorphous zinc sulfide prepared by the thiosulfate procedure are attributed by Grillot to complete absence of oxygen in the final phosphor, in contrast to phosphors obtained from the ordinary sulfide even after their deoxidation by $H_2S$.

Inasmuch as some of the points in Grillot's report appeared obscure to us, we undertook an investigation of the reaction of sodium thiosulfate with zinc sulfate and a study of the phosphors prepared of the resultant "zinc disulfide."

**Luminescence of Glasses Containing Cerium,** G. O. Karapetyan, pp. 1368–1371.

*Introduction:* Investigation of glasses activated by cerium is of considerable theoretical and practical interest inasmuch as these glasses exhibit an exceptional resistance to coloring by ionizing radiation. At the same time cerium is a luminescence activator and its behavior as such in glasses merits attention. Yet it is not feasible in general to extend to glass with cerium the data on the absorption and luminescence of allied systems, i.e., crystals and solutions containing Ce ions.

Investigation of the absorption and luminescence spectra of glasses containing Ce showed that the element may be present in either the trivalent or the tetravalent state. Each valence state is characterized by its own distinctive absorption spectrum. Change in the type of glass (phosphate, silicate or borate) affects the level of oxidation of the cerium and also leads to quantitative changes in the absorption and luminescence spectra.

It is known that only glasses containing cerium in the trivalent state luminesce. Transition of part of the cerium to the tetravalent state results in a substantial decrease in the intensity of luminescence. Some authors, including Ginther, report that with increase in the cerium concentration its absorption spectrum in crystals undergoes great modifications connected with the formation of aggregations or clumps of Ce ions.

The present communication is concerned with a number of concentration dependences in glasses activated by cerium. The glasses used in the experiment were characterized by high purity: The iron content did not exceed 0.005%. Carbon or ammonium salts were introduced into the initial batch in order to produce reducing conditions. The glasses were founded in quartz crucibles in an oil fired furnace.

The absorption spectra were measured on a Beckman spectrophotometer using samples 0.1 to 0.5-mm thick and then normalized to a sample thickness of 1 mm. The absorption spectra of cerium were obtained in the form of differential curves: The ordinates of the absorption spectrum of the glass without cerium were subtracted from the corresponding ordinates of the

absorption curve for the glass with cerium. The absolute luminescence efficiencies were measured by the sphere procedure on the photoelectric setup of V. A. Arkhangel'skaya. The total experimental error did not exceed 10% of the measured values.

**Improvement of the Color Rendition of "Fluorescent" Lamps,** R. A. Nilender, pp. 1377–1382.

**Vol. 23, no. 12, 1959.**

**Nuclear Reactions of Multiply Charged Ions With Carbon and Oxygen and Their Influence in Investigation of Coulomb Excitation,** D. G. Alkhazov, A. P. Grinberg, G. M. Gusinskii and I. Kh. Lemberg, pp. 1451–1457.

*Introduction:* Investigation of Coulomb excitation of high lying levels requires increasing the energy of the bombarding particles. The use of protons or $\alpha$-particles in such experiments leads to a sharp increase of the $\gamma$-background (particularly in the case of bombardment of low mass number nuclei) that arises due to reactions involving the formation of a compound nucleus. In principle, the intensity of the background $\gamma$-lines must decrease greatly if heavy ions are employed as the projectiles.

However, even in our first attempt to use 25 Mev nitrogen ions for excitation of high energy nuclear levels in Sn isotopes we encountered a background of $\gamma$-lines, the intensity of which was much greater than the expected intensity of $\gamma$-rays emitted as a result of Coulomb excitation.

For the purpose of elucidating the origin and character of this background $\gamma$-radiation we investigated the $\gamma$-spectra of over 40 different elements, their compounds and isotopes, arising as a result of bombardment by $C^{12}$, $N^{14}$, $O^{16}$, $Ne^{20}$ and $Ne^{22}$ ions. The $\gamma$-radiation was detected by means of a scintillation spectrometer consisting of a 40-mm diameter, 40-mm thick NaI(Tl) crystal coupled to an FEU-11 photomultiplier and a 50-channel pulse height analyzer. In these experiments we used the same "close geometry" as in our earlier work on the $\gamma$-rays emitted as a result of Coulomb excitation of nuclear levels. As before, the distance from the target to the face of the crystal was 2.7 mm. The $\gamma$-radiations were studied in the region from 0.1 to 2 Mev. The spectrometer was calibrated in energy by means of "standard" radioactive $\gamma$-sources.

By way of bombarding particles, we used the following ions accelerated in a cyclotron: 13.6 Mev $C^{12}$, 11 to 40 Mev $N^{14}$, 18.1 Mev $O^{16}$, 23.1 to 27.8 Mev $Ne^{20}$ and 25.6 Mev $Ne^{22}$.

**Inelastic Neutron Scattering by Odd Nuclei,** A. M. Korolev, pp. 1470–1474.

*Introduction:* Excitation of collective nuclear surface levels through direct interaction between the nucleus and an inelastically scattered neutron is ordinarily described in terms of the Bohr-Mottelson model. It is possible, however, that at resonant energies the neutron may remain for some time close to the nuclear surface, and then a metastable state, which is not a compound nucleus state, may form. We have included this mechanism in treating inelastic neutron scattering by spherical nuclei by Heitler's theory of damping.

In the present work we use the methods of our previous analysis to study inelastic neutron scattering by nuclei with half-integral spin. It was found that because of its complexity the problem can be solved only for weakly deformed nuclei and only taking into account excitation of the first two collective levels.

**Magnetic and Quadrupole Moments of Weakly Deformed Nuclei,** B. D. Konstantinov and A. M. Korolev, pp. 1480–1485.

*Introduction.* Bohr's generalized model of the nucleus is now commonly used to explain the experimentally observed magnetic and quadrupole moments of nuclei.

Several authors have used this model to treat these moments while taking account of the interaction of an odd nucleon with the nuclear surface. Investigations have been published both for strong and weak coupling. Nevertheless, there remain some questions, for instance, as to the validity of the adiabatic approximation in finding the energy levels and the contribution of two-phonon states to the magnetic and quadrupole moments. Although Choudhury has extended the investigation to three-phonon states with intermediate coupling, the analytic dependence of these quantities on the ground state quantum numbers of the nucleus has yet to be given.

The method used in the present work is essentially the same as that of Kerman and Choudhury. We shall investigate the magnetic and quadrupole moments of nuclei by approaching intermediate coupling from the direction of weak coupling and making use of the results of our preceding work, in which we obtained the wave functions and energy levels of odd nuclei. Nonadiabatic terms and two-phonon states are included in the calculation. Further, the influence of the odd "extra" nucleon on the magnitudes of the nuclear moments will be considered.

**Some Characteristics of New Photomultiplier Tubes,** A. G. Berkovskii, I. Ya. Breido, O. S. Korol'kova and L. G. Leiteizen, pp. 1498–1500.

*Introduction:* There have been developed two new photomultipliers for use in scintillation spectrometers. The FEU-35 photomultiplier has a 25-mm diameter cathode, a maximum diameter of 34 mm and an overall length of 108 mm. The tube has a 10-pin key-type base and no side leads.

The other photomultiplier has a cathode diameter of 38 mm, a maximum diameter of 48 mm and an overall length of 190 mm. Like the FEU-35 it has no side leads.

## *INDUSTRIAL LABORATORY (Zavodskaia Laboratoriia).* Published by Instrument Society of America, Pittsburgh.

**Vol. 25, no. 9, Sept. 1959.**

**Determination of Diffusion Coefficients in Polycrystals According to Concentration Curves,** V. T. Borisov, V. M. Golikov and G. V. Scherbedinskii, pp. 1115–1118.

*Introduction:* The present article describes a method of determining the volume $D$ and the boundary $D_l$ diffusion coefficients according to integral $\gamma$-radioactivity curves for the residue. This method can be applied in those cases where $\gamma$-radioactive isotopes are used in experiments and the concentration on the surface of specimens under investigation remains constant during diffusion annealing.

**Determination of the Diffusion Coefficient by the Method of Residual Gamma Activity,** V. Z. Krasil'shchik, I. L. Svetlov and M. B. Bronfin, pp. 1118–1121.

**Optical Method of Determining the Total Volume of Foreign Matter in Solid Bodies,** A. F. Naumov, pp. 1143–1145.

**Method for Determining the Saturated Vapor Pressure of Nonvolatile Substances,** G. I. Novikov, A. V. Suvorov and A. K. Baev, pp. 1148–1150.

*Introduction:* In our method the substance being tested is evaporated in a closed vessel in the atmosphere of a chemically inert gas, which acts as an elastic medium in transmitting the vapor pressure to a U-tube manometer placed outside the high temperature region. During this process, the vapor of the substance being investigated is forced to condense after entering the low temperature part of the apparatus. However, the rate of condensation is so slow that the equilibrium of evaporation will not be disturbed, provided that the transfer of the substance resulting from the evaporation in the hot part, and condensation in the cold part of the device, is eliminated.

**Determination of the Elastic Moduli of Heat Resistant Materials by the Dynamic Method at High Temperatures,** A. I. Kovalev and I. I. Vishnevskii, pp. 1154–1159.

*Introduction:* We developed a method for the high temperature measurement of dynamic elastic moduli of heat resistant materials, which permitted the simultaneous determination of the normal elastic modulus and of the shear modulus at each temperature point. This method has been used earlier by one of the authors of the present article in measurements of elastic properties of metallic materials.

**Apparatus for Determining the Thermal Expansion of Films and Fibers,** A. V. Sidorovich and E. V. Kuvshinskii, pp. 1179–1181.

*Introduction:* We have developed an apparatus designed for a quantitative linear dilatometric study of polymers in a $10^{-2}$ to $10^{-5}$ mm Hg vacuum under dynamic rigidly controlled temperature-time conditions over temperature ranges from 20–250 deg. This apparatus makes it possible to heat and to cool samples during measurement at constant rates varying from 0.5 deg/hr to 2 deg/min; it maintains a constant temperature during annealing to an accuracy of $\pm 0.2$ deg for several days, etc. While the samples are studied dilatometrically, they can also be weighed (in order to check and control the invariability of their contents while the experiment is being carried out).

**Automatic Measurement ot the Density of Flowing Liquids,** B. Z. Votlokhin, pp. 1184–1186.

**Vol. 25, no. 10, Oct. 1959.**

**Volumetric Determination of Microgram Quantities of Rare-Earth Elements,** V. I. Kuznetsov and L. A. Okhanova, pp. 1218–1221.

*Introduction:* After the separation of rare-Earth elements, by chromatography or some other method, the absolute quantities available may be very small, of the order of a few micrograms. It is difficult to determine such small quantities by the normal methods. Complexometric methods for the determination of rare-Earth elements are described in the literature. For this purpose, instead of trilon B, we have used citric acid and arsenazo indicator. The method developed for 10–20 $\gamma$ and upward of these elements, gave a mean error of 1–2% relative.

**Application of Polarography to the Identification of Plastics,** V. D. Bezuglyi and V. N. Dmitrieva, pp. 1235–1239.

*Introduction:* A number of methods of identifying plastics and other high-molecular compounds are described in the literature. However, they do not make it possible to determine the nature of these materials sufficiently rapidly and accurately. We set out to develop a polarographic method for use in determining different plastics quantitatively. Many of the monomers and also other destruction products, obtained by dry distillation of plastics, are reduced on a mercury dropping electrode and are characterized by definite half-wave potentials. Some of the depolymerization products are not reduced directly, but they may be converted into nitro-, nitroso- and halogen derivatives which are polarographically active and have definite polarographic characteristics. The values of the half-wave potentials of the dry distillation products and their derivatives for definite forms of plastic may be compared with the characteristics obtained by polarographic examination of analysis samples.

**Use of Hard X-Ray Radiation for Determining Residual Stresses,** M. Ya. Fuks and L. I. Gladkikh, pp. 1248–1252.

**Determination of the Gas Content in Liquids From the Change of Electrical Conductance,** K. E. Perepelkin, pp. 1265–1268.

*Introduction:* During the processes of removal of gas from liquids: Flotation, electrolysis, etc., it is necessary to know the amount of gas dispersed or dissolved in the liquid phase. A number of different methods has been suggested for determining the gas contained in liquids; they are, however, not universally applicable or not entirely satisfactory, while some of them exclude the possibility of remote or automatic measurement.

For determining the content of gases dispersed in a liquid, a method can be used which is based on the dependence of the properties of the dispersion system on the content of the dispersed phase (for example the electrical conductance), which has been considered earlier.

The known methods of determining the relationship between the resistivity of the dispersion systems and the content of the electrically nonconductive inclusions for measuring the gas content in the liquid were found to be unsuitable for the intended purpose since the exact value of the electrical conductivity of the medium must be known and also its constancy in time, which in some cases cannot be realized.

We therefore developed a new method, the dilatometric conduction method, which is based on the relationship between the gas content in the liquid (and, consequently its electrical resistance) and the absolute pressure in the system.

**Dynamic Method of Studying the Degassing Process,** B. I. Gorfinkel' and Yu. A. Arkhipov, pp. 1268–1271.

*Introduction:* A knowledge of the mechanism of the gassing processes is indispensable for solving many problems connected with the use of a vacuum. The nature and the speed of such processes determine the requirements imposed on the equipment used, and make possible the correct choice of parameters for the production processes.

The emission of gases by various bodies in vacuum was studied by a number of investigators. However, the necessity of studying fast, often highly unsteady processes calls for the use of techniques different from the usual static methods. The dynamic method was found to be the best in the study of unsteady processes.

This paper describes a dynamic method of investigation of the aggregate emission of gas.

**Rapid Method of Calculating the Damping Factor From Oscillograms,** R. I. Garber and Yu. G. Miller, pp. 1291–1292.

**Initial Amount of Dust in Work With Models of Dust Collecting Devices,** V. E. Maslov and Yu. L. Marshak, pp. 1317–1318.

*Introduction:* A simple and reliable method of studying the separation of aerosols in models of various dust collecting devices has been developed at the All-Union Institute of Calorics. According to this method, the catching surface is covered with a viscous liquid (for instance, vaseline). The amount of dust settled on the surface can be determined by various physicochemical methods.

**Method of Sampling Liquid Hydrocarbons,** A. G. Cheglikov, p. 1333.

*Introduction:* In transferring samples into low pressure gas meters, liquid gas, which is throttled after it is let out from the storage tank, is evaporated in a small heat exchanger. In this, a portion of heavy hydrocarbons can remain in liquid form. In further heating, the hydrocarbons evaporate and then partially condense in the gas meter.

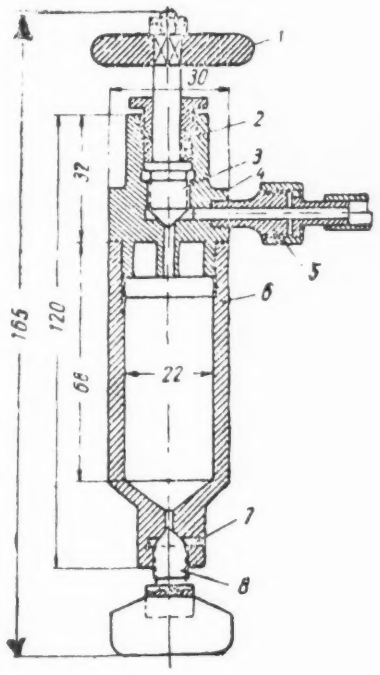


Diagram of the sampler. 1) Inlet valve; 2) packing gland; 3) inlet valve stem with the shuting cone; 4) cover; 5) inlet fitting; 6) frame; 7) check opening; 8) check valve.

We developed a device for the sampling of liquid hydrocarbons directly from the storage tank. The sample can be kept in the sampler for a long time and can be easily transported to the place of analysis. In filling the gas meter, the liquid hydrocarbons evaporate, and heavy hydrocarbons which do not evaporate at room temperature, remain in the sampler. They are measured and taken into account in the processing of analysis data.

***JOURNAL OF APPLIED MATHEMATICS AND MECHANICS (Prikladnaia Matematika i Mekhanika).* Published by Pergamon Institute, New**

**York, in conjunction with American Society of Mechanical Engineers.**

**Vol. 24, no. 3, 1960.**

**Problems of the General Theory of Plasticity,** A. A. Il'iushin, pp. 587–603.

*1. The isotropy postulate.* The general mathematical theory of plasticity is being developed primarily for solid bodies, whose material in the undeformed state is isotropic or quasi-isotropic (polycrystalline), obeys Hooke's law in the elastic region and in which the formation of plastic deformations is characterized by a plasticity condition which coincides with sufficient accuracy with the Huber-Mises condition (as, for example, the Tresca and other conditions, which replace the Mises surface by polygones which are close to it, etc.). For the sake of brevity such bodies will be called isotropic in the initial state.

In approaching the problem of stress-strain relations, which determine the basis of the theory, the various plasticity conditions of the indicated type may be called approximate representations of the Mises condition in all those cases in which the ensuing consequences do not differ essentially.

**Stability in the Critical Case of a Zero Root for Systems With Time Lag,** S. N. Shimanov, pp. 653–668.

*Abstract:* A practical method is given for solving the problem on the undisturbed motion of a system with time lag for the critical case when one of the roots is zero.

**Equations of Motion for Systems With Non-Ideal Constraints,** G. K. Pozharitskii, pp. 669–676.

*Abstract:* The mechanics of systems subject to constraints is based on the assumption that the equations of constraints are satisfied exactly during the whole course of motion for arbitrary forces acting on the system and for arbitrary initial conditions consistent with the constraints. It is clear, however, that in an arbitrary mechanical system, the model of which is a system with constraints (for example, ideal and holonomic), the reactions of constraints arise in consequence of violating the latter. In the majority of problems known in the literature, the reactions arise in consequence of elastic deformations of bodies belonging to the system and those exterior to the latter.

Since the disturbances of the reactions which arise during the motion are very small, their neglect does not cause any essential differences between the theory and experiment. This model together with a certain hypothesis concerning the properties of reactions (their being ideal) permits us to obtain in quite a general form the equations of motion for systems with ideal holonomic as well as nonholonomic constraints, and also the equations of motion for holonomic systems with friction, provided that a certain law of friction holds.

However, due to a frequent appearance of automatically controlled systems, it seems to us interesting to consider systems with automatic devices, the action of which can be interpreted as that of a constraint, not belonging to any of the fore-mentioned types.

**Explosions Above Surfaces of Liquids,** V. M. Kisler, pp. 724–734.

*Abstract:* The problem of explosions above surfaces of liquids is studied under the following assumptions:

(a) The effect of the external explosion on the motion of the free surface of the liquid can be simulated by an appropriate unsteady pressure distribution over a time-varying area.

(b) The motion of the liquid is linearized, which can be justified by the large difference between densities of liquid and gas.

(c) The liquid is considered as incompressible. This assumption increases in validity as the ratio of the speed of sound in the real liquid to the propagation speed of the shock wave over the surface increases.

These assumptions make it possible to reduce the problem at hand to a problem of infinitely small surface wave disturbances over a heavy incompressible ideal liquid. Apparently, this conceptual setting was first used by Lamb in connection with problems of long surface waves. In modern times, wave motion from this point of view has been studied in some detail by Finkelstein. A similar approach was also used by Voit, Cherkesov, and others.

From the results for explosions above heavy liquids, it is easy to derive the motion of free surfaces of weightless fluids by letting the gravitational constant $g$ approach zero. This condition corresponds to the initial effects of the explosion when the pressure forces dominate the gravitational forces.

**Calculation of Flow Past Axisymmetric Bodies With Detached Shock Waves Using an Electronic Computing Machine,** O. M. Belotserkovskii, pp. 745–755.

*Abstract:* In solving the title problem, the majority of authors have assumed the shape and position of the shock wave, after which the inverse problem was solved; a detailed review of existing methods is given in the paper. The method of Dorodnitsyn permits the direct problem to be solved with the necessary degree of accuracy, in its exact formulation.

Such calculations have been carried out at the Computing Center of the Academy of Sciences USSR, on the electronic computing machine BESM-1.

The problem is posed of treating the calculation by a method that would be equally suitable for handling both plane and axisymmetric bodies of various shapes (smooth, with corners, combinations) with detached shock waves, for different values of the adiabatic index $\kappa(\kappa > 1)$ and of the free-stream Mach number $(1 < M_\infty \leqslant \infty)$. The plane problem was considered by the author, and calculation of flows at $M_\infty = 1$ was carried out by Chushkin. The calculation scheme and also results of computations for certain simple shapes (ellipsoids, spheres and disks) are given.

**Flow of an Electrically Conducting Fluid in Tubes of Arbitrary Cross Section in the Presence of a Magnetic Field,** S. A. Regirer, pp. 790–793.

*Abstract:* One of the problems of magnetohydrodynamics is the study of the flow of a conducting viscous fluid in a tube located in a magnetic field. Its solutions are known for plane and round cylindrical tubes. The general problem treated here of the steady flow in an infinitely long tube of arbitrary cross section reduces to the successive solution of two linear boundary value problems. A result of a similar nature was obtained earlier for a limited class of externally applied magnetic fields.

**Almost-Periodic Solutions of Nonlinear Systems of Differential Equations,** V. Kh. Kharasakhal, pp. 838–842.

**Stability of a Gyroscope Having a Vertical Axis of the Outer Ring With Dry Friction in the Gimbal Axes Taken Into Account,** V. V. Krementulo, pp. 843–849.

*Abstract:* Rumiantsev has investigated the influence of viscous friction on the stability of vertical rotation of a gyroscope on gimbals. Other authors have investigated the vertical rotation of a gyroscope taking into account dry friction in the suspension. The latter problem is further investigated in this paper.

## *JOURNAL OF PHYSICAL CHEMISTRY (Zhurnal Fizicheskoi Khimii).* Published by The Chemical Society, London.

**Vol. 34, no. 5, May 1960.**

**Thermodynamics of Equilibria in Similar Reactions,** V. A. Kireev, pp. 449–455.

*Abstract:* The number of chemical compounds used in the various branches of the national economy increases so rapidly that it is impossible to keep pace with requirements for thermodynamic data. It is therefore important to be able to calculate the equilibrium of one reaction from data for another similar reaction. The accuracy of such results is, in general, comparable with that of the usual experimental determinations. This increases the utilization of the existing data and enables the equilibrium to be determined for experimentally difficult conditions such as very high temperatures.

We shall consider three of the numerous thermodynamic methods of determining chemical equilibrium, differing in the initial assumptions.

*Comparison of Two Reactions at the Same Temperature*

The second method of calculation is based on the equation

$$\ln K_Y = \ln K_X + \frac{\Delta H^\circ_X - \Delta H^\circ_Y}{RT} - \frac{\Delta S^\circ_X - \Delta S^\circ_Y}{R} \qquad [11]$$

which was obtained by the author from

$$\ln K_Y = -\frac{\Delta H^\circ_Y}{RT} + \frac{\Delta S^\circ_Y}{R} \qquad [12]$$

and an analogous expression for $\ln K_Y$. When Eq. 11 is expressed in terms of activities it becomes a rigorous thermodynamic relation.

*Comparison of Two Reactions With the Same Values of Equilibrium Constants*

*Summary:* Basic thermodynamic relationships, which correlate the parameters of chemical equilibrium in similar (monotypical) chemical reactions, have been given and the more important analytical methods of calculating the chemical equilibria have been considered. It has been shown that the accuracy of the results obtained by such methods is practically the same as that of the direct experimental determinations. Approximate results may be obtained from very meager initial data, or for the less similar (monotypical) reactions.

**Burning Velocity of Ozone-Oxygen Mixtures,** N. A. Slavinskaya, V. E. Kazakevich, S. A. Kamenetskaya, V. M. Cherednichenko and S. Ya. Pshezhetskii, pp. 462–464.

*Introduction:* Kamenetskaya and Pshezhetskii have shown that the critical ignition conditions for ozone and its mixtures with oxygen correspond to the kinetics of its slow decomposition. Values of the lower inflammability limit and the ignition parameters, calculated from Semenov's theory of thermal ignition and from kinetic data were in satisfactory agreement with experiment.

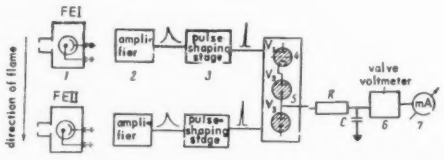


**Fig. 1. Circuit for measuring flame-propagation velocity: 1) photocells; 2) pulse amplifiers; 3) pulse-shaping stages; 4) charging valve; 5) voltage regulators; 6) valve voltmeter; 7) milliammeter.**

It is of interest to establish whether there is a similar relation between the kinetics of the slow reaction and the burning velocity of ozone. Until recently there has been only limited information in the literature about the burning velocity of ozone, and we have therefore measured the flame propagation rate for various mixtures of ozone and oxygen. The measurements were made in a horizontal tube, using a photoelectric method because of the low actinic value of the flame.

*Summary:* The burning velocity of ozone in ozone-oxygen mixtures in a horizontal tube has been measured by a photoelectric method. Calculations based on the thermal theory of flame propagation have shown that the burning velocity of ozone conforms to the kinetics of its thermal decomposition.

**Kinetics and Mechanism of Methane Oxidation. II. Kinetics of the Accumulation of Intermediate Products,** L. V. Karmilova, N. S. Enikolopyan and A. B. Nalbandyan, pp. 470–473.

*Introduction:* The present paper deals with the kinetics of accumulation of formaldehyde and hydrogen peroxide during the oxidation of methane in a quartz vessel, treated with HF, and operating during the course of a year, with a wide variation of experimental conditions

*Summary:*

1 Formation of hydrogen peroxide as well as formaldehyde has been shown to occur during the oxidation of methane at 423–513 deg in a quartz vessel treated with HF.

2 Formaldehyde is a primary intermediate in the reaction, and peroxide is formed by oxidation of the formaldehyde.

3 The maximum yield of formaldehyde is a linear function of the initial pressure of the reaction mixture and of methane, and is independent of the oxygen concentration over a wide range of pressure.

4 The activation energy for the formation of formaldehyde has been determined ($E_{CH_2O} \cong 7.8$ kcal). The relative yield of hydrogen peroxide has been shown to fall with rise in temperature.

**Aerosols Formed in Radiochemical Reactions,** V. S. Bogdanov, pp. 496–500.

*Summary:*

1 An optical method has been used to study the formation of aerosols during the exposure of gaseous organic substances to fast electrons under various conditions, and their subsequent changes.

2 The particle sizes of aerosols formed from methane are a few tenths of a micron; the particles carry both positive and negative changes (1–11 elementary charges); the majority of the charged particles (66%) having 1–3 elementary changes. The number of charged particles depends on the degree of dilution of the aerosol.

3 A study has been made of the variation of the weight concentration and the yield $G$ with the amount of energy absorbed for aerosols obtained from methane. The yield for ethylene is 32 times as great as the maximum yield reached with methane.

**Inhibition and the Structure of Inhibitors. III. Inhibited Polymerization of Vinyl Acetate,** Z. A. Sinitsyna and Kh. S. Bagdasar'yan, pp. 529–532.

*Introduction:* In a previous paper the inhibition of polymerization was used to investigate the reactivity of different aromatic compounds toward the methacrylate radical. The inhibited polymerization of vinyl acetate has been investigated in the present work.

*Summary:*

1 Each inhibitor molecule terminates two kinetic chains: chain regeneration does not occur, and each kinetic chain leads to the formation of a single polymer molecule.

2 Electron-donor and electron-acceptor substituents intensify the reactivity of the benzene ring toward the polyvinyl-acetate radical.

3 The value of $k_x/k_p$ is about $10^3$ times as great for nitrobenzene as for the other benzene derivatives. The effect of substituents in nitrobenzene is governed by the Hammett rule, with $\rho = 0.76$.

4 The reactivity of the polyvinyl acetate radical exceeds that of the polymethacrylate radical by a factor of $10^3$–$10^4$.

5 It has been shown by the inhibited-polymerization method that $k_p/k_0^{1/2} = 0.275$ for vinyl acetate at 50 deg.

**Apparatus for Determination of Temperature at Different Heights in the Jet of Flame From Gunpowder,** P. F. Pokhil, V. M. Mal'tsev and L. N. Gal'perin, pp. 539–541.

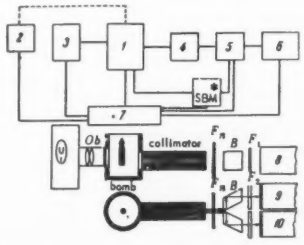


**Fig. 1. Block diagram of apparatus for measuring temperatures at different heights of jet of flame from gunpowder: 1) constant-pressure bomb; 2) incandescent tungsten lamp; 3) xenon lamp; 4) optical system; 5) photomultiplier bank; 6) MPO-2 recording oscillograph; 7) power pack; 8)–10) FEU-42 photomultipliers; $F_r$ red filter; $F_b$ blue filter; $F_n$ neutral platinum filter; $B$ biprism; $Ob$ objective.**

* Transliterated from the Russian—significance not clear (Ed. of Translation).

*Introduction:* The apparatus described was designed for measuring temperatures between 1300 and 3000 deg at different heights in the jet of flame from gunpowder at different pressures. The temperature was investigated by means of the blue:red ratio with a flame emitting a continuous spectrum in the visible region. The apparatus enables the absorption to be measured at the height of the jet of flame (at definite wave lengths), thus giving the true temperature of combustion.

**Simple Apparatus for Production of Pressures up to 200 Atmospheres,** S. I. Sklyarenko, I. V. Smirnov, L. B. Belyaeva and E. A. Malysheva, pp. 541–543.

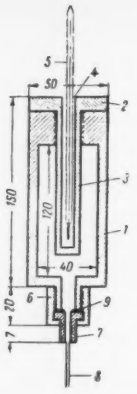


**Diagram of apparatus for the production of specified pressures up to 200 atm (dimensions in mm).**

*Introduction:* In many kinds of physico-chemical investigations it is often necessary to produce high pressures in various types of apparatus. Most frequently pressures not exceeding 100–200 atm are adequate.

The production of high pressures usually requires quite complicated apparatus, which may not be available in a nonspecialist laboratory. In the absence of such special apparatus, a simple device may be employed for producing pressures up to 200 atm (and if necessary somewhat higher) in a closed vessel of small volume.

**Calculation of Rotational Partition Function for Molecules in a Liquid,** A. M. Evseev, p. 548.

For complex molecules possessing rotational degrees of freedom, the self-consistent field method[1] allows the asymmetry of the force field of the molecule to be taken into account on the assumption that the effective field of the other molecules is isotropic. This circumstance simplifies calculation of the partition function. For this calculation the rotation of the molecules in the liquid should not be considered free, but hindered, as in intramolecular rotation, in accordance with the hypothesis put forward by Evseev and Lebedev.[2]

To find the energy spectrum of rotation of the molecule it is necessary to solve the Schrödinger equation in a general form

$$\frac{\partial^2\psi}{\partial\varphi^2} + \frac{8\pi^2 I}{h^2}\{E - V\}\psi = 0$$

for potential energy $V$. In order to allow for hindered rotation we can separate that part of the molecules for which the wave equation has the form

$$\frac{\partial^2\psi}{\partial\varphi^2} + \frac{8\pi^2 I}{h^2}E = 0$$

with the condition $E > V$. Obviously these molecules will be freely rotating.

For the rest of the molecules the potential energy can be expressed by

$$V = \tfrac{1}{2}f\varphi^2$$

where $\varphi$ is the angle of rotation of the molecule. These molecules will perform torsional oscillations or librations. The frequency of oscillation is

$$\nu = \frac{1}{2\pi}\sqrt{\frac{f}{I}}$$

or

$$\nu = \frac{\sigma}{2\pi}\sqrt{\frac{\epsilon_0}{2I}} \qquad \epsilon_0 = V_{\max}$$

The fraction of the molecules possessing free rotation is[2]

$$\eta = e^{-\epsilon_0/kT}$$

[1]Evseev, A. M., *Zhur. Fiz. Khim.*, 1957, vol. 31, p. 2414.
[2]Evseev, A. M. and Lebedev, V. P., *ibid.*, 1953, vol. 27, p. 1068.

the fraction performing torsional oscillations is

$$1 - \eta = 1 - e^{-\epsilon_0/kT}$$

The energy of the system of interacting molecules can be divided into the following parts:

1 Transitional energy of all molecules, $\sum_1^N p_i^2/2m_i$.

2 Potential energy of interaction of all molecules, calculated by the self-consistent field method, $U = \sum u_i$.

3 Rotational energy of $N_1$ molecules, $N_1 = Ne^{-\epsilon_0/kT}$ with energy spectrum from $\epsilon_0$ to $\infty$.

4 Energy of torsional oscillation of $N_2$ molecules, $N_2 = N(1 - e^{-\epsilon_0/kT})$, with energies of oscillation from 0 to $\epsilon_0$.

Consequently, the Hamiltonian of the system of $N$ molecules can be written in the following way

$$H_j = \sum_{i=1}^{N}\frac{p_i^2}{2m_i} + \sum_{i=1}^{N}u_i + \sum_{i=1}^{N_1}\epsilon_{i\text{rot}} + \sum_{i=1}^{N_2}\epsilon_{i\text{libr}}$$

Hence the partition function is equal to

$$Z = \frac{1}{N!}Q_v Q_r\left\{e^{-\epsilon_0/kT}\sum_0^\infty e^{-\epsilon_{\text{rot}}/kT}\right\}^{N_1}\left\{\sum_0^{\epsilon_0} e^{-\epsilon_{\text{libr}}/kT}\right\}^{N_2}$$

where

$$\sum_0^\infty e^{-\epsilon_{\text{rot}}/kT} = Q_r$$

$$\left\{\sum_0^{\epsilon_0} e^{-\epsilon_{\text{libr}}/kT}\right\} = \frac{1 - e^{-\epsilon_0/kT}}{1 - e^{-h\nu/kT}} \cong \frac{kT}{h\nu_0}(1 - \epsilon^{-\epsilon_0/kT})$$

## *PHYSICS OF METALS AND METALLOGRAPHY (Fizika Metallov i Metallovedenie).* Published by Pergamon Institute, New York.

**Vol. 8, no. 6, 1959.**

**Electrical Conductivity of Ferromagnetic Metals in a Radio Frequency Field,** P. S. Zyryanov, T. G. Izyumova and G. V. Skrotskii, pp. 1–5.

*Introduction:* We know that ferromagnetic metals have additional specific resistance compared with nonferromagnetic metals. This additional resistance is usually explained by dispersion of conductance electrons on thermal fluctuations in the degree of magnetization.

In metals which are in conditions of ferromagnetic resonance the character of the fluctuations in the degree of magnetization can be materially altered.

The specific resistance $\rho$ of a metallic ferromagnetic can be considered to consist in the following parts

$$\rho = \rho_{\text{lattice}} + \rho_{fm} + \rho_{fm}' \qquad [1]$$

where $\rho_{\text{lattice}}$ and $\rho_{fm}$ are, respectively, the resistances caused by dispersion of conductance electrons on lattice variations thermodynamically in equilibrium (phonons) and on variations in magnetization (ferromagnons), and $\rho_{fm}$ is the additional resistance caused by a change in magnetization in a radio frequency field. The temperature relation and order of magnitude of $\rho_{\text{lattice}}$ are well known; $\rho_{fm}$ was calculated by Turov for low temperatures on a spin wave model. The temperature relation of $\rho_{fm}$ agrees qualitatively with experience. Here an attempt is made to construct a qualitative theory for the increase in resistance of ferromagnetics in a radio frequency field.

**Development of Metal Physics and Physics of Metallurgy in the Chinese Peoples' Republic During Ten Years,** Chou Chih-Hung, Ko Tsun and Tsin Lin-Chao, pp. 16–23.

**Electric Conductivity of Iron at Elevated Temperatures,** V. S. Gumenyuk and V. V. Lebedev, pp. 38–41.

*Abstract:* The paper gives data on the study of the temperature dependence of the electric conductivity of high purity iron, which was obtained by vacuum distillation. The curve plotting the electric resistivity as a function of temperature shows clearly the points of magnetic and phase transition. Comparison is made

with the measured values of the electric resistance for armco iron and with the results of other authors. A description is given of a high temperature (up to 2500C) furnace.

**Concentration Inequalities Experimentally Detected in Solid Bodies,** V. I. Arkharov, pp. 51–55.

*Conclusion:*

1 The phenomena of the appearance of concentration nonuniformity in alloys investigated by Zav'ialov and Bruk are different in their nature from the phenomena of internal adsorption.

2 The phenomena studied by Zav'ialov and Bruk can be explained on the basis of simple thermodynamic conditions influencing the form of the constitutional diagram of the alloy; however, these explanations are unsuitable for the phenomena of internal adsorption because of the completely different nature of the latter.

3 The thickness of the zones of intercrystalline internal adsorption estimated from the experimental data obtained by different methods has a value of $10^2$–$10^3$ Å; direct auto-radiographic detection of these zones is extremely difficult and possible only in particularly favorable conditions in exceptional cases. The zones detected in the work of Zav'ialov and Bruk have a thickness which exceeds the transverse size of the zones of intercrystalline internal adsorption.

4 The remarks of Zav'ialov and Bruk relating to some of the aspects of the phenomena of internal adsorption, apart from the fact that they (the remarks) are made on the basis of incorrect identification of internal adsorption with the phenomena of stratification in solid solutions, contain also a series of misunderstandings caused by a much too simplified conception of the mechanism of internal adsorption.

5 Despite the shortcomings noted in our article, we consider that the work of Zav'ialov and Bruk contains a description of phenomena which are important for metallography and correct explanations of these phenomena on the basis of the laws represented by the constitutional diagrams of alloys.

**Failure of a Martensite Crystal Under the Simultaneous Action of External Tensile and Compressive Stresses,** A. Mashin, pp. 95–100.

*Abstract:* The present article deals with changes in a martensite crystal which is actually a martensite monocrystal, under the simultaneous action of external tensile and compressive stresses. It is found that the martensite crystals in failing, first form microcracks, break up, then fracture completely. The interpretation of these changes was based on an analysis of stresses acting on the martensite crystal during its loading. The crushing of the crystals is explained by the fact that the compressive stresses on one side of the crystal are not compensated in these cases. The problem considered here is solved in connection with problems of propagation of elastic and plastic waves in an austenitic-martensitic medium.

**Effect of the Original Structure and Temperature of Deformation on Phase Transformations During Plastic Formation,** B. A. Apaev and Yu. A. Sysuev, pp. 101–106.

*Introduction:* Several papers express an opinion on the differences in processes caused by plastic deformation, when equilibrium and nonequilibrium alloys are subjected to plastic deformation. It is usual to consider that, in the first case, the deformation causes fragmentation of the phases, change in the block structure and stressed state of the alloy. In the second case, as well as these processes, on reaching a certain degree of deformation more important changes can take place in the alloy, characterized by the formation of new phases, which can differ from the original phase both in their crystallographic structure and in the chemical composition.

In the light of a number of papers, this classification is more than arbitrary, since the results of these papers indicate the presence of phase transformations during deformation of the alloys in the equilibrium and states close to the equilibrium.

The opinion held by some authors that the deformation of equilibrium systems cannot cause the formation of new phases has led, in our opinion, to incorrect conclusions. Taking as a starting premise the fact that plastic deformation in equilibrium systems only causes those processes mentioned, and observing the similar change of the physical properties during the heating of a plastically deformed alloy and also the alloy in the hardened state, these authors consider it sufficient proof that during tempering in the range of the "third transformation" processes occur which are caused only by the change in the block structure of the $\alpha$ phase, of its stressed state, by destruction of the coherent bonds and by the change in shape and dimension of the carbide particles.

If the equilibrium state of the alloy is characterized only by the ratio and chemical composition of the phases, then, on the basis of the existing point of view, the conclusion would be drawn that there should be no essential difference in the processes arising during the deformation of tempered steel, when the structure of the latter is characterized for example, by lamellar and granular cementite. In our opinion, this point of view should be made more specific, i.e., there should be a more complete determination of the equilibrium state of the system, taking into account the equilibrium of the form of the phases.

The present paper deals partly with problems similar to those already published and also studies the effect of the deformation temperature and the original structure on the character of phase transformations and the character of hardening during deformation.

**Vol. 9, no. 1, 1960.**

**Determination of the Number of Independent Parameters of Short-Range Order in Multicomponent Solid Solutions,** A. N. Men', pp. 16–19.

*Introduction:* When investigating the temperature and concentration dependence of correlation parameters $\epsilon$ in different coordination spheres for a binary solid solution by the methods of the statistical theory of ordering, the problem has to be solved for an arbitrary extreme, as the parameters $\epsilon$ are not independent. In the case of $n$-component solid solutions with a complex lattice, the number of independent parameters of short-range order has to be determined in each special case.

In the present note an attempt is made to construct a general scheme for calculating the number of independent parameters of short-range order $\sigma$ in any coordination sphere for $n$-component solid solutions with a complex lattice, allowing for the dependence of $\sigma$ on the distribution of the atoms with respect to the sublattices.

**Mechanism of the Formation of Lüders Lines,** L. B. Erlikh, pp. 49–52.

*Abstract:* The mechanism of the formation of Lüders lines—the wrinkles on the surface of soft steel loaded in tension—has not so far been established. It is proposed to explain this mechanism on the basis of the loss of the rigidity of the thin surface layers under compression. It has been shown that in soft steel testpieces in the process of tension, the conditions necessary for this phenomenon do actually occur.

*Conclusions:*

1 The process of the formation of Lüders lines is made up of a number of successive stages.

2 Lüders lines—these are wrinkles—are the result of the loss of stability in the thin surface layer under the action of residual compressive stresses.

**Structure of Electrolytically Deposited Metals From the Data of Structural Investigations,** K. M. Gorbunova, V. V. Bondar', V. P. Moiseev, O. S. Popova, I. M. Polukarov and A. A. Sutiagina, pp. 62–67.

*Introduction:* As is generally known, the structure of electrodepositions determines a number of technical characteristics of metallic coatings. With their help it is possible to give desired properties (decorative, electric magnetic, mechanical, etc.) to the products made from very different metals. The interest in the coatings of this type will rise still more when polymeric materials commence to be used for construction purposes.

A wide range of permissible fluctuations in the conditions of electro-deposition processing makes it possible to change the structure and the properties of coatings of the same metal. At the same time the mechanism by which the conditions of electrolysis affect the structure and properties of coatings remains unknown to a considerable degree and requires further investigations.

**Investigation of Internal Friction in Metal-Ceramic Bodies. II. The Ternary System Cu-Ni-Fe,** B. Ia. Pines and Den Ge Sen, pp. 72–76.

*Abstract:* In studying internal friction in metal-ceramic specimens from a ternary mixture of powders of Cu-Ni-Fe, six peaks (maxima) of internal friction were observed, corresponding to relaxation effects at the contacts of like and unlike grains.

*Conclusions:*

1 An experimental study of internal friction has been carried

out for metal-ceramic specimens from a Cu-Ni-Fe ternary mixture of powders, by a torsional oscillation method.

2 On the temperature internal friction curve of specimens from the Cu-Ni-Fe ternary mixture of powder, six maxima (peaks) are observed, which are evidently due to diffusion transitions of atoms along grain boundaries. Of these, three maxima correspond to processes at the contacts of like grains, and the other three to contacts of unlike grains. The position (temperature) of the maxima coincides with those found (separately) for the three binary systems.

3 The energy of activation of "internal friction processes" has been found from frequency displacements and the background of the internal friction curve.

4 The values of energy of activation $E$, corresponding to internal friction maxima, agree within the limits of uncertainty with those found earlier for the same maxima in the case of specimens of the pure components or of binary mixtures of the powders.

5 The energy of activation $E'$ found from the "background" of the temperature-internal friction curve is appreciably less than the values $E$ determined from the frequency displacement of peaks. If the presence of the background corresponds to fluctuating transitions of atoms then there may be taking part only those atoms in highly distorted region of the crystal (for instance on the core of edge dislocations).

6 All the values of energy of activation for specimens from a ternary mixture of powders depend on the duration of preliminary annealing; on increasing the time the values of energy of activation $E$ increase, and those for $E'$ are somewhat decreased.

**Uniqueness of Physical Explanation of the Slope of Stress Relaxation Curves,** G. N. Kolesnikov and A. I. Moiseyev, pp. 84–86.

**Investigation of Grain Boundary Displacement During Creep,** V. M. Rozenberg and I. A. Epshtein, pp. 106–113.

*Abstract:* A study is made of grain boundary displacement during creep in aluminium. It is shown that the extent of grain boundary displacement is independent of the boundaries' orientation with respect to the elongation axis. Displacements of grain boundaries make no contribution to the value of overall elongation but they do increase the plasticity of the material.

## *RADIO ENGINEERING* (*Radiotekhnika*). Published by Pergamon Institute, New York, in conjunction with Massachusetts Institute of Technology.

**Vol. 15, no. 7, 1960.**

**Dependence of the Voltage Standing Wave Ratio and Losses in a Balanced Aerial Switch on the Distance Between the Magnetron and the Dischargers,** B. E. Rubinshtein, pp. 24–32.

*Abstract:* A study is made of the operation of a balanced aerial switch with discharge protection for the receiver under reception conditions. It is shown that the losses under reception conditions are greatly dependent on the distance between the magnetron and dischargers if the dischargers produce a shift in phase.

**Problem of "Jumps" in Electrical Circuits,** S. A. Drobov, pp. 47–60.

*Abstract:* A method is elaborated for determining the moments at which voltage and current "jumps" arise in circuits with nonlinear two-poles and three-poles. It is shown that the solution does not require a complete set of differential equations for the system being studied. It is sufficient to know certain parameters. Several examples are given in the conclusion of circuits widely used in radio engineering.

**Establishing the Frequency at the Output of an Ideal Narrow Band Filter With Frequency Phase Modulation,** L. I. Iaroslavskii and B. I. Iakhinson, pp. 72–83.

*Abstract:* This article is devoted to a study of transient processes, or, more accurately, the establishment of the instantaneous frequency and instantaneous amplitude at the output of a narrow band system with a frequency phase modulated input signal, i.e., when sharp and large changes occur in its frequency and phase (jumps). Purely frequency and purely phase modulation are regarded as special cases of frequency phase modulation.

**Investigation Into Transient Processes, Caused by the "Reactance" of the Supply Sources, in Class B Amplifiers,** A. T. Balanov, pp. 112–126.

*Abstract:* The results are given of a theoretical and experimental investigation into periodical recurrent transient processes, caused by the reactance of the supply sources in reference to large class B-type amplifiers. The effect is shown of feedback on the magnitude of nonlinear distortions caused by these transient processes. Criteria are given for the design of output filter capacitors, rectifiers and blocking capacitors in automatic bias circuits.

**Vol. 15, no. 8, 1960.**

**New Theory of Active Four-Poles and Its Application to Distributed Amplifiers,** E'. V. Zeliakh, pp. 18–35.

*Abstract:* The author introduces new parameters for active four-poles called characteristic (or "image") voltages and currents. He formulates the theory of cascade connection for matched active four-poles with symmetrical bodies and gives formulas for calculating the currents and voltages at the ends of the circuit under any load. The theory can be used to analyze distributed amplifiers. Formulas are produced for the amplification factors of amplifiers. Account is taken of "unmatched conditions" at both ends of the grid and anode circuits.

**Contribution to the Analysis of Harmonic Frequency Dividers,** I. Kh. Rizkin, pp. 47–59.

*Abstract:* It is shown that the analysis of harmonic frequency dividers described by differential equations of a higher order than two can in some cases be reduced to the analysis of an equivalent divider described by a second-order equation. The method of devising the equivalent system is indicated for two common types of system.

**Improving the Frequency Phase Characteristics of Selective Feedback Amplifiers for Excessive De-Tuning,** V. L. Zmudikov, pp. 75–80.

*Abstract:* In selective, frequency-dependent, feedback amplifiers, amplification greatly off-tune from the quasi-resonance frequency approaches unity and not zero, unlike resonance amplifiers. This brings about a deterioration in the selectivity and interference resistance of feedback amplifiers. Two methods of eliminating this residual amplification by means of subtracting circuits are described.

**Interpolation of Functions by Exponential Polynomials and Its Application to the Synthesis of Electrical Circuits With Respect to the Characteristics,** N. S. Kochanov, pp. 87–95.

*Abstract:* A study is made of the makeup of exponential polynomials, with respect to the values of a time function and its first derivative at a number of equidistant points of interpolation. The use of this method is shown for the synthesis of a four-pole forming a sine-squared pulse.

**Spectrum Analysis in Amplitude Phase Modulation,** L. E. Kliagin, pp. 96–106.

*Abstract:* Exact theoretical formulas are produced which make it possible to evaluate the spectra produced in the Kahn-type transmitter by amplitude phase modulation. It is shown that oscillations with optimum amplitude phase modulation cannot be produced and that the second sideband can only be partially suppressed; in this respect, the system has no advantages over the quadrature modulation system.

## *RADIO ENGINEERING AND ELECTRONICS* (*Radiotekhnika i Elektronika*). Published by Pergamon Institute, New York, in conjunction with Massachusetts Institute of Technology.

**Vol. 4, no. 12, 1959.**

**Theory of Detecting the Useful Signal in the Background of Gaussian Noise and an Arbitrary Number of Interfering Signals With Random Amplitudes and Initial Phases,** Ia. D. Shirman, pp. 9–21.

*Abstract:* The detection of a "composite" signal, when the useful high frequency signal $u_A(t)$ (is known completely, including the initial phase or the amplitudes and the initial phase) is not only superimposed on a white Gaussian noise but also on $m$ high frequency signals $u_{Bi}(t)$ $(i = 1, 2, \ldots, m)$ with a Rayleigh-type

amplitude distribution and with an equiprobable initial phase is examined. It is shown that the addition of interfering signals changes the pulse characteristic of the optimum filter $v(t) = A_0 r_{m+1}(t_0 - t)$ and the energy of the threshold signals, but it does not change the character of the optimum process and the form of the detection curve. Recurrent formulas are given for the determination of $r_{m+1}(t)$, and the energy utilization factor for composite detection is derived.

**Some Methods of Detecting Fluctuating Signals in Two-Channel Systems,** Iu. B. Chernyak, pp. 22–35.

*Abstract:* The problems of detecting signals in a two-channel receiving system with linear composition of the amplitudes, with maximum amplitude selection and also with detection approaching the quadratic composition of amplitudes are examined. The comparison of these methods with the quadratic composition and with the multiplication of the amplitudes is carried out.

**Accuracy of Measuring the Parameters of Oscillations Distorted by Low Intensity Gaussian Noise,** B. A. Dubinskii, pp. 36–46.

*Abstract:* We examine the problem of determining the accuracy of the parameters of oscillations during ideal reception in Kotel'nikov's sense, in the presence of Gaussian low intensity noise. The derivation is given of expressions for the matrixes of the second moments of the parameter errors, which are the generalizations of the corresponding expressions given elsewhere to the case when the partial differentials of the oscillations with respect to the parameters are non-orthogonal functions. As an example of using these expressions, the matrix of the second moments of the errors of measuring the parameters of a sinusoidal pulse signal is calculated.

**Dependence of Irregular Ionospheric Radio Wave Refraction on the Zenith Angle,** Iu. L. Kokurin, pp. 47–53.

*Abstract:* The dependence of the vertical and horizontal irregular refraction of radio waves ($\lambda = 4$ m) in the ionosphere on the zenith angle is calculated. It is shown that these dependences are fundamentally different for various models of the ionospheric layer. The necessity of measuring the irregular refraction at small zenith angles, in order to establish a model of the layer, is indicated.

**Application of Chaplygin's Method for the Solution of Some Nonlinear Problems of Radio Engineering,** V. I. Kaganov, pp. 54–58.

*Abstract:* The advantages of using Chaplygin's method for the solution of the dynamic equations of systems, containing nonlinear inertia-free elements are shown. This method enables us to find a solution quickly and to evaluate the error. As an example we examine the transient process in an automatic frequency control system.

**Method of Solving Boundary Problems of Electrodynamics,** Ia. N. Fel'd, pp. 74–90.

*Abstract:* A method is developed for finding the distribution of currents in a system of $N$ metal bodies excited by an incident wave or external emf, applied to their surfaces. The solution is given in the form of series in special orthonormalized functions with finally defined coefficients. The method is illustrated by a problem of exciting a system of $N$ finite parallel tubular dipoles and infinite strips.

**Spectral Analysis of Quasi-Static Electric Field Space Harmonics,** G. M. Gershtein and A. V. Khokhlov, pp. 127–137.

*Abstract:* A new method proposed earlier for modelling static fields, based on the Shockley-Ramo induced-current theorem is used for transforming the space harmonics of a quasi-static electric field in a periodic structure to time harmonics of induced current, with subsequent analysis of the spectrum of the latter. Using a low frequency spectrum analyzer the experimental analysis of the space-harmonic spectrum of the azimuthal field component of a four-segment structure rotating about a charged probe is carried out. Comparisons of the spectra obtained in this way with theoretical spectra and with spectra obtained using an electrolytic tank, show satisfactory agreement.

***SOVIET PHYSICS-DOKLADY* (*Doklady Akademii Nauk SSSR, Otdel. Fiziki*). Published by American Institute of Physics, New York.**

**Vol. 5, no. 3, Nov.–Dec. 1960.**

**Method for Estimating the Temperature of Hot Stars From Their N III Emission Spectrum,** A. A. Nikitin, pp. 461–462.

**System of Programing Concepts,** R. I. Podlovchenko, pp. 483–485.

*Introduction:* The analysis of logical schemes arising in the composition of programs has led to the introduction of the concepts of operator, logical condition and operator sequence. In this paper, one of the possible methods of defining these concepts is investigated, and certain relations between operator sequences are established on the basis of their functions.

**New Principle for the Construction of a Memory Device,** G. G. Stetsyura, pp. 486–488.

*Introduction:* In this paper, a principle for the construction of a parallel-type memory device is set forth. This type of device will allow rapid access to information stored in it when an arbitrary portion of the information itself is given as a guide to the search, rather than its storage location.

**Analyzing the Flow of an Aerated Fluid Assuming a Two-Parameter Permeability Characteristic,** D. A. Efros and I. F. Kuranov, pp. 497–500.

*Introduction:* In hydrodynamic calculations of the flows of an aerated fluid, it is the usual procedure to make use of relative permeabilities specified in the form of functions $F_g(\rho)$ and $F_l(\rho)$, which are determined in filtration experiments with a mixture of liquid and gas introduced from without. The data of recent investigations show, however, that, in the stationary filtration of a gas-impregnated fluid, the process is described with considerably more completeness by two-parameter relations of the form

$$\frac{k_g}{k} = F_g(\rho, P^*) \qquad \frac{k_l}{k} = F_l(P^*, \lambda)$$

Here $k_g$ and $k_l$ are the permeabilities for the gas and for the liquid, respectively, $k$ is the initial permeability, $\rho$ is the saturation of the liquid, $P^* = P/P_1$, where $P_1$ is the pressure at the inflow: $\lambda = \Gamma^{3*}/S(P)$, here $S(P)$ and $\Gamma^*$ are the solubilitycoefficient and gas factor, both reduced to the pressure $P_1$.

**Motion of an Axially Symmetric Solid in Space About a Stationary Point Under the Action of Moments Slowly Varying With Time,** G. E. Kuzmak, pp. 526–529.

**Speeding up the Limiting Process for Obtaining Roots to Secular Equations by the Method of Mayants,** B. L. Livshits, pp. 575–579.

**Apparatus for High Pressure and High Temperature With a Conical Piston,** L. F. Vereshchagin, V. A. Galaktionov, A. A. Semerchan and V. N. Slesarev, pp. 602–604.

*Introduction:* In order to carry out physical investigations, the authors have made several different types of apparatus for high pressure and high temperature. An apparatus with conical pistons is described here. This setup, similar to the recently described "belt" setup, was made independently in the development of an idea published earlier and differs from the "belt" in that it has a large working volume.

Fig. 1 shows the essentials of the apparatus. The working

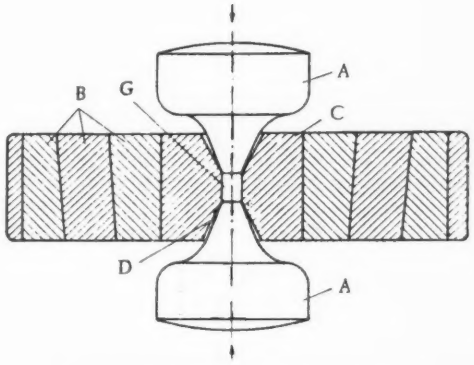


**Fig. 1. Essentials of the apparatus.**

substance $G$, which is subjected to the high pressure, is placed in the cylinder of a matrix $C$, and is compressed by two pistons $A$, which have the form of truncated cones. Pyrophyllite sealing material $D$ is packed between the conical surfaces of the matrix and the plungers. The purpose of this packing is to support, and therefore to strengthen, the narrow part of the conical pistons, at the cross section where the stress exceeds the elastic limit of the piston material. In addition, the pressure gradient along the generators of the cone, which arises in the packing when the plunger is loaded, provides confinement of the pressure in the volume $G$, not permitting flow of the working substance in the gap between the conical surfaces of the pistons and the matrix. To reduce the deformation of the matrix when the pressure is applied, and to strengthen it, support is provided by three backing rings $B$, pressed sequentially into one another. Another variation was also used, in which support was accomplished by the rods of four hydraulic presses, whose axes were situated in a horizontal plane, passing through the middle of the working volume and at an angle of 90 deg to one another.

## *SOVIET PHYSICS-SOLID STATE (Fizika Tverdogo Tela).* Published by American Institute of Physics, New York.

**Vol. 2, no. 6, Dec. 1960.**

**The Dispersion and Re-Establishment of Contacts Between Microblocks During Plastic Deformation,** R. I. Garber, I. A. Gindin and L. M. Polyakov, pp. 984–990.

*Abstract:* In order to explain the reason for the weak strength of real solids we must assume that there arises during the deformation process an accumulation of dislocations, ruptures and microcracks leading to large strain concentrations reaching into the microregion of the theoretical values of strength.

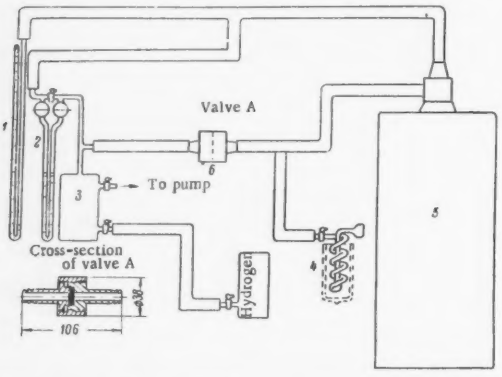


Fig. 1. Schematic of set-up used to control the porosity of metallic plates. 1) Mercury manometer, 2) differential oil manometer, 3 and 5) reservoirs 4) trap for the drying and purification of air entering the set-up, 6) valve (junction) for monitoring the samples. The porosity is computed using the formula $\gamma = l\,n(\Delta p_1/\Delta p_2)/k\tau$ where k is a constant determined by the set-up, $\tau$ the time interval, and $\Delta p_1$ and $\Delta p_2$ are the initial and final pressures registered by the manometer 2.

In the case of plastic deformation it is usually considered that during all stages of this complex process the complexity is preserved even though crushing and disorientation of the microblocks are observed. In the present paper we examine the dispersion phenomenon and the processes involved in the re-establishment of contacts between microblocks which insure the macroscopic integrity of the plastically deformed material.

**The Effect of Heat Treatment on the Photo-EMF in Cuprous Oxide,** I. D. Kirvalidze, pp. 1043–1045.

*Introduction:* Cuprous oxide which is well known for its semiconducting properties exhibits an exceptionally wide scatter in conductivity values in dependence on the excess oxygen concentration. The stoichiometric excess oxygen value depends on the previous heat treatment of the specimen. Excess oxygen also affects the photo-activity of cuprous oxide.

The aim of the present investigation was to explain the effect of heat treatment in vacuo on the photo-emf in the cuprous oxide surface layer.

**Temperature Dependent Quantum Green's Functions,** Sh. M. Kogan, pp. 1074–1084.

*Introduction:* The effectiveness of the method of quantum Green's functions in application to the problem of many bodies has been very well demonstrated in quite a number of papers. In papers by Bonch-Bruevich, it has been shown that quantum Green's functions contain extremely full information about the energy spectrum of the quasi-particles in a many-body system The connection of Green's functions with the density matrix has been established, and a spectral theorem has been proved on the connection of the poles of the Green's function with the energy spectrum of the system. The method of quantum Green's functions has been used to solve problems on plasma oscillations and on the screening of an external field in a degenerate electron or electron-hole gas for an arbitrary type of anisotropy of the isoenergy surfaces. This method has been successfully used for the approximate solution of the problem of chemical adsorption on a metal. The method of quantum Green's functions is also used in the latest papers of Migdal, Galitskii and Migdal, Galitskii, and Belyaev to study the spectrum of the quasi-particles in non-ideal Fermi and Bose gases.

In all of these papers the systems studied are either in the ground state or in the immediate neighborhood of the ground state. This situation is associated with the use of Green's functions defined as averages of $T$-products of field operators over the ground state of the system in question. In particular, to study the thermodynamic properties of quantum systems it is necessary to generalize the method of Green's functions to systems that are at arbitrary temperatures $T > 0$. The present paper is devoted to the realization of such a generalization

**Theory of Infrared Absorption in Crystals,** L. E. Gurevich and Z I. Uritskii, pp. 1123–1133.

*Abstract:* Absorption of long wave radiation by crystals was investigated at frequencies $\omega < \omega_i$ ($\omega_0$ is the photoelectric threshold) and also in the fundamental absorption region.

In the first case, phonon absorption was investigated by inducing with light in crystals virtual excitations which decayed with the production of phonons. It was shown that in the continuous and discrete absorption regions the most important is absorption accompanied by the production of two phonons. Absorption by free carriers in a magnetic field was also investigated. The absorption coefficient was found to oscillate when degeneracy was present and also in the case when there was no degeneracy, but in a strong magnetic field $h\,\Omega \gg T$($\Omega$ is the Larmor frequency and $T$ is temperature expressed in energy units).

For the fundamental absorption in a magnetic field, oscillations of the absorption coefficient were a function of $(\omega - \omega_0)/\Omega$ with a period equal to 1. In the case of degeneracy the absorption edge was displaced, and oscillated owing to the oscillations of the Fermi level.

**Ejection of Electrons From Metals by Ions,** N. N. Petrov, pp. 1182–1188.

*Introduction:* In order to explain the nature of the kinetic ejection of electrons, the present paper treats the excitation of bound electrons in a metal. On the basis of the discussions offered, recent experimental data on ion-electron emission are evaluated.

The temperature dependence of potential ejection of electrons, the dependence of $\gamma$ on the energy expended in the formation of the bombarding ion, and the role of energy losses by the excited electrons are also discussed

Despite the fact that the study of ion-electron emission has drawn a great deal of attention in the last few years, there remains yet quite a number of unanswered questions. The present paper represents an attempt to explain the kinetic ejection of electrons by ions, and on the basis of recent data to discuss certain special aspects of ion-electron ejection.

**Interaction of Acoustic Oscillations in Ion and Electron-Ion Plasmas,** P. S. Zyryanov and E. G. Skrotskaya, pp. 1196–1200.

*Abstract:* The role of nonlinear effects in ion and electron-ion plasmas in the case of acoustic oscillations is considered. The mean free path of Debye phonons is computed, the phonon thermal conductivity and relaxation time in the phonon system are determined.

## *SOVIET PHYSICS-TECHNICAL PHYSICS (Zhurnal Tekhnicheskoi Fiziki).* Published by American Institute of Physics, New York.

**Vol. 5, no. 2, Aug. 1960.**

**Optical Properties of Axially Symmetrical Magnetic Fields With Central Location of the Source of Charged Particles,** S. A. Kuchai, pp. 131–140.

*Abstract:* In this paper it is shown that axially symmetrical fields with central location of the source can be used for isotope separation of wide angle and high beams.

**The Mechanism of Space Charge Fluctuations in Quasi-Compensated Ion Beams,** M. V. Nezlin, pp. 154–164.

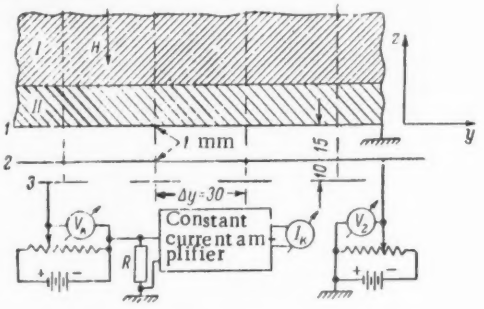


Fig. 1. The experimental apparatus. I) Ion beam; II) secondary plasma; 1, 2) diaphragms; 3) collector. The dimensions are in mm. R = 500,000 ohms.

*Abstract:* This paper describes a study of the state of compensation of the space charge in an intense ion beam passing through a rarefied gas in a strong magnetic field. The mechanism is determined that causes the fluctuations that produce strong decomposition of the space charge in the beam, so that the electric field in the beam reaches some tens of volts per centimeter.

**Method of Investigating the State of Explosion Products by Measuring Shock Wave Parameters,** O. A. Tsukhanova, pp. 219–224.

*Abstract:* A method of determining the state of the reaction products and the range of the chemical process by the experimental investigation of the parameters of the shock waves formed during the explosion of gaseous mixtures in closed pipes is investigated. The results obtained for the mixture $2O_2 + H_2$ are given and the heat emitted by the reaction products during nonstationary flow in pipes is determined.

*Summary:* On the basis of the experimental measurement of shock wave velocity, and of the pressure and velocity of gas flow in front of and behind a shock wave propagating in the explosion products of a gaseous mixture in a cylindrical chamber, we can determine the density distribution along the length of the chamber and compute the value of $p/\rho = RT/\mu$ as functions of time. These data also permit us to judge the degree of completion of the chemical process and to compute the heat transfer from the combustion products and the sides of the chamber. Processing of the experimental results for explosions of the mixture $2O_2 + H_2$ has shown that the equilibrium condition is reached after a time interval of the order of $10^{-3}$ sec.

**Vol. 5, no. 3, Sept. 1960.**

**Study of a Magnetic Trap,** K. D. Sinel'nikov, V. D. Fedorchenko, B. N. Rutkevich, B. M. Chernyi and B. G. Safronov, pp. 236–240. [See illustration at right.]

*Abstract:* Experiments are described that indicate the accumulation of particles in a magnetic trap with a spatially periodic magnetic field and the formation in it of a sizable potential well for positive ions.

**Experiments on Electrodynamic Acceleration of Plasmas,** I. F. Kvartskhava, R. D. Meladze and K. V. Suladze, pp. 266–273.

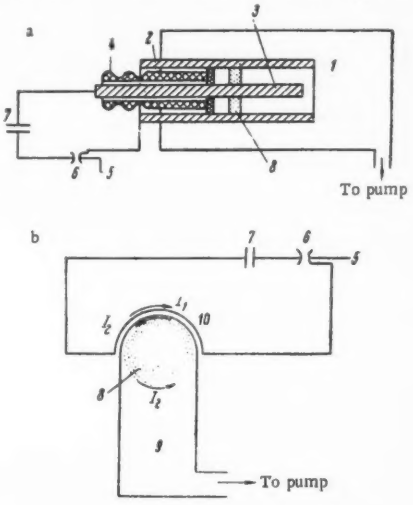


Fig. 1. a) Diagram of the coaxial accelerator; b) diagram of the induction accelerator; 1) vacuum chamber; 2) outer electrode; 3) inner electrode; 4) porcelain insulator; 5) trigger electrode; 6) discharge unit; 7) condenser bank; 8) plasma bunch; 9) vacuum chamber; 10) current-carrying turn.

*Abstract:* The results of experiments on electrodynamic acceleration of plasmas in coaxial and induction accelerators are presented. It is found that three different kinds of plasma bunches can be produced in a coaxial accelerator. The maximum bunch velocities have been determined. An estimate of the total mass of the bunches accelerated during one discharge cycle of the condensers in a coaxial device is made. A qualitative description of the described effects is given.

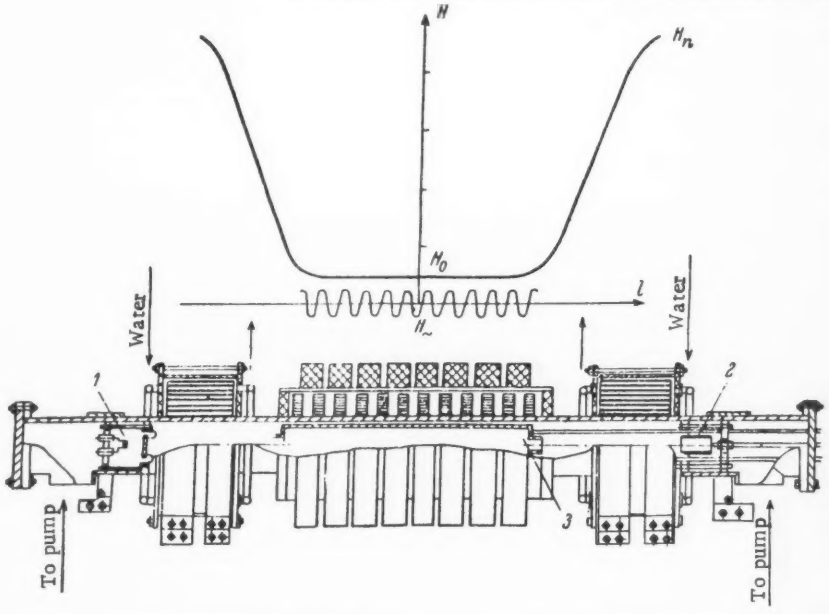


Fig. 1. Diagram of experimental apparatus: 1) electron gun; 2) collector; 3) resonator.

**Magnetohydrodynamic Effects Observed in Pulsed Contraction of a Plasma,** I. F. Kvartskhava, K. H. Kervalidze and Yu. S Gvaladze, pp. 274–281.

*Abstract:* Streak photographs of a pulsed contraction of a plasma in strong magnetic fields are discussed. These photographs indicate an instability which involves the expulsion of plasma formations from the surface of the pinch. The expulsion of plasma apparently results from the interaction of radial shock waves which are reflected at the pinch axis and the surrounding magnetic field. This eruptive instability can be observed in both induction and linear pinches Probe measurements of the magnetic field are discussed

**High Frequency Oscillations in a Bounded Plasma,** R. A. Demirkhanov, A. K. Gevorkov, A. F. Popov and G. I. Zverev, pp. 282–289.

*Abstract:* An investigation has been made of oscillations excited in a bounded plasma in the frequency range from $100 \cdot 10^6$ to $1000 \cdot 10^6$ cps. It is shown that these plasma oscillations are due to oscillations of electrons in the potential well created in the plasma. Several oscillations at different frequencies are excited simultaneously; these frequencies are lower than the plasma frequency. The oscillations are accompanied by electromagnetic radiation. A possible mechanism for the excitation of these oscillations is proposed. [See illustration at right.]

**Radiation Energy Losses in a Plasma,** V. D. Kirillov, pp. 295–304.

*Abstract:* Experiments are described which have been undertaken to investigate the mechanism for the loss of energy from a stable plasma pinch which is isolated from the chamber walls. The experiments have been carried out in a cylindrical porcelain system (with electrodes) at discharge currents of tens of kiloamperes, a longitudinal magnetic field of 24,000 oe and a deuterium pressure of $2 \cdot 10^{-1}$ to $10^{-2}$ mm Hg. The duration of the half-cycle of the discharge current is approximately 500 $\mu$sec. It is found that the flow of charged particles to the walls of the chamber is small. Experiments with an ionization chamber, vacuum spectrograph and thermal phosphors show that a considerable portion of the energy loss from the plasma is due to ultraviolet radiation from the impurities.

*Conclusion:* The results of this group of measurements indicate that under the present experimental conditions most of the energy in the plasma is lost as impurity radiation. Even under unstable discharge conditions, in which case the plasma is in contact with the walls of the chamber the charged particles carry only a small part of the Joule heat to the walls.

The problem of the amount of impurities and the evolution of these impurities in the discharge process in the present experiments remains open. However, the uniformly low electrical conductivity in the majority of experiments described in the literature leads us to believe that the level of the impurities in those experiments (as well as in the present ones) is still very high.

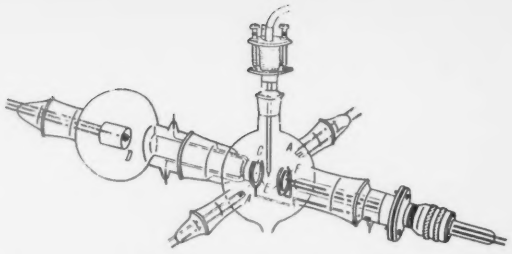

Fig. 1. Construction of the discharge tube.

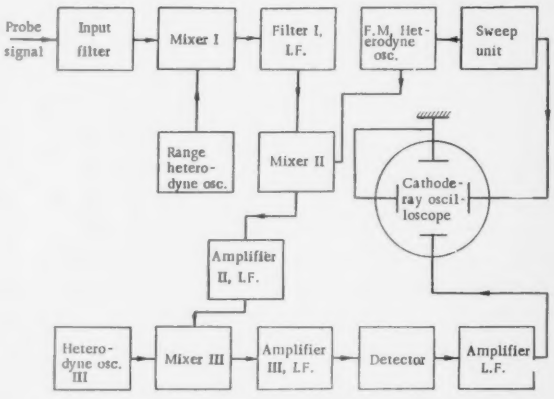


Fig. 2. Block diagram of the UHF receiver with a sensitivity of $10^{-11}$ w.

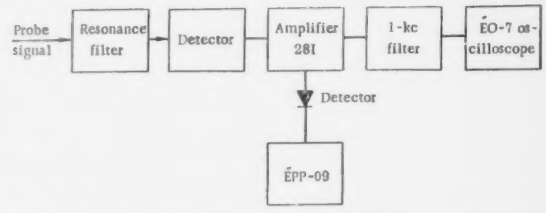


Fig. 3. Block diagram of the apparatus used for detecting oscillations between 200 and 1000 Mcps.

It would be difficult to achieve any success in heating a deuterium plasma by Joule heating without first removing these impurities.

# HOW TO ADD DEPTH TO THE RF SPECTRUM

Faced with an almost unsolvable problem, Martin engineer McKay Goode helped parlay a unique concept and three years of research into a spectacular advancement in radio communications. ● The problem turned over to Goode and a team of specialists was to design a flexible, interference-free, mobile communications system that would reliably perform in high-density military operations. ● Their answer: a system called RACEP.* Here, speech signals are pulse-coded into millionth-of-a-second fragments, combined at random and transmitted all at once over the same frequency. Only receivers preset for the proper code can receive and reconstruct the fragments into normal speech. ● *Result: Engineers working in the creative environment at Martin in Florida have given the almost saturated rf spectrum a new life.*

*Random Access and Correlation for Extended Performance

**MARTIN**
ORLANDO

Breakthroughs like this are achieved when men with talent are allowed to seek their own solutions. At The Martin Company in Orlando, Florida, there is a continuing need for engineers and scientists who can help push forward technological frontiers. ● For information about your place in one of our six major missile and electronics systems, or in one of our future programs, write: C. H. Lang, The Martin Company, Orlando 62 Florida.

*Immediate technical staff openings include:*

COMMUNICATIONS / DIGITAL COMPUTER RESEARCH / HUMAN FACTORS / OPERATIONS RESEARCH / WEAPONS SYSTEMS ANALYSIS / GUIDANCE & CONTROL SYSTEMS / HIGH RESOLUTION RADAR / FLUID DYNAMICS / AEROSPACE DYNAMICS / INFORMATION THEORY

*All qualified applicants will receive consideration for employment without regard to race, creed, color or national origin.*